

# POLYTECHNIC UNIVERSITY OF TURIN

MASTER'S DEGREE

## ENERGETIC AND NUCLEAR ENGINEERING

**Innovation in Energy Production**



MASTER'S THESIS

## **Advantages of metal hydrides usage for hydrogen storage in stationary applications**

*Supervisor*

Prof. Massimo Santarelli

*Candidate*

Matteo Marinelli

**Academic year 2018-2019**

## Sommario

Il presente lavoro è stato impostato in modo da fornire nel primo capitolo informazioni generiche sintetizzate riguardanti problemi di rilevanza globale, quali il cambiamento climatico e la transizione energetica in atto, per poi incentrarsi sulla necessità dell'accumulo di energia in un settore elettrico alimentato sempre più da fonti rinnovabili intermittenti, che rendono la rete potenzialmente instabile. Nel secondo capitolo viene spiegato come tale compito può essere adempito dall'idrogeno tramite un accumulo chimico stabile di lungo termine (o stagionale) che permetterebbe di colmare i deficit di produzione, presenti per la natura stessa delle fonti, tramite l'energia stoccata durante i periodi di surplus delle stesse che, in questo modo, non andrebbero sprecati, incrementando l'efficienza del sistema. L'idrogeno non è una risorsa energetica primaria essendo raro in natura nelle sue forme elementare e molecolare, ma è comunque visto con interesse come potenziale combustibile e mezzo di accumulo d'energia, essendo il suo valore di densità energetica massica il più alto in natura. Le tecnologie basate sull'idrogeno sono molteplici. Alcune sono carbon-free e potrebbero avere un importante ruolo per combattere i cambiamenti climatici. Attualmente il sistema di accumulo d'idrogeno più utilizzato è sicuramente quello di gas compresso a pressioni elevate, dai 200 ai 700 bar, il quale causa notevoli problemi di sicurezza, costi ed ingombri (nonostante i precedenti valori).

In seguito ai primi due capitoli introduttivi, viene descritta un'alternativa molto promettente: gli idruri metallici. Questi materiali sono interessanti per la loro densità volumetrica d'idrogeno, superiore anche alla densità dell'idrogeno liquido, le basse temperature e pressioni d'esercizio e l'intrinseca sicurezza degli stessi materiali, i quali rilasciano il gas solo in seguito ad un assorbimento di calore in particolari condizioni termo-fisiche molto semplici da attuare. Migliaia di leghe differenti sono state testate dagli anni '70, ma questa tecnologia è stata sempre scartata sia per l'assenza di una vera e propria necessità di eliminare le fonti fossili convenzionali ai fini energetici in passato, sia per l'elevato peso delle strutture adibite all'accumulo causato da valori troppo bassi

di densità gravimetrica per applicazioni automobilistiche (problema trascurato nelle applicazioni stazionarie). La descrizione di suddetti materiali viene affrontata in maniera ordinata e completa: prima di tutto, vengono spiegate nel dettaglio termodinamica cinetica caratterizzanti, viene proposta una classificazione delle leghe analizzate e spiegati i possibili metodi di sintesi, layout del reattore, adeguamenti in impianti per la produzione di idrogeno gassoso da fonti rinnovabili e rispettiva re-elettrificazione. Il lavoro termina con un possibile adattamento ad un impianto in fase di costruzione su un'isola della regione Sicilia (Ginostra) con relative analisi preliminari tecnica ed economica. Questa fase finale del lavoro viene portata avanti e confrontata costantemente con la soluzione odierna (gas compresso) così da evidenziare tutti gli eventuali vantaggi e svantaggi. Dal punto di vista economico, ci saranno maggiori svantaggi data la bassa commercializzazione odierna della tecnologia e quindi la sua scarsa maturità, per cui viene infine tracciata un'ipotetica learning curve, che considera una possibile futura maggiore penetrazione nel mercato.

# Index

## 1. Introduction

1.1. Climate change, the main problem of this century.....	1
1.2. The “Energy Transition” .....	5
1.3. The necessity of Energy Storage.....	9

## 2. The Hydrogen prospective

2.1. General Overview .....	13
2.2. The role of hydrogen in the energy transition.....	15
2.3. Fuel Cells and Electrolysers.....	18
2.4. Stationary application.....	22
2.5. Automotive application.....	23
2.6. Hydrogen storage.....	25
2.6.1. Compressed gas .....	
2.6.2. Liquid hydrogen.....	
2.6.3. Metal Hydrates.....	
2.7. Hydrogen Embrittlement.....	33

## 3. Hydrogen Storage in Metals and Alloys

3.1. Thermodynamics.....	36
3.2. Kinetics.....	48
3.3. Ternary hydrides classification.....	49
3.3.1. AB.....	
3.3.2. AB <sub>2</sub> .....	

3.3.3. AB <sub>5</sub> .....	
3.3.4. Others.....	
3.4. Today's best options.....	56
3.4.1. LaNi <sub>5</sub> .....	
3.4.2. TiFe.....	
3.4.3. TiMn <sub>1.5</sub> .....	
3.5. Synthesis of intermetallic compounds.....	60
3.6. Tank design.....	62
3.7. Plant design.....	66
<b>4. Application to the off-grid plant in Ginostra (Sicily)</b>	
4.1. Introduction.....	71
4.2. MH-based system adoption.....	74
4.3. Economic assessment.....	84
4.4. Possible future trends .....	86
<b>5. Conclusions.....</b>	<b>91</b>

## **Bibliography**

## **Ringraziamenti**

*“ Climate change is real and it is happening right now. It is the most urgent threat facing our entire species, and we need to work collectively together and stop procrastinating.*

*We need to support leaders around the world who do not speak for the big polluters, but who speak for all of humanity, for the indigenous people of the world, for the billions and billions of underprivileged people out there who would be most affected by this.*

*For our children’s children, and for those people out there whose voices have been drowned out by the politics of greed.”*

**Leonardo DiCaprio, Oscars 2016**

# 1. Introduction

## 1.1. Climate change, the problem of this century

Today, almost all scientist all over the world agree on the reality of Climate Change. It is caused predominantly by the release of greenhouse gases as result of human activities; the energy sector covers the biggest part of this global amount of about 35 [Gton<sub>CO<sub>2</sub></sub>/year], of which only less than a half could be absorbed by oceans and land biosphere causing an average global temperature increase of about 25 – 30 [mK/year]

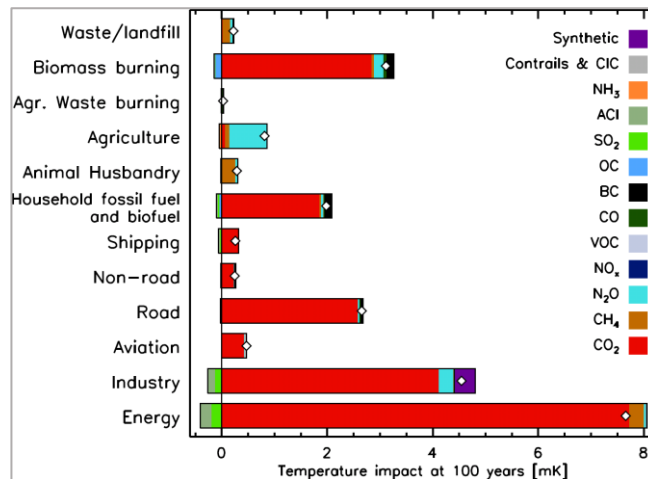


Figure 1 global mean temperature change by source sector after 100 years (for 1-year pulse emissions). Emission data for 2008 are taken from the EDGAR database. For BC and OC anthropogenic emissions are from Shindell et al. (2012) and biomass burning emissions are from Lamarque et al. (2010) [1]

The greenhouse effect consists in the action of several chemical compounds like H<sub>2</sub>O, CO<sub>2</sub>, CH<sub>4</sub>, N<sub>2</sub>O and others which absorb and emit infrared radiation in the wavelength range emitted by Earth; in practice, the action of Green House Gases (GHG) changes the radiative equilibrium between Earth and outer space, not allowing the surface re-irradiated fraction to go outside. This is mostly caused by the molecules of carbon dioxide (CO<sub>2</sub>) which can absorb energy from infrared radiation: the energy from the photon causes the vibration of the molecule so that it gives out this extra energy by emitting another infrared photon. Once the extra energy has been removed by the emitted photon, the carbon dioxide molecule stops vibrating. The temperature of a gas is a measure of the speed of its molecules, so, a faster vibration of a particle raises the

temperature of the gas and causes, on a macroscopic scale, the global warming phenomenon. A second problem of the carbon dioxide is represented by its high stability, which characterizes its higher lifetime in the atmosphere, compared to other GHG and its difficult removal, especially at low concentrations.

The correlation between the average temperature and the yearly average concentration of CO<sub>2</sub> enhancements are evident from samplings carried out worldwide by the scientific community during the last century. This last year has been characterized by the highest value of CO<sub>2</sub> concentration of 415.7 [ppm] [2], registered in May 15, value never so high since Pliocene (2.5 – 3.6 Million years ago), in which the average global temperature and sea levels were 2-3 [°C] and 25 [m] higher than today's values [3]. July 2019 was the hottest month ever recorded [4] and, contemporary, deforestation acts all around the world are touching alarming levels, especially in the Amazon forest, also known as “the planet lung”. It is important to notice that plants chlorophyll photosynthesis represent the only effective known tool to decrease the CO<sub>2</sub> levels in the atmosphere. Researchers are currently studying the possibility to apply carbon capture sequestration processes (CCS) to conventional power plants, responsible of almost all emissions in the energy sector.

The Peterhead power station, located in Aberdeenshire on the north-east coast of Scotland, will be the world's first gas-fired power plant (1180 [MWe]) to host a full-

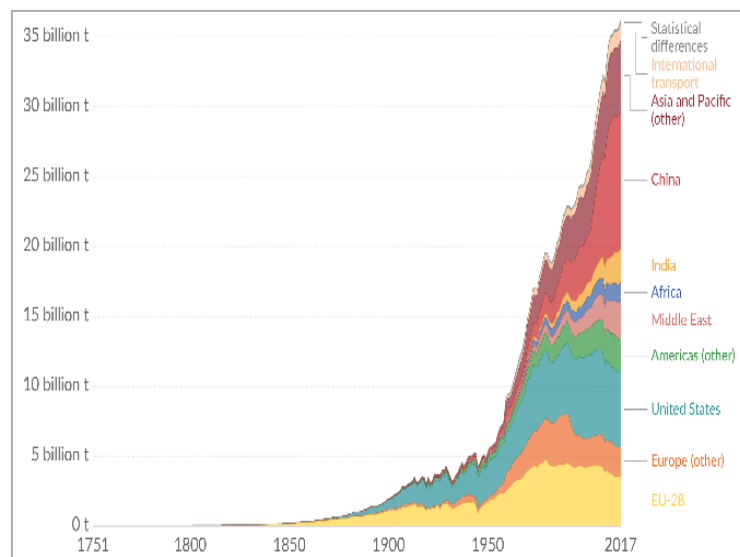


Figure 2 Annual CO<sub>2</sub> emissions by world region [6]

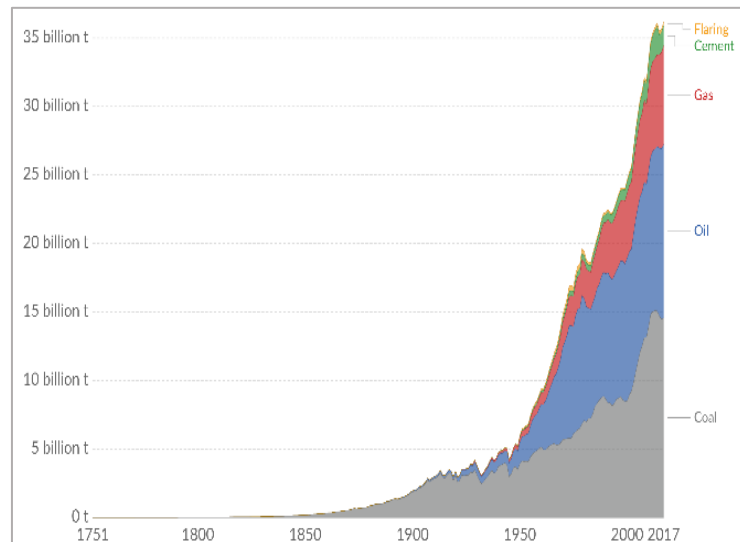


Figure 3 Annual CO<sub>2</sub> emissions by fuel [6]

chain carbon capture and storage (CCS) project on a commercial scale; the project is scheduled to be operational by the end of 2020, and will power approximately half a million homes with clean electricity [5].

Paris, December 12, 2015: 195 countries sign a legally binding agreement to limit global temperature below to 2°C above the era prior to mass industrialization, with an aspiration to limit this to 1.5°C. The world average temperature has already warmed by around 1°C and, unless the energy system changes in almost every field, from power generation to end-users across sectors, the global climate will be affected in the coming 50 to 100 years. The greenhouse gases emitted in a business-as-usual scenario would lead to an increase of the average global temperature of about 4 – 5 [°C] by 2100 [8]. Higher temperatures are already causing many types of weather anomalies all around the world, including storms, heat waves floods, sea levels rise due to world's ice melting in Artic and Antarctica; this least registered the second lowest minimum in the satellite record on September 2019, only behind September 2012 [7]. The direct consequences relies in increasing human's death rate, wildlife extinction rates, ocean acidity (by CO<sub>2</sub> absorption), etc.

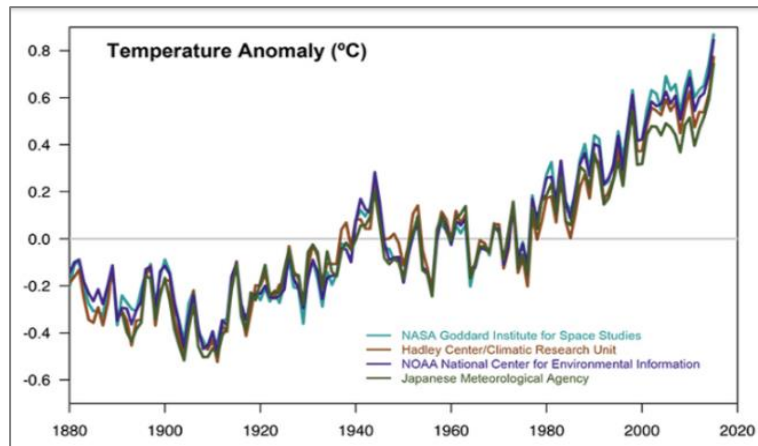


Figure 4 Temperature data from four international science institutions: all show a rapid warming in the past few decades on that the last one has been the warmest on record.

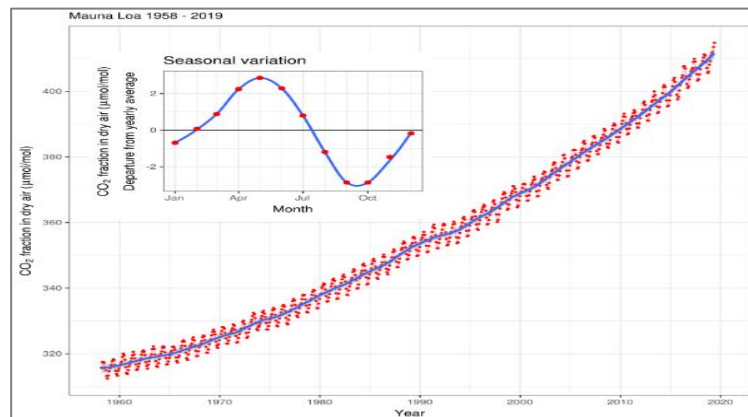


Figure 5 Mauna Loa (Hawaii) was chosen as a monitoring site because, located far from any continent, the air was sampled and is a good average for the central Pacific. Being high (3397 m), it is above the inversion layer where most of the local effects are present.

The primary effect of burning coal, oil, gasoline in vehicles etc. is air pollution. Ninety percent of people worldwide breathe polluted air, according to new estimates released today by the World Health Organization (WHO). In 2016, polluted air resulted in 7 million deaths globally, 4.2 million from ambient air pollution and 3.8 million from the burning of solid fuels for heating and cooking, with low- and middle-income countries bearing the brunt of the burden [9]. Carbon dioxide is not harmful for humans and animals, since it is a natural component of the atmosphere and essential for plant life. Chemical compounds that are dangerous in this field are sulphur and nitrogen oxides (in particular dioxides), carbon monoxide, volatile organic compounds, particulate matter, toxic metals, chlorofluorocarbons, ammonia and ground level ozone. The WHO also recognized the role of air pollution, which includes major climate forcers such as black carbon, as a critical risk factor for non-communicable diseases, contributing to a

significant percentage of all adult deaths from heart disease, stroke, chronic obstructive pulmonary disease and lung cancer.

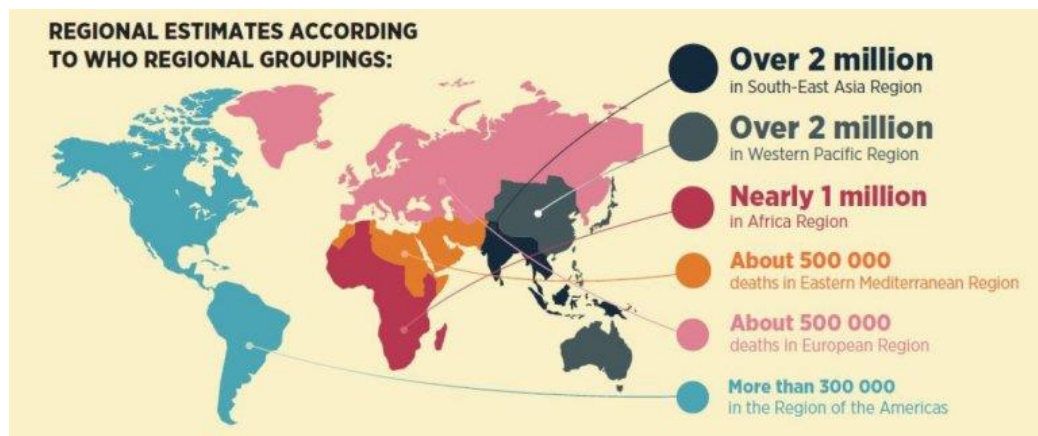


Figure 6 Deaths by air pollution worldwide [9]

But, despite these big problems, fossil fuels account for 82% of primary energy consumption today yet, with renewable energy sources contribute only 14%, and nuclear sources 4%. The global population increase, and the constant economic growth of developing countries (in particular China and India), causes the increase of the global energy demand in electricity, heating, cooling and transportation. In 2018 it increased around 2.3% (the greatest rise in a decade) with a rise of fossil fuel consumption, so, bringing the global energy-related emissions to grow of an estimated 1.7%. This trend has been maintained for all the 2010s, although the best carbon-emitting countries have been also the best investors in sustainable technologies [11].

Today, the problem is still far from being solved and current global efforts seem to be not enough, but signs of change are emerging. Renewable power supply, electrification and energy efficiency measures are appearing across sectors: over the past ten years, global investments in renewable energy sources have been spurred with 16% per year to a total amount of more than USD 2.5 Trillion in this decade, amplifying price drops of solar and wind power in particular, 70% and 50% respectively [12].

## 1.2. The “Energy Transition”

The world needs to embark on one of the most profound transformation in its history: a transition of energy supply and consumption from a system fuelled primarily by non-

renewable, carbon-based energy sources to clean, low-carbon energy sources. The current energy architecture evolved to serve social needs, such as lighting, mobility, heating and safety, and to fuel economic growth and the rising population and increasing demand for energy supply urged us to explore more sustainable energy fonts. Ensuring a secure and reliable energy supply to meet these socio-economic objectives requires a vast array of technologies for energy extraction, conversion and end use, and an infrastructure to integrate these activities.

These last decades, scientific and political communities together have been focused on carry an unprecedented revolution in the energy sector in order to reduce the energy-related emissions of the 90% from fossil fuels by 2050 (Paris Agreement objective), increasing the renewable energy production (50% of the global mix by 2030, EU long-term targets). Electricity is at the centre of energy transition because of its role for economic and social development and its potential to support the decarbonisation. Electricity is in fact a primary link to the use of carbon-free energy sources, such as renewables and nuclear, and its penetration in sectors like transport and heating/cooling can facilitate their decarbonisation.

Energy transition is generally defined as a long-term structural change in energy systems and it's seen as the principal step to do in order to solve the global warming problem. Its principal targets are:

- A full renewable and nuclear power production characterized by conventional plants used as backup systems that could be equipped with carbon sequestration technologies.
- This will unbalance supply and demand in the power sector, so the adoption of short-term (peak shaving) and long-term (seasonal) energy storage systems is needed to solve the problem of source intermittency of wind and solar sources in order to stabilize the grid.

- Important focus on energy efficiency, that means achieving the same level of service (measured as economic output, production quantity or distance travelled) while consuming less energy/fuel;
- Heat production (equal to the 45% of the entire amount of energy consumption worldwide), by using of biomass, solar thermal technologies and heat pumps;
- Zero-emission vehicles development, like battery electric v. and fuel cell v. powered by hydrogen;
- Industrial emissions cutting with the adoption of CCS or renewable energy sources to provide process heat at high temperatures, such as concentrated solar power and hydrogen combustion.
- A transformation of the energy infrastructure, to give more stability to the grid by a new mix of centralized and decentralized energy supply. Moreover, the digitalization of the electric grid can be another possibility: most of the energy consumption should be focused when electricity is abundant and reduced when intermittent RES are scarce. Therefore, this offers further opportunity for energy efficiency improvements since in intelligent buildings, automatic centralised control of HVAC, lighting, and appliances ensures that energy is consumed when and where it is needed;

According to the IEA, only four of 38 energy technology areas were on track in 2018 to meet its Sustainable Development Scenario, which the agency describes as “a major transformation of the global energy system”.

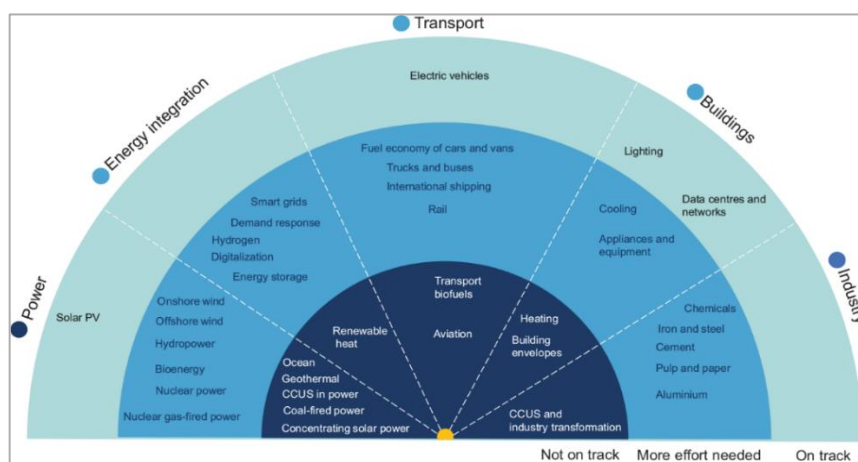


Figure 7 International Energy Agency radar of energy technology areas [13]

An effective energy transition implies a difficult balance between sustainability, competitiveness, affordability, and security of supply and it surely requires massive investments in all the fields involved in this enormous process that is happening right now. Global investments in renewable power and fuels in 2018 totalled USD 288.9 billion (USD 304.9 billion including hydropower), that has been an 11% decrease from the previous year, largely as a result of a significant fall in China, but it's been the fifth year in a row that investments exceeded the USD 230 billion mark. Moreover, with a stable growth in renewable power capacity, the decline in investment reflects to some extent the renewable power falling costs. Nearly all the investments were in solar PV and wind power, with developing and emerging economies that accounted for 53% of total renewable energy investment (with China alone accounting for 32% of the total) [10].

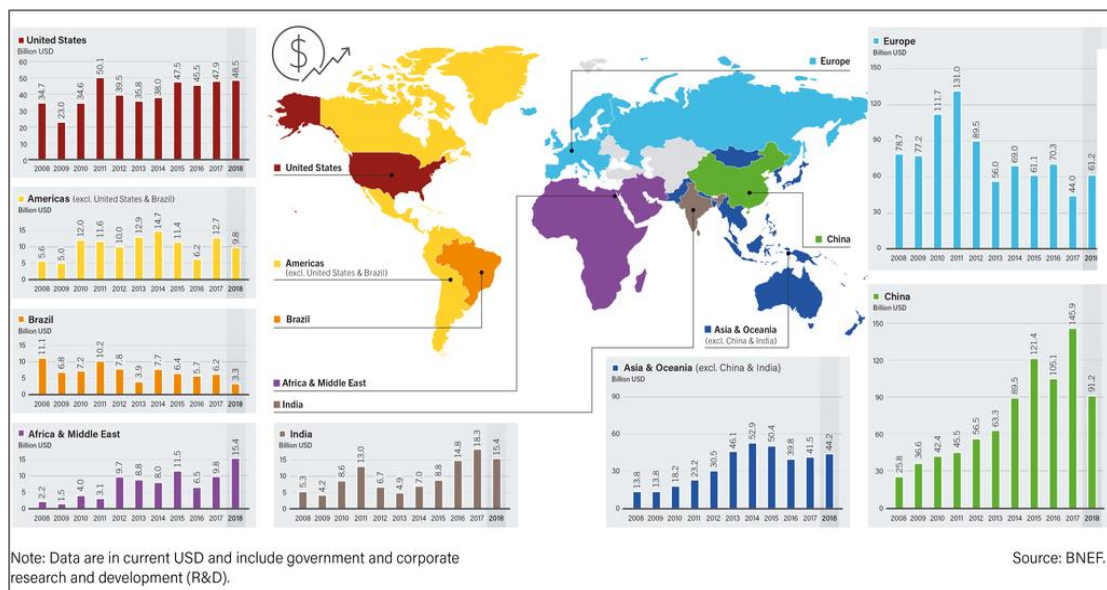


Figure 8 Global new investment in renewable power and fuels by country region, 2008-2018 [11]

Renewable power is increasingly cost-competitive compared to conventional fossil fuel-fired power plants. By the end of 2018, electricity generated from new wind and solar photovoltaics (PV) plants had become more economical than power from fossil fuel-fired plants in many places. Moreover, in some locations it was more cost-effective to build new wind and solar PV power plants than continue to run existing fossil fuel power plants.

As in previous years, renewables saw far less growth in the heating, cooling and transport sectors than in the power sector. The approval of modern renewable energy for heating and cooling in buildings and industrial applications progressed at a slow rate, while the use of biofuels for transport grew moderately during the year.

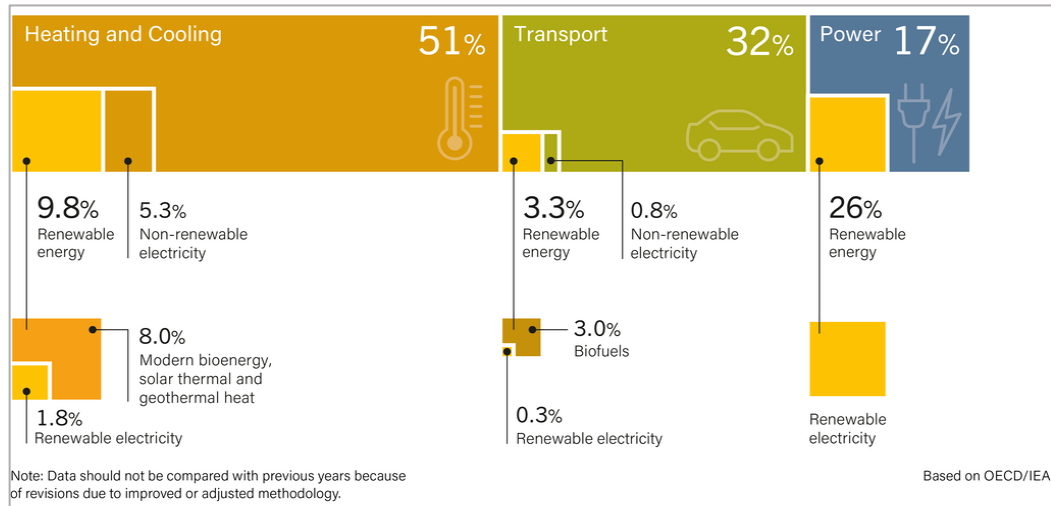


Figure 9 Renewable energy in total final energy consumption by sector, 2016 [11]

It's important to underline how Global Warming is increasing the social concern worldwide about all principal environmental issues, especially regarding younger generations; for instance, the “Fridays for Future” movement, organized by Greta Thunberg, has been received an attendance of more than one million people in 4000 cities around the world between September 20-27 2019 and this can only increase the general efforts to face up this problem.

### 1.3. The necessity of Energy storage

Towards 2050, growth in population and GDO will increase energy demand by 16%, despite projected energy efficiency achievements and renewables are expected to increase their share of the energy mix by 3 to 5 times the current amount. Wind and solar PV are at the vanguard of power-sector decarbonization and set to expand rapidly [11]. The variable output of wind and solar PV makes demand-supply matching more difficult due to their fluctuating nature, caused by weather conditions as well as diurnal and seasonal patterns. This increases the need for new flexibility resources within the system. With the exception of pumped hydro storage, the deployment of electricity storage is at an

embryonic stage. Pumped storage hydropower currently amounts to 153 GW or just over 2% of power generation capacity worldwide, and accounts for most of the capacity to store electricity. Beyond pumped hydro, energy storage systems encompass a largely decentralised, fast growing, diverse and complex set of technologies. While the current installed capacity of these other technologies combined totals around 4 GW, battery storage capacity is growing fast: its installed base has tripled in less than three years, largely driven by lithium ion batteries, which now account for just over 80% of all battery capacity. In particular, small-scale battery storage systems, are making inroads, and 45% of all annual capacity additions are now behind-the-meter<sup>1</sup>[16]. So, the electricity system is currently in a great transition from today's demand-driven centralized and fossil-based generation, where flexibility<sup>2</sup> is predominantly provided by dispatchable generation, toward increasing supply-driven distributed energy production where additional sources of flexibility will be needed. In the electricity grid, supply and demand must be equal during all times. The system frequency (50 [Hz] in Europe, 60 [Hz] in USA) is a measure of balance between supply and demand: it rises if generation is higher than demand and decreases in the opposite case. Short-medium term energy storage systems can balance generation and demand, but today the grid capacity is almost null. Today in fact, when the intermittent renewable share is lower than 15 – 20 % of the overall electricity consumption, grid operators are able to compensate the intermittency; when, instead, it exceeds 25 %, as sometimes it happens in Denmark or Spain, renewable electricity need to be curtailed during the low consumption periods in order to avoid grid perturbation and congestion [17].

---

<sup>1</sup> Widely known in the photovoltaic industry, with the term “Behind The Meter”, a BTM system is a renewable energy generating facility that produces power intended for on-site use in a home, office building, or other commercial facility. The location of the solar PV system is literally “Behind The Meter”, on the owner's property, not on the side of the electric grid/utility.

<sup>2</sup> Flexibility Is the ability of the power system to match perfectly generation with demand.

The second typology of energy storage is the seasonal storage: in a 100% renewable scenario, seasonal storage can compensate seasonal fluctuations in power supply. Considering PV for example, excess energy can be stored in summer when the energy produced is higher than the required quantity, and finally supplied during winter when the source is scarce. There are also thermal ESS that will be as important as the electric or chemical ones but they need further development as the others, in terms of commercialization and research; this work is focused on the chemical storage of hydrogen that can be produced in several ways and stored reversibly for week or months, providing a more reliable seasonal performance compared to electrical and thermal technologies.

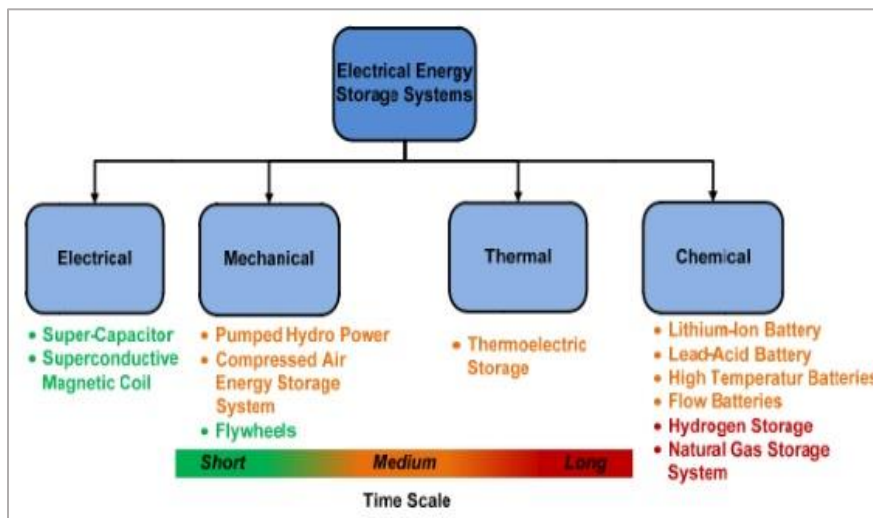


Figure 10 Energy storage technologies classification with examples for each type

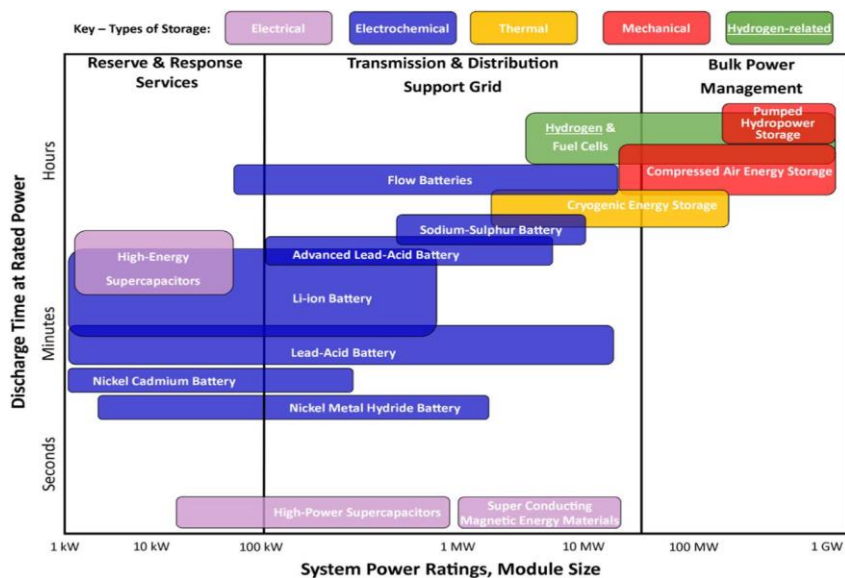


Figure 11 Comparison of key-type energy storage technology in sense of storage capacity and discharge power duration

In off-grid solar applications for energy access, most of systems now include a storage unit. Pumped hydro remains important, though constrained by the location of suitable sites: around 26 GW of additional capacity are expected by 2023, almost (70% of it in China). Lithium-ion batteries are expanding rapidly and are mostly aimed at providing short-term storage. To meet even long-term needs such as seasonal storage, hydrogen is a valid option. Hydrogen storage, however, has a very low round-trip efficiency (in Power-to-Power systems) and the costs of production from green electricity remain a key barrier.

In the following table the current costs of different energy storage technologies are listed:

Table 1 List of the current energy storage systems with respective levels of maturity and system costs [16]

<b>Technology</b>	<b>Maturity</b>	<b>[USD/kWh] (Approximated from plots in [17] , [18])</b>
Pumped Hydro	Mature	350
Li-ion Batteries (NiCoAl)	Maturing	380
Li-ion Batteries (LiFeP)	Emerging	590
Lead-Acid Batteries	Mature	180
FlyWheels	Emerging	1500 – 6000
CAES	Maturing	50 (+ cost of service due to poor RTE)

## 2. The Hydrogen perspective

### 2.1. General Overview

The physical and chemical properties of hydrogen are in many cases unique, despite the fact that hydrogen appears to be the most simple element with  $Z=1$ . Hydrogen is the most abundant element of universe, accounting for the 75% of the mass of all normal matter and for 15 mol% on the surface of earth (the third most abundant element), predominantly bound in water; a minor amount is bound in hydrocarbons and biomass, but there is only a very small concentration of molecular hydrogen in the atmosphere. Three isotopes are known: protium (the most common, 99,98 %), deuterium (0.0026-0.0184%) and the unstable tritium. Molecular hydrogen,  $H_2$ , is a gas at ambient conditions and the lightest molecule of all substances, therefore, it is difficult to condense to a liquid due to the very low critical point ( $T_c = -240.01$  [°C],  $p_c = 12.96$  [bar]).

Table 2 Main physical characteristics of molecular hydrogen

<b>Hydrogen Properties</b>	<b>Value</b>	<b>Unit of measure</b>	<b>Notes</b>
<b>Density (normal conditions)</b>	0.08376	kg/m <sup>3</sup>	The real problem of hydrogen applications
<b>Specific Heat</b>	14.33	kJ/kgK	Very High
<b>Low Heating Value</b>	119.96	MJ/kg	More than double of methane (55.5 MJ/kg) and oil (45 MJ/kg)
	33.333	kWh/kg	
	232.92	kJ/mol	
<b>Molecular Weight</b>	2.0159	g/mol	The lowest value in nature
<b>Diffusion coefficient in air at 25 °C</b>	0.61	cm <sup>2</sup> /s	Very high compared to other gases (0.16 for CH <sub>4</sub> )
<b>Ignition limits</b>	4-75	/	Related to safety problems

It is a non-poisonous, tasteless, colourless, and odourless gas and it is characterized by the fastest diffusion speed in air; therefore, it quickly disperses uniformly from a leak, which contributes to safety, although the explosion range in air is broad. Pure hydrogen-oxygen flames emit ultraviolet light and with high oxygen mix are nearly invisible to the naked eye and the detection of a burning hydrogen leak may require a flame detector; such leaks can be very dangerous. Hydrogen is a very reactive element and forms compounds with most of other elements in the periodic table and with a variety of chemical bonds, in fact it has an ambivalent behaviour towards other elements, occurring as an anion ( $H^-$ ) or a cation ( $H^+$ ) in ionic compounds, forming covalent bonds. Hydrogen can be used as an excellent energy vector thanks to its high specific energy (120 MJ/kg compared to 45 MJ/kg for oil). The advantage to use hydrogen is that it can be stored and will produce water when reacting with oxygen. This will allow reducing the greenhouse gas emission and limiting the use of fossil fuel. However, its low energy density at ambient pressure and temperature (about 10 MJ/Nm<sup>3</sup>) is a serious drawback for a practical use and it is necessary to store it in a more compact form.

Currently, the total annual hydrogen demand worldwide is around 330 [Mtoe<sup>3</sup>], equivalent of around 70 million tonnes, mostly for oil refining and chemical production, almost entirely supplied from fossil fuels with significant associated CO<sub>2</sub> emissions, with 6% of global natural gas and 2% of global coal going to hydrogen production. It is responsible of emissions of around 830 [Mton<sub>CO<sub>2</sub></sub>/year], equivalent to Indonesia and the United Kingdom productions combined [20]. Today hydrogen is used in several industrial processes. The principal one is its usage as raw material in chemical industry for the production of different compounds like methanol, ammonia, hydrochloric acid. It is also used as fuel for rockets, metalworking applications and in the energy industry to produce electricity directly (Fuel Cells) or store energy in chemical form, acting as an energy carrier. Other applications exist but are far from the penetration in the market, like fuel cell vehicles (car, trains and even airplanes) [21].

---

<sup>3</sup> MTOE is the acronym of Million Tonne of Oil Equivalent. 1 MTOE  $\equiv$  11.63 MWh  $\equiv$  41.868 GJ



Figure 12 Main hydrogen production and usage path today (19th June 2019) in millions of tons per year [20]

## 2.2. The role of hydrogen in Energy Transition [23]

Today's growing interest in the widespread use of hydrogen for clean energy systems relies principally on:

- The possibility to be produced without any carbon footprint if renewable electricity is used for electrolysis or bio-methane is processed in steam methane reforming equipped with CCS;
- Its chemical properties that also allow for its use as feedstock in chemical processes, including production of ammonia and methanol;
- Absence of SO<sub>x</sub> emissions in case of combustion, with only limited NO<sub>x</sub>.

As it's been explained previously, energy sector is currently experiencing a radical transformation worldwide. The expansion of renewable energy generation capacity creates new challenges associated with storing large amounts of energy, because of the increasing amounts of RES that lead to a rapid rise in intermittent energy from wind and solar power in the electricity grid. Great significance is attached to storage in the form of "renewable gases" (power-to-gas) such as hydrogen or methane, with hydrogen being produced by electrolysis from surplus electricity generated from renewable sources.

Hydrogen is expected to play an important role in a future energy economy, based on environmentally clean sources and carriers with principal strengths in its light

weight, high energy density and its clean combustion emissions with no harmful chemical by-products. The Hydrogen Council [23] has declared that it has principally seven roles in decarbonizing major sectors of the economy alone:

- **Enable large-scale, efficient renewable energy integration:** as already said, an increased integration of renewable, intermittent energy sources will require adequate storage solutions and hydrogen offers valuable advantages in this context, as it avoids carbon dioxide and particles emissions, can be deployed at large scale and can be made available everywhere. Electrolysis can convert excess electricity into hydrogen during times of oversupply; the produced H can be used to provide back-up power during power deficits (Power-to-Power) or can be used in other sectors such as transport, industrial or residential. Moreover, Hydrogen can serve as long-term carbon-free seasonal storage medium: it represents the optimal overall solution for long-term, carbon-free seasonal storage, together with pumped hydro that today offers more than 95% of global power storage (162 [GW]), but it remains subjected to local geographic conditions.
- **Distribute energy across sectors and regions:** Some countries, such as Japan, are not well positioned to generate energy with wind and solar power alone, so that importing renewable energy might be more economical than produce it at low efficiency. While transporting electricity over long distances can cause energy losses, pipeline transportation of hydrogen and storage in metal hydrides reaches almost 100% efficiency, making hydrogen an economically attractive option when transporting renewable energy at scale and over large distances.
- **Act as a buffer to increase system resilience:** Due to its high energy density and long-term storage capacity, hydrogen can be well suited to serve as an energy buffer and strategic reserve, so to align global energy storage with charging energy demand. Today, the energy system has a backup capacity of about 24% of final annual energy consumption, almost exclusively held by fossil fuels.

- **Decarbonize transport:** Fuel cell electric vehicles (FCEVs) can have an important role in future to decarbonize a sector which accounts the 21% of global emissions alone, since it's actually oil dominated. This topic is elaborated on in chapter 2.3.2.
- **Decarbonize industry energy use:** Today, natural gas, coal and oil provide energy for industrial processes and generate about 20% of global emissions. In this field, energy efficiency must be improved, reducing the need of energy, and the process heat at low- and high-grade could be decarbonized by means of hydrogen usage. In fact, it's often available as by-product of chemical industry and can be used in burners or fuel cells to produce heat and electricity. The waste heat of SOFC or MCFC is characterized by higher qualities due to the higher process temperature and offer a zero-emissions alternative for heating. An important project in this field is the first pilot hydrogen-based steelworks plant ever that will be constructed in Sweden in 2020 in which hydrogen the direct reduction of iron ore (i.e. the separation of oxygen from the iron ore using hydrogen and synthesis gas) could develop into an important industrial process in steel manufacturing, substituting the blast furnaces and cutting the carbon emissions completely. The steel production alone is responsible of the 7 – 9 % of the total CO<sub>2</sub> emissions [15].
- **Serve as feedstock using captured carbon:** if carbon capture and utilization technology takes off, hydrogen will be needed to convert the captured carbon into usable chemicals like methanol, methane, formic acid, urea, plastics and pharmaceutical goods, that today are produced by crude oil as feedstock.
- **Help decarbonize building heating:** space heating and warm water supply accounts for about 80 % of residential energy consumption, responsible for 12% of global emissions. Hydrogen technologies such as fuel cell micro CHPs offer high efficiency for heat and power generation, and houses linked to the gas grid can handle a mixture of hydrogen and natural gas with relatively small adjustments and investments.

German analysts of the German company Energy Brainpool argue that hydrogen could become more economic than natural gas in 20 years, due to current investments in hydrogen production from renewable energy surplus. Today green hydrogen costs 0.18 €/kWh that goes to more than 0.35 €/kWh considering taxes. In 2030 it should decrease to 0.12 €/kWh and to 0.021 – 0.032 €/kWh in 2040, depending on the renewable energy rate in the electric grid and on its available surplus. On the opposite side, EIA estimates an increase of natural gas costs from 0.017 €/kWh today to 0.32 – 0.041 €/kWh in 2030-2040.

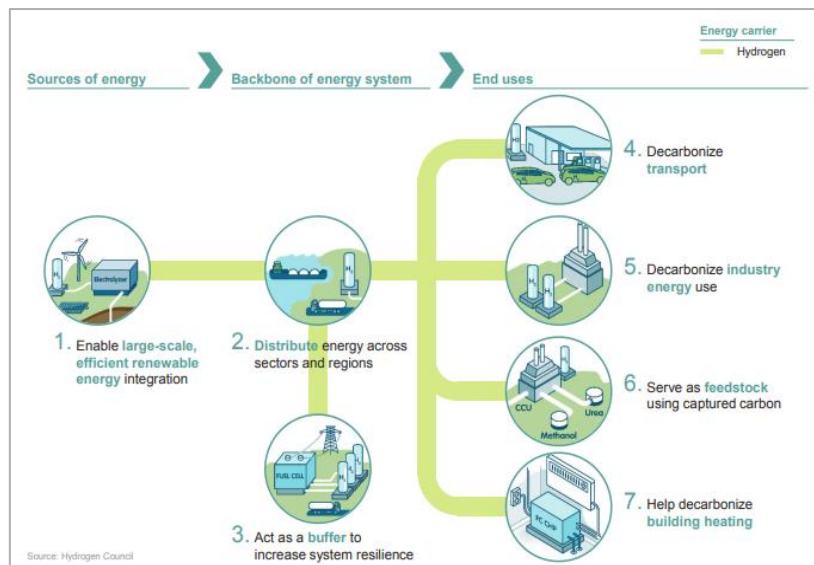


Figure 13 The seven roles explained

### 2.3. Fuel Cells & Electrolysers

A fuel cell is an electrochemical device that generates electricity directly from a fuel and an oxidant in one step, exploiting the thermodynamic effects of an oxidation changing its “pathway” by the interposition of an artificial structure between the reactants. There are several type of fuel cells available and typically they are categorized by both their operating temperature and electrolyte typology, but the only technology considered in this work is the low temperature proton-exchange membrane fuel cell (PEMFC). They are made up of three adjacent segments: anode, electrolyte and cathode. At the anode a catalyst oxidizes the fuel ( $H_2$ ,  $CH_4$ ,  $CH_3OH$ , etc.), turning it fuel into an ions and electrons. The electrolyte is a substance specifically designed so that only ions can pass through it. Electrons travel through a wire creating the electric current sustained by an

external voltage. The ions travel through the electrolyte to the cathode where are reunited with electrons and reacting with a second chemical (usually oxygen) to generate water and other compounds depending on the FC typology.

The operation of an electrolyser is exactly the opposite. It is needed an external electric power able to dissociate the water molecules in pure hydrogen and oxygen that are divided and collected separately, as shown in figure 14. The chemical reactions implicated in PEM machines are very simple and involve only hydrogen and oxygen:

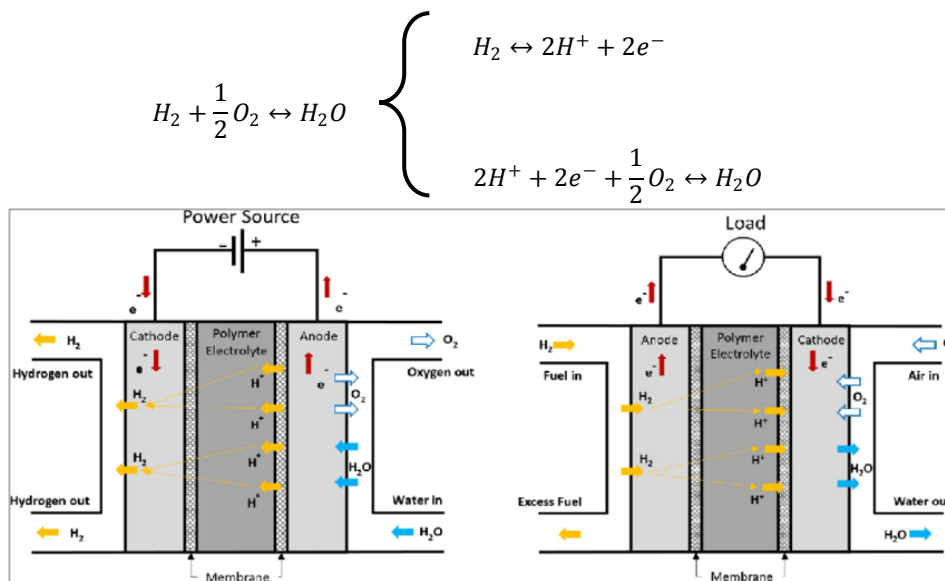


Figure 14 Structure of a PEM electrolyser / fuel cell system

The principal parts of the system are:

- Two electrodes, characterized by a catalyst, where the reaction occurs, and a three-phase boundary that enables the electrode to conduct ions (towards the electrolyte), electrons (towards the external circuit and the load) and molecules that are transmitted in a porous media from/to the bulk flow;
- A membrane in between (electrolyte) able to transfer only the wanted ions. The state of art material is NAFION, a polymeric material that needs constant humidification to conduct  $H^+$  in form of hydrated protons ( $H_5O_2^+$ ,  $H_7O_3^+$ );
- Metallic interconnectors between single cells to increase the current generated and the power produced by the stack. It must be a good conductor not permeable to molecules.

The PEM systems are characterized by the following main features:

- High purity level of Hydrogen requirement, at least 99.99%, due to the high carbon sensitivity (in particular CO), which would irreversibly damage the system in a very short time;
- Low temperature operation (50 – 90 °C), that makes necessary the usage of platinum as catalyst to increase the kinetic of the reaction. The material for electrolysers are instead ruthenium or iridium;
- The possibility of efficient dynamic operations, which makes it suitable for distributed power generation, backup power, portable power, as well as automotive applications. This make it uniquely suitable to transform renewable electricity generated by unsteady power sources to generate hydrogen, like wind or PV;

The applications in which FC systems can be beneficial in future are stationary and mobile power generation (even for remote areas not linked to the main electric grid), fuel cell electric vehicles, satellite power systems and military applications (submerged vehicles, in particular due to the very low sound and infrared signatures). The principal fuel cell properties that justify the current efforts on the R&D are high efficiency, long system life and low maintenance, higher energy density relative to batteries and cogeneration potential, especially regarding the high temperature systems (SOFC, MCFC).

The technology considered in chapter 4 for the electrolyser is the alkaline one. It is characterized by two electrodes inside a liquid electrolyte with 20-30 wt.% KOH that circulates inside the system without any pump requirement (so-called “smart” closed loop) and dissociates in  $K^+$  and  $OH^-$ . It is the less expensive technology in the electrolysers frame but it does not respond quickly to high-fluctuating input signals, like RES (Renewable Energy Sources) and the relative efficiencies are the lowest.

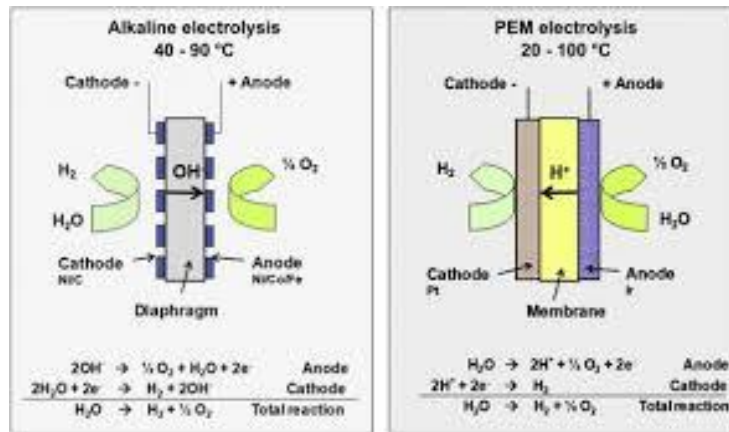


Figure 15 Alkaline water electrolysis, compared with PEM

Product development for low temperature electrolysis began 40 years ago, but scarcer commercial products are currently on the market and the amount of hydrogen produced today with this technology is around 2 [Mtoe/year], (the 0.6% of the total). Electrolysis is a key technology to attempt to convert electrical energy produced by renewable energy sources into chemical energy to be easily stored. The main disadvantages relate on the current high price, due to the usage of noble materials as catalyst, the low efficiencies compared to conventional methods to produce hydrogen. Almost all hydrogen today is produced from fossil fuels, with direct production from electricity through water electrolysis under 1%. However, investment in electrolysis for renewable applications is quickly on the rise, which could help reduce costs and provide additional flexibility. If all planned or under construction projects materialise, cumulative hydrogen electrolysis capacity will rise from 55 [MW] in 2017 to over 150 [MW] by 2020 [20]. Currently, several projects are under construction, as showed in figure 15.



Figure 16 Electrolyser capacity installed per year [24]

PEM fuel cells have an average efficiency in the range 48% - 55%, while the alkaline electrolyzers are characterized by a value around 50% - 70%, with a corresponding low round-trip efficiency compared to other storage technologies of 24% - 38.5%.

## 2.4. Stationary Application

Power-to-gas plants convert electrical power into a storable gas (hydrogen or synthetic methane), suitable to absorb excessive power produced by renewable generators like wind and photovoltaic systems. As a gas, this excessive renewable power may be stored within the gas network and made available to all energy sectors and the chemical industry in a reliably and stable form.

This work is focused on Power-to-Power systems, in which there is no link to the gas grid and hydrogen is produced and stored during excessive renewable power generation which would be inevitably curtailed. Then, once the renewable source is scarce, hydrogen can be re-electrified in a direct electrochemical process, using fuel cells.

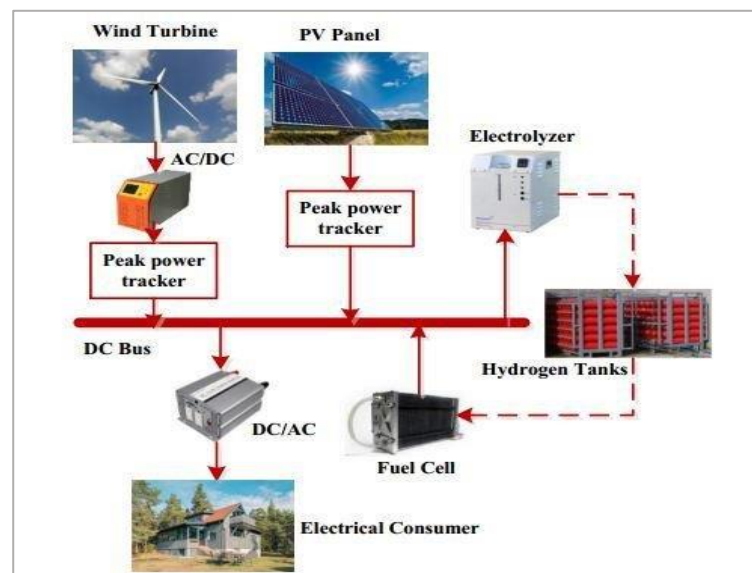


Figure 17 Hydrogen based energy conversion routes in P2P plants

It is important to say that, due to the poor round-trip efficiency of hydrogen re-electrification, the development in the short term is unlikely. Converting electricity into a new energy carrier enables extracted energy to be used after many months or

transported through alternative infrastructure opening possibilities for de-carbonizing other sectors, such as transportation, chemical industry, etc.

Today, the majority hydrogen-based P2P plants regards micro-grid or off-grid locations since no large size P2P plants have been constructed yet. In places difficult to reach, like islands or mountain towns, a plant of this kind can be economically advantageous compared to conventional methods of electricity production. Some international projects are focused on the development of renewable electricity production with hydrogen-based P2P systems, with the aim of making these considered communities independent by fossil fuel and totally decarbonized without any CO<sub>2</sub> emission. The REMOTE project is one of these, coordinated by the STEPS team, composed by researchers and professors of Polytechnic University of Turin. This European project, started in 2018, wants to pursue the zero-emission goal in 4 locations difficult to access and to link with the main electric grid unless with big investments. In chapter 4, the attention will be focused on one of these DEMO plants.

## **2.5. Automotive application [27]**

As the world grapples to eliminate fossil fuels, electric cars have seen an incredible boom: last year over one million electric cars were sold around the world and the overall number today passes the three million units. While there are many brands of electric car to choose from, there are only two choices when it comes to powering electric vehicles: fuel cells or batteries. Both produce electricity to drive electric motors, eliminating the pollution and inefficiencies of the internal combustion engine, both electricity and hydrogen can be produced from low or zero carbon sources including solar and wind power, and therefore both are being pursued by car manufacturers and researchers as the possible future of electric vehicles. Hydrogen has a specific energy of 33.3 [kWh/kg], while lithium ion batteries at best have a specific energy of just 0.28 [kWh/kg] (most fall around 0.17[kWh/kg]): that's more than 120 times as much energy per kg for hydrogen. Additionally a hydrogen fuel cell vehicle can be refuelled in less than 5 minutes, while a battery-powered electric vehicle, like Tesla model S, takes over 3 hours to fully recharge,

but important progresses are done each year from this point of view. The big disadvantage of hydrogen stays in the price of refuelling of about 0.18 [\$/km] compared to battery-powered electric vehicle, 0.02-0.03 [\$/km], 8 times less; here lies the problem, hydrogen simply requires more energy to produce. Moreover, the charging efficiency of batteries reaches 99%, very high compared to electrolyser technologies.

The next hurdle in getting hydrogen fuel cell vehicles on the road is the transport and storage of pure hydrogen; its cost is problematic: hydrogen has extremely low density as a gas and it needs to be increased. This can be made in two ways: compress in gaseous form, liquefy by cryogeny, or host it in metal hydrides, more precisely in complex hydrides. On-board compressed hydrogen-gas storage 700 [bar] is today introduced in vehicles, due to comparable refuelling time ( $< 3$  min) and driving range ( $\geq 500$  km) to conventional gasoline-fuelled vehicles. However, hydrogen compression to 700 bar consumes an amount of energy comparable to 13–18% of the lower heating value. Additionally, when hydrogen is compressed to 700 bar the volumetric energy density becomes 5.6 [MJ/L] which is far less than 32.0 [MJ/L] for gasoline. Thus, solid-state hydrogen storage is considered. By combination of a high-pressure cylinder and a solid-state material containing hydrogen, the driving range of a hydrogen-fuelled vehicle could be extended significantly or the tank volume could be reduced while maintaining the same driving range. The Energy Department of United States has a specific unit that is studying a solution to make hydrides for storage in automotive applications reliable and cost-effective, with a proper list of targets to reach: by 2020, the FCTO (Fuel Cell Technology Office) aims reach these specific system targets:

- 1.5 kWh/kg system (4.5 wt.% hydrogen);
- 1 kWh/lt system (0.030 kg hydrogen/lt);
- \$10/kWh (\$333/kg stored hydrogen capacity).

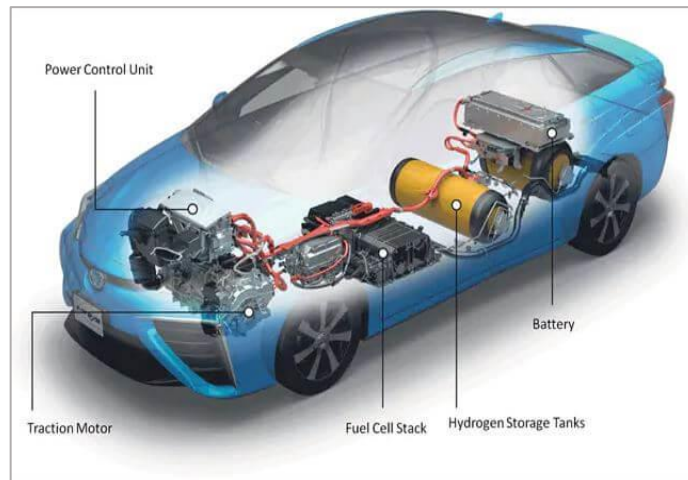


*Figure 18 Schematic representation of a hydrogen-powered car at the state of art*

The global fuel cell electric vehicle (FCEV) stock reached 11 200 units at the end of 2018, with sales of around 4 000 in that year (80% more than in 2017). Most of the sales continue to be Toyota Mirai cars in California, supported by the Zero Emission Vehicle (ZEV) mandate and expanding refuelling infrastructure. Japan has announced its intention to become the world's first hydrogen society with its government and the auto industry that are working together to introduce 160 hydrogen stations and 40000 FCEV by 2021. At the end of 2018, 376 hydrogen refuelling stations were in operation. And leading countries have announced targets to build a total of 1 000 more during 2025-2030 [28].

## **2.6. Hydrogen Storage [32]**

It is obvious that hydrogen storage will have a fundamental role in the future hydrogen economy as it covers a big part of the mentioned applications.

The most common method to store hydrogen in gaseous form is in steel tanks, although lightweight composite tanks are designed to withstand higher pressures and are becoming more and more common. Gaseous hydrogen cooled to near cryogenic temperatures, is another alternative that can be used to increase the energy density of gaseous hydrogen. A more novel method to store hydrogen gas at high pressures is to use glass micro spheres.

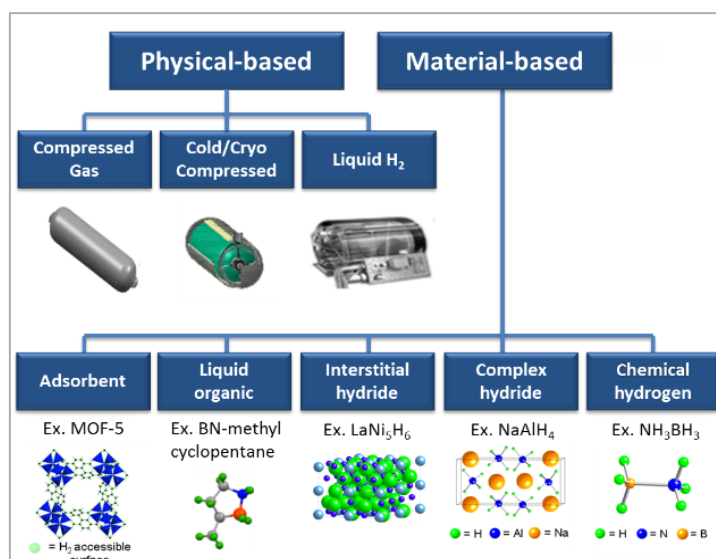


Figure 19 Overview of hydrogen storage technologies [27]

Hydrogen can be stored physically as either a gas or a liquid: the first one typically requires high-pressure tanks (>200 [bar]), the other requires cryogenic temperatures because of the low boiling point of hydrogen at ambient pressure of  $-252.8[^\circ\text{C}]$ . Both solutions are characterized by large volume requirements, high energy penalties, high investment cost and safety problems. It can also be stored on the surfaces of solids (by adsorption) or within solids (by absorption in metal hydrides). This last option allows a big enhancement of hydrogen volumetric density, even higher than the liquid phase. The main drawbacks that limited their commercialization in past are the low gravimetric capacity of intermetallic compounds, which makes them unsuitable for mobile applications, and the high energy required by lighter compounds, known as complex hydrides.

### 2.6.1. Compressed gas

The most common method of hydrogen storage today is by gas compression at high pressures in steel or composite material-based cylinders. New lightweight composite cylinders have been developed, able to withstand pressures up to 800 bar, so that hydrogen can reach a maximum volumetric density of  $36 [\text{kg}/\text{m}^3]$ , almost half as much in its liquid form at normal boiling point. It can be easily observed that hydrogen density does not follow a linear function over the increase of pressure. A hydrogen density

of 20 [kg/m<sup>3</sup>] is reached at 300 [bar]. The volumetric density can be increased to around 40 up to 70 [kg/m<sup>3</sup>] by compressing the gas to a pressure of up to 700 or 2000 [bar], respectively. However, 2000 bar is technically not feasible and liquid density cannot be pursued with the current knowledges. The main advantages with such composite tanks are their low weight, and their commercial availability; they are also well-engineered and safety tested thanks to the very long experience collected during the decades. The main disadvantages are the large physical volume required and the energy penalties associated with compressing the gas to very high pressures. There are also some safety issues that still have not been resolved, such as the problem of rapid loss of H<sub>2</sub> in an accident and the embrittlement of cylinder material, during the numerous charging/discharging cycles.

The wall thickness of a cylinder capped with two hemispheres is given by the following equation:

$$\frac{d_w}{d_0} = \frac{\Delta p}{2 \cdot \sigma_v + \Delta p} \quad (1)$$

Where  $d_w$  is the wall thickness,  $d_0$  the outer diameter of the cylinder,  $\Delta p$  the overpressure and  $\sigma_v$  the tensile strength of the material, which varies from 50 – 1100 [MPa]. The density of hydrogen at elevated pressure can be estimated using the principles of thermodynamics. While the behaviour of most gases can be approximated with a high accuracy by the simple equation of state of an ideal gas, the behaviour of hydrogen deviates significantly from the predictions of the ideal gas model. The resulting deviation from the ideal gas law is always in the form of expansion (the gas occupies more space than the ideal gas law predicts). One of the simplest ways of correcting for this additional compression is through the addition of a compressibility factor, designated by the symbol  $Z$ . Compressibility factors are derived from data obtained through experimentation and depend on temperature, pressure and the nature of the gas.

$$pV = nZRT \quad (2)$$

By reducing the pressure  $p$  to the critical pressure  $p_{CR}$  and the temperature  $T$  to the critical temperature  $T_{CR}$ , a generalised compressibility factor for all gases, can be drawn as a function of  $P_R = P/P_{CR}$  and  $T_R = T/T_{CR}$ . The value of compressibility factor  $Z$  for hydrogen at high pressures and low temperatures in Figure 18 shows that, at ambient temperature, a value of 1.2 is reached at 300 [bar], and at low temperatures even earlier. This means that a calculation of the hydrogen mass in a container from a measurement of temperature and pressure using the ideal gas equation will result in a mass 20% greater than in reality

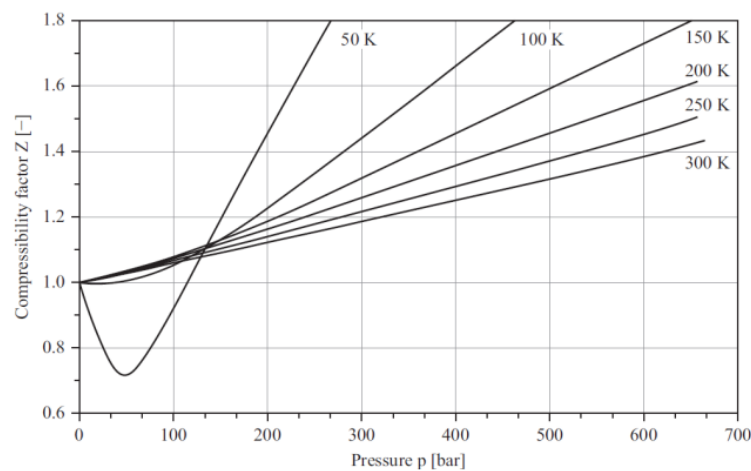


Figure 20 Hydrogen compressibility factor

### 2.6.2. Liquid hydrogen

The energy density of hydrogen can be improved by storing hydrogen in a liquid state to 70.8 [kg/m<sup>3</sup>]; liquefaction of hydrogen is a well-established technology, which is especially applied in space exploration. However, liquefaction is an energy intensive process: the condition of low temperature is maintained by using liquid helium. Hydrogen does not liquefy until -252 [°C]  $\equiv$  21 [K] at ambient pressure and a lot of energy must be employed to achieve this temperature. Furthermore, issues are remaining with tanks due to the hydrogen boil-off, the energy required for the liquefaction process, system volume, weight and cost. About 40 % of the energy content of hydrogen can be lost due to the storage methods and safety is also an issue with the handling of LH<sub>2</sub>.

The theoretical volumetric density is 71 [kg/m<sup>3</sup>]. This means that liquid hydrogen has a much better energy density than the pressurized gas solutions mentioned above. It is interesting to note that more hydrogen is contained in a given volume of water (111 [kg/m<sup>3</sup>], or gasoline (84 [kg/m<sup>3</sup>]) than in pure liquid hydrogen. The simplest hydrogen liquefaction cycle is the Linde cycle, based on the Joule-Thompson effect, which occurs when a gas or a mixture experiences a change in temperature during isenthalpic pressure change.

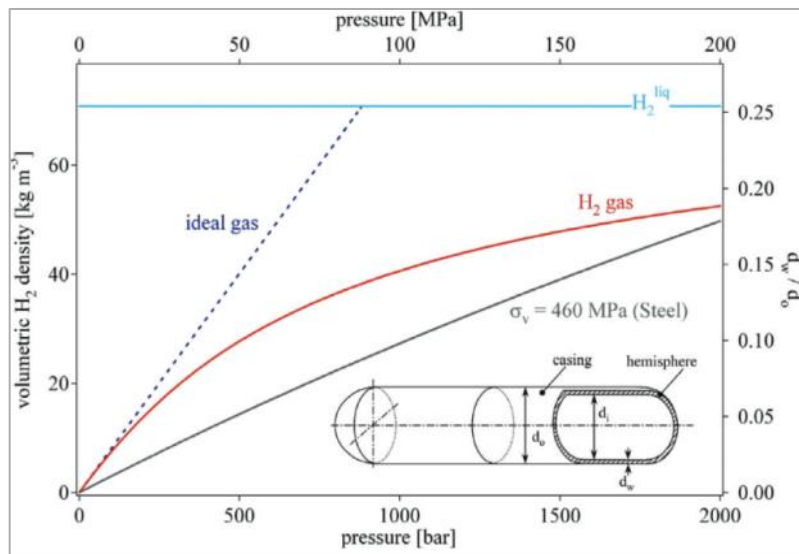
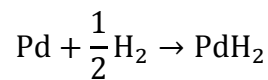


Figure 21 Volumetric density of compressed hydrogen as function of gas pressure, compared to an ideal gas behaviour and liquid hydrogen

### 2.6.3. Metal Hydrates

The first discovery of the absorption of hydrogen in a metal dates back to 1866 thanks to Thomas Graham (1805-1869), who obtained palladium hydride thanks to the reaction;



It is not a stoichiometric compound: the H<sub>2</sub> is dissolved in the metal matrix in atomic form, occupying the interstitial positions in the crystal lattice. This casual find was the start point of thousands of studies involving other metal hydrides.

The elevated reactivity of hydrogen, linked to its electronegativity value (2.2), enables this element to form chemical bonds with the majority of elements in the periodic table,

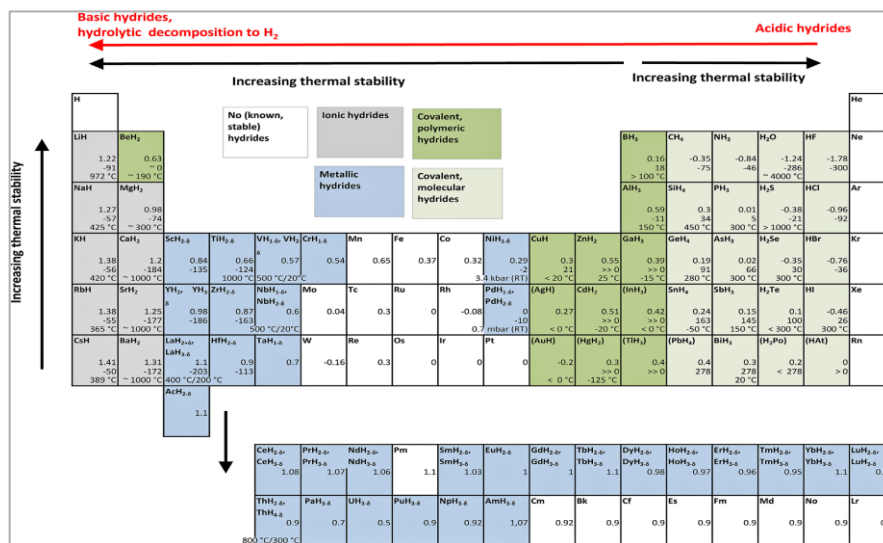


Figure 22 Overview of the (stable) binary hydrides of all elements. In addition to the stoichiometry, the electronegativity difference, the formation enthalpy, and the decomposition temperature for the hydride of each element are given.

except noble gases and some transition metals that compose very unstable compounds (figure 19). There can be 4 possible typologies of metal hydrides, that correspond to different chemical bonds between atom and Hydrogen.

- Ionic hydrides:** binary compounds formed with alkaline or alkali-earth metals; hydrogen, due to its very high electronegativity, can take the most external electron of the metal completely, forming the ion  $[H^-]$ . These compounds can react with water causing large hydrogen release, but they are too stable to be used as hydrogen storage materials. The most important material of this kind is the  $MgH_2$  that is considered a transition hydride since its chemical bond is partially ionic and covalent. It is rising a lot of interest by the American department of energy for both stationary and automotive applications, thanks to its relatively high gravimetric density (5.5 %wt.). A lot of studies and experimentations with important investments are going on to improve its performances.
- Covalent Hydrides:** binary compounds formed with non-metallic elements which have an electronegativity value comparable with hydrogen, so the chemical bond

between them is covalent. Typically, these compounds can be found in liquid or gaseous form at ambient conditions and are thermodynamically unstable. They are not suitable for hydrogen storage since their sintering is too complicated.

- **Complex Hydrides:** they are characterized by the formation of a certain anionic group, a crystalline structure in which hydrogen is covalently linked to a central atom as the general formula  $A_xM_yH_z$ . A represents an element of the first or second group and M can be boron, aluminium or a transition metal. The usage of these compounds for hydrogen storage has been reevaluated since 1997, when Bogdanovic & Schwickardi, studying the  $NaAlH_4$ , found that it is possible to reduce the kinetic barrier of desorption, making the process reversible, by means of catalysts usage (in that case Titanium). The systems  $Mg_2FeH_6$  and  $Al(BH_4)_3$  are characterized by very high volumetric densities of 150 [ $kg/m^3$ ] (the highest ever discovered) and 70 [ $kg/m^3$ ]. Since the elements involved are relatively light compared to transition metals, the gravimetric densities are higher in this case, making this typology interesting especially for automotive applications. The real problem stays in the large temperatures and pressures required to operate in this field. Characteristic that is overwhelmed with the following chemical compounds.
- **Intermetallic or Interstitial Hydrides:** These compounds are composed by transition metals and rare-earth materials. Hydrogen in this case forms a metallic bond with the hosting metal:  $H_2$  dissociates and electrons pass to the metal conduction band, while protons occupy the interstices of the octahedral or tetrahedral crystal lattice. As already seen, most of the 91 natural elements above H will hydride under appropriate conditions, but unfortunately the Pressure-Composition-Temperature (PCT) properties are not very convenient relatively to the 1-10 [bar], 0-100 [ $^{\circ}C$ ] ranges of utility chosen for practical applications (PEM). So, in order to exploit on practical applications of reversible hydrides, strong hydride forming elements A are

coupled with weak hydrating elements B, forming alloys characterized by intermediate thermodynamic affinities between the two.

Their advantages are the good volumetric capacity, that can be up to 60% higher than that of liquid hydrogen, the safe way of storage, the high energetic rate at moderate pressure and temperature. They should also present high reversible capacity, fast kinetics, resistance to oxidation, or corrosion and long cycle life. Their thermodynamic properties can be tuned by appropriate chemical substitutions.

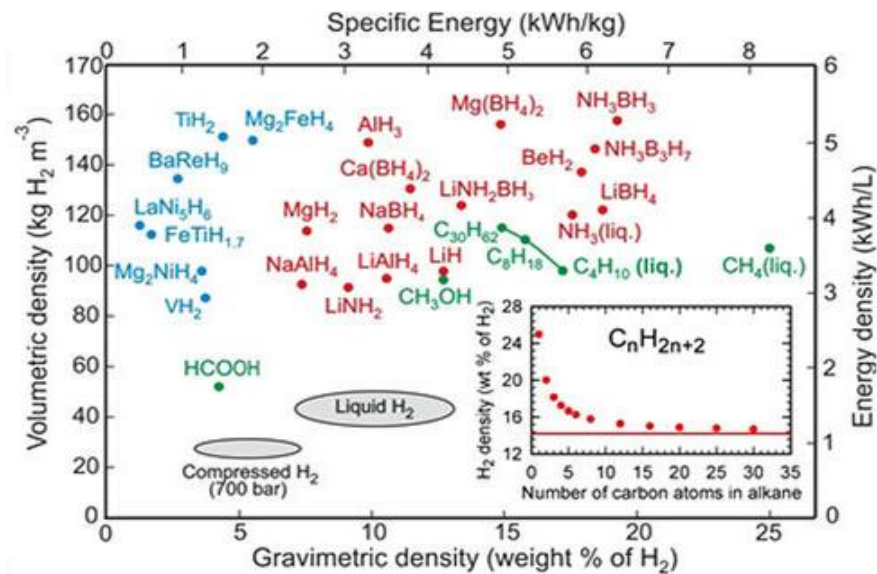


Figure 23 Overview of the main available chemical compounds able to store hydrogen, compared to liquid and compressed gas methods, with their main thermodynamic characteristics. (Intermetallic hydrides in blue, complex and ionic hydrides in red, hydrocarbons in green)

High density hydrogen storage is a challenge for stationary and automotive applications. Presently available storage options typically require large-volume systems that store hydrogen in gaseous form and a further development of metal hydride systems can help in future, making possible to store seasonally hydrogen with the best safety characteristics. Another way to store hydrogen is the physisorption of hydrogen molecules at low temperature on materials with high surface area. Hydrogen molecules are adsorbed at the surface of the materials without dissociation in which Van der Waals interactions type only are involved, with consequent low energy in bounding. This means that it is necessary to work at very low temperatures (using liquid nitrogen) and sometimes high pressure to obtain a good weight capacity. The different types of

materials which are studied for their high specific surface area are carbons and nanocarbons, zeolites, and metal organic frameworks (MOFS).

Table 3 Overview of the principal hydrogen storage methods with relative properties

<b>Storage Methods</b>	$\rho_m$ [mass %]	$\rho_v \left[ \frac{\text{kg}_{\text{H}_2}}{\text{m}^3} \right]$	T [°C]	P [bar]	<b>Phenomena and remarks</b>
<b>High pressure gas cylinders</b>	13	<40	Room Temperature	200-800	Compressed gas (molecular H <sub>2</sub> ) in light weight composite cylinders (tensile strength of the material around 2000 [MPa])
<b>Liquid hydrogen in cryogenic tanks</b>	Size dependent	70.8	-252	1	Liquid hydrogen (molecular H <sub>2</sub> ) on materials e.g. carbon with large specific surface area, fully reversible
<b>Complex compounds</b>	<18	≤150	>100	1	Complex compounds ([AlH <sub>4</sub> ] <sup>-</sup> , [BH <sub>4</sub> ] <sup>-</sup> ) desorption at elevated temperatures, absorption at high pressures
<b>Absorbed on interstitial sites in a host metal</b>	≤2	≤150	Room temperature	1-5	Hydrogen (atomic H) intercalation in host metals, metallic hydrides working at RT are fully reversible.

## 2.7. Hydrogen Embrittlement [33], [34]

Hydrogen embrittlement (HE) also known as hydrogen-assisted cracking (HAC) and hydrogen-induced cracking (HIC), describes the embrittling of metal after being exposed to hydrogen. It is a complex process not completely understood yet because of the variety and complexity of mechanisms that can lead to it. The dynamics that have been proposed to explain embrittlement include the formation of brittle hydrides, the creation of voids that can lead to bubbles and pressure build-up within a material and enhanced decohesion or localised plasticity that assist in the propagation of cracks. Hydrogen embrittles a variety of substances including steel, aluminium (at high temperatures only), and

titanium. Austempered<sup>4</sup> iron is also susceptible, though austempered steel (and possibly other austempered metals) display increased resistance to hydrogen embrittlement.

The main thermo-physical parameters involved with this phenomenon are:

- Temperature: During hydrogen embrittlement, hydrogen is introduced to the surface of a metal and individual hydrogen atoms diffuse through the metal structure. The solubility of hydrogen increases at higher temperatures, so raising in temperature can increase the hydrogen diffusion. Moreover, If steel is exposed to hydrogen at high temperatures, hydrogen will diffuse into the alloy and combine with carbon to form tiny pockets of methane at internal surfaces that does not diffuse out of the metal and collects in the voids at high pressure and initiates cracks in the steel
- Concentration gradient: When assisted by a concentration gradient where there is significantly more hydrogen outside the metal than inside, hydrogen diffusion can occur even at lower temperatures.
- As the strength of steels increases, the susceptibility to hydrogen embrittlement increases (steels, above a hardness of HRC 32 may be susceptible to early hydrogen cracking).

It may be not permanent: after the hydrogen embrittlement, if the cracking doesn't occur, and there is no source of hydrogen, its atoms start re-diffusing from the stainless steel restoring the original metal ductility.

HE can be prevented through several methods centred on minimizing contacts between the metal and hydrogen. Another way of preventing this problem is through material selection. Certain metals or alloys are highly susceptible to this issue so choosing a material that is minimally affected while retaining the desired properties would also provide an optimal solution. Much research has been done to catalogue the compatibility of certain metals with hydrogen. In tensile tests carried out on several structural metals

---

<sup>4</sup> Austempering is heat treatment that is applied to ferrous metals, most notably steel and ductile iron, used to improve mechanical properties or reduce / eliminate distortion.

under high-pressure molecular hydrogen environment, it has been shown that austenitic stainless steels, aluminium (including alloys), copper (including alloys, e.g. beryllium copper) are not susceptible to hydrogen embrittlement along with a few other metals.

The main actions to prevent HE are:

- The steel used to manufacture any part must have very low levels of impurities such as phosphorous and sulphur;
- The hardness of the stainless steel should be low;
- The high percentage of Chromium and Molybdenum in stainless steel restricts hydrogen to diffuse.

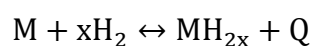
### 3. Hydrogen Storage in Metals and Alloys

A sustainable low-carbon society does not base its energy supply on further exploitation and consumption on fossil forms of carbon. The great potential of carbon-free renewable energy is strongly linked with storage. Among all technical feasible forms of storable energy (gravitational, electric, heat, chemical), the production of hydrogen and its reversible storage in metal hydrides have high promising potential. Research on hydrogen storage materials has attracted high interest over the last 40 years. Storing hydrogen in solids is one of the most promising solutions to the issue of safe, compact, and affordable hydrogen storage for its use as energy carrier. It could solve problems related to compressed gas storage since application of MH can provide very high hydrogen storage capacity per unit volume, increased safety due to the lower pressure of stored hydrogen and limited rate of hydrogen release in case of accidental leaks or even rupture of the containment, reliability and high purity of the supplied H<sub>2</sub>.

Hydrogen can be stored chemically in intermetallic alloys, or in complex hydrides. High volumetric capacity (80–160 [kg<sub>H<sub>2</sub></sub>/m<sup>3</sup>]) can be obtained using appropriate systems. The main drawback of hydrogen absorption in solids is its low weight capacity, which is negative for mobile applications. In the 70s, hydrogen absorption near ambient conditions was discovered for LaNi<sub>5</sub> and FeTi, opening the way to a new research field: the hydrogen storage in intermetallic compounds. The different families of intermetallic compounds are classified on the basis of their formula unit such as AB, AB<sub>2</sub>, AB<sub>5</sub>, AB<sub>3</sub>, A<sub>5</sub>B<sub>19</sub>, A<sub>6</sub>B<sub>23</sub> that are extensively explored in the section 3.3

#### 3.1. Thermodynamics

Many metals and alloys react reversibly with hydrogen to form metal hydrides according to the reaction:



Here, M is a metal or an intermetallic compound,  $MH_x$  is the respective hydride, x the ratio of hydrogen to metal and Q the heat of reaction. Since the entropy of the hydride is lowered in comparison to the metal and the gaseous hydrogen phases separated, the hydride formation is exothermic and the reverse reaction of hydrogen release accordingly endothermic. Therefore, the reaction can be read by both senses and its direction is determined by temperature, pressure and reactants concentration (PCT). Under precise values, the reaction reaches the equilibrium. For hydrogen storage purposes, storage density and reversibility at around ambient conditions are the most important properties; in addition, for economic and sustainability reasons abundant materials and low-cost processing are needed. The working temperature and pressure ranges on which focus are 1-10 [bar] and 10-100[°C] and, fortunately, most of intermetallic compounds integrated with PEM fuel cells stay in these operating regions.

The mechanism of  $H_2$  absorption consists in the following steps:

- Far from the metal surface, molecular hydrogen and two H atoms potential energies differ in the value of dissociation energy ( $E_{D_{H_2 \rightarrow 2H}} \cong 436$  [kJ/mol]). When a molecule arrives at around 1 molecular radius far from the metallic surface (0.2 [nm]), attractive Van der Waals forces act on it starting a physisorption process ( $\cong 10$  [kJ/mol]).
- Then, the molecule must overwhelm the dissociation activation and the formation of the metallic bond energetic barriers. The process is shown in figure 20, in which the intersection between physisorption and chemisorption curves points out the passage between the two phases. It can be in the positive or negative region, indicating if the process needs an activation energy or not. Molecular  $H_2$  dissociates prior to dissolution in the metal.

- After dissociation on the metal surface, the H atoms have to diffuse into the bulk to form a M-H solid solution commonly referred as  $\alpha$ -phase. In conventional room temperature metals / metal hydrides, hydrogen occupies interstitial sites - tetrahedral or octahedral - in the metal host lattice. The chemisorption energy is typically in the range of  $E_{\text{Chem}} \approx 20 - 150 \text{ [kJ/mol}_{\text{H}_2}]$  and thus significantly higher than the respective energy for physisorption.

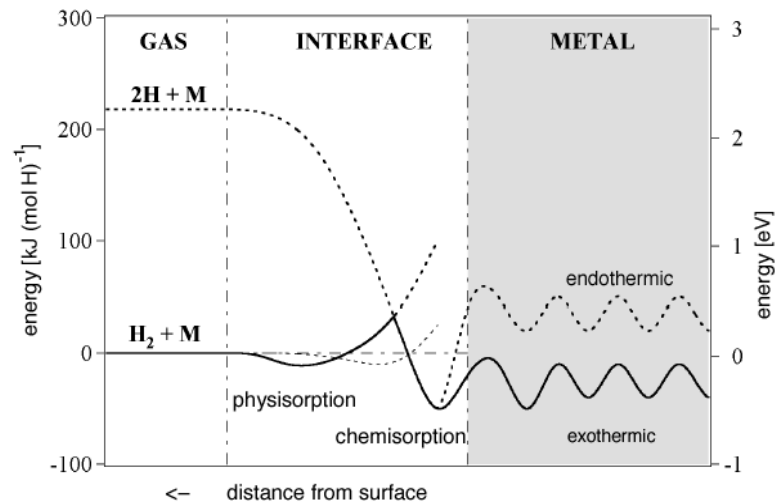


Figure 24 Schematic of potential energy curves of hydrogen in molecular and atomic form approaching a metal. [36]. The usual path is characterized by the continuous line with an highly exothermic absorption

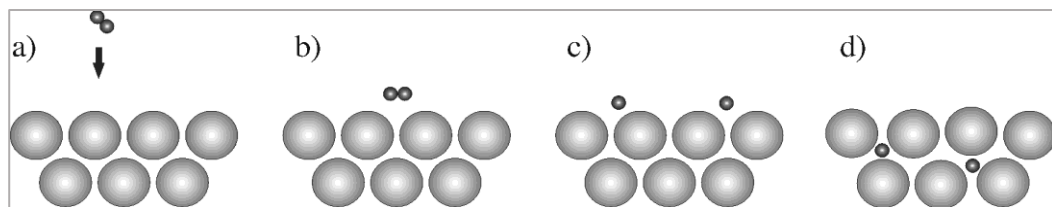


Figure 24 Reaction of a H<sub>2</sub> molecule with a solid storage material [36]

- H<sub>2</sub> molecule approaching the metal surface;
- Interaction of the H<sub>2</sub> molecule by Van der Waals forces (physisorbed state);
- Hydrogen molecules dissociates.;
- Occupation of subsurface sites and diffusion into bulk lattice sites

Transition metals can react directly with hydrogen gas (thermal formation). At a low partial pressure of hydrogen and small hydrogen concentrations in the metal, a solid solution of atomic hydrogen can be observed in the original metal lattice ( $\alpha$ -phase) with a random diffusion in the metal lattice. H-atoms do not take a fixed and ordered positions and are usually quite mobile, even at room temperature. The host lattice expands with increasing hydrogen concentration in the order of  $3\text{ \AA}$  per H-atom. For small hydrogen concentrations in the metal, this is described by Sievert's law: it states that the solubility

of a diatomic gas in metal is proportional to the square root of the partial pressure of the gas in thermodynamic equilibrium.

$$\frac{c_H^2}{p_{H_2}} \cong K \quad (4)$$

The concentration of the dissolved H atoms into the metal is proportional to the square-root of the hydrogen partial pressure (considering an ideal gas behaviour) on the metal surface with respect to the Sievert's constant  $K=K(T)$ .

$$c_H = \frac{H}{M} = \sqrt{Kp_{H_2}} \quad (5)$$

At a higher partial pressure and higher hydrogen concentrations in the metal, the  $\alpha$ -phase becomes saturated with hydrogen and starts nucleating into a hydride phase  $\beta$  at nearly constant pressure (plateau pressure), with higher hydrogen content and an own structure. Accompanied by the transition from the solid-solution to the hydride phase, a volume expansion of the metal lattice of 8–30% can occur which can lead to pulverization of the material. This expansion can be anisotropic, depending on the initial structure and the location of the interstitial sites. The right end of the plateau represents the 100 %  $\beta$ -phase.

$$\frac{a_{MH_x}}{f_{H_2, Gas}^{x/2} a_M} = k_{MH_x} \quad (5)$$

$$\frac{a_{MH_x}}{a_M} \cong \left( \frac{p_{H_2}}{p^0} \right)^{\frac{x}{2}} k_{MH_x} \quad (6)$$

$p_{H_2}$  is characterized by an equilibrium value in which  $\alpha$ -phase and  $\beta$ -phase coexist (that is,  $a_M = a_{MH_x} = 1$ ) but with different hydrogen concentrations ( $c_{H,M} \neq c_{H,MH_x}$ ), called equilibrium pressure. Its value depends on the Gibbs free formation enthalpy of the hydride ( $\Delta_f G_{MH_x}^0$ ) and thus on temperature T:

$$\left(\frac{p_{H_2,eq}}{p^0}\right) = \frac{1}{k_{MH_x}} = e^{-\frac{\Delta_f G_{MH_x}^0}{RT}} \quad (7)$$

$$\left(\frac{\delta \ln k_{MH_x}}{\delta T}\right)_p = \frac{\Delta_f H_{MH_x}^0}{RT^2} \quad (8)$$

In the case of a negative formation enthalpy ( $\Delta_f H_{MH_x}^0$ ), the equilibrium constant ( $k_{MH_x}$ ) decreases with increasing temperature, resulting in an increased equilibrium pressure,  $p_{H_2,eq}$ . R is the universal constant of gases and T is the hydride absolute temperature.

Absorption and desorption processes and the relative thermodynamic aspects are described in semi-logarithmic Pressure-Composition-Temperature (PCT) diagrams. Composition can be listed in either weight percent, atomic H/M ratio or volumetric density. In PCT diagrams the continuous lines are isotherms, experimentally determined, and highlight the H<sub>2</sub> pressure trend as function of the composition. The equilibrium conditions are also shown, in specific points in the middle of the plateaus, under the “bell”. Here, as previously explained,  $\alpha$ -phase and  $\beta$ -phase coexist and the equilibrium pressure is kept constant forming a plateau, in ideal conditions. When instead the two phases don't coexist, the pressure increases rapidly with the H-content. Here, the principal advantage of metal hydrides usage: the property of absorbing/desorbing large amounts of hydrogen at a constant pressure, that is, the pressure does not increase with the amount of hydrogen absorbed as long as the phase transition takes place. The plateau length represents the hydrogen quantity that can be reversibly stored in the metal, so, the lower the temperature the higher this amount is.

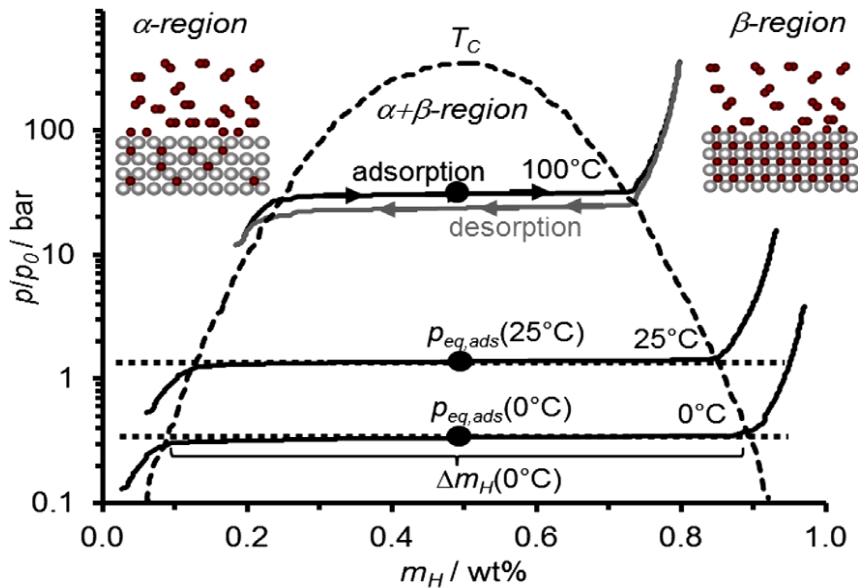


Figure 25 Pressure isotherms for the hydrogen incorporation of a typical interstitial transition metal hydride ( $\text{LaNi}_5\text{H}_6$  --  $\delta$ ) at different temperatures, and the different phase-regions. [35]

At a hydrogen partial pressure ( $p_{\text{H}_2}$ ) above the equilibrium value ( $p_{\text{H}_2,\text{eq}}$ ) the  $\alpha$ -phase is completely transferred to the  $\beta$ -phase and additional hydrogen is dissolved as a solid solution in the  $\beta$ -phase. As the temperature increases, so too does the solubility of hydrogen in the  $\alpha$ -phase and the  $\beta$ -phase, this results in a narrowing of the equilibrium plateaus. Finally, the two-phase region disappears above a critical temperature  $T_c$ , that is, the passage from one phase to the other is continuous.

Moreover, the degree of freedom, following the Gibbs' phase rule, is  $f = n - r + 2 = 2 - 3 + 2 = 1$ , that is the system has one degree of freedom, following an isotherm process. Changing the hydrogen partial pressure upstream, only  $\alpha$  and  $\beta$  quantities change, while  $f = 2$  outside.

Many compounds have a variable stoichiometry, so that the  $x$  value (in  $\text{MH}_x$ ) can vary. For instance, there are two main structures for  $\text{TiFe}$ , with different properties and plateau pressures, that are  $\text{TiFeH}_2$  and  $\text{TiFeH}_{1.7}$ . So, an alloy can show multiple plateaus with more than one distinct hydride phase formation. Sandrock [] always considers only the first plateau.

- To have a hydrogen absorption, its partial pressure (or supply pressure) must be higher than the equilibrium pressure, so to move toward right in the PCT diagram. The

difference  $P_{app} - P_{eq}$  is the main driving force for mass transfer. Moreover, if the thermal energy is not managed effectively inside the reactor, and the metal hydride bed temperature increases, even the equilibrium pressure increases. This brings to a deterioration of performances and vice versa if the hydride bed is cooled down;

- In the opposite way, a desorption process needs an underpressurized ambient and a contemporary heat release to reaction bed. The higher the temperature, the higher the released hydrogen flow rate.

The equilibrium pressure in the plateau directly depends by temperature, enthalpy and entropy variations through the Van't Hoff equation, which can be found starting from equation 7:

$$\ln(p_{eq}) = \frac{\Delta H}{RT} - \frac{\Delta S}{R} \quad (9)$$

This equation explains the relation between pressure, hydrogen concentration and temperature, that is a characteristic property of the metal hydride material. It has been experimentally demonstrated that the entropy variation depends almost entirely by the hydrogen dissociation value (from gaseous to solid form), equal to  $-130.9$  [J/mol K] at  $25$  [°C] and  $1$  [bar] (negative in case of absorption). This value is representative of the stability of the metallic bond between hosting metal and hydrogen. Hence the formation enthalpy can be estimated from the equilibrium temperature at the same pressure, that depends on the material involved:

$$\Delta_f H_{MH_x}^0(1 \text{ bar}) = \Delta_f S_{MH_x}^0 \cdot T_{eq}(1 \text{ bar}) \quad (10)$$

From the Van't Hoff relation, the homonym plot can be drawn:

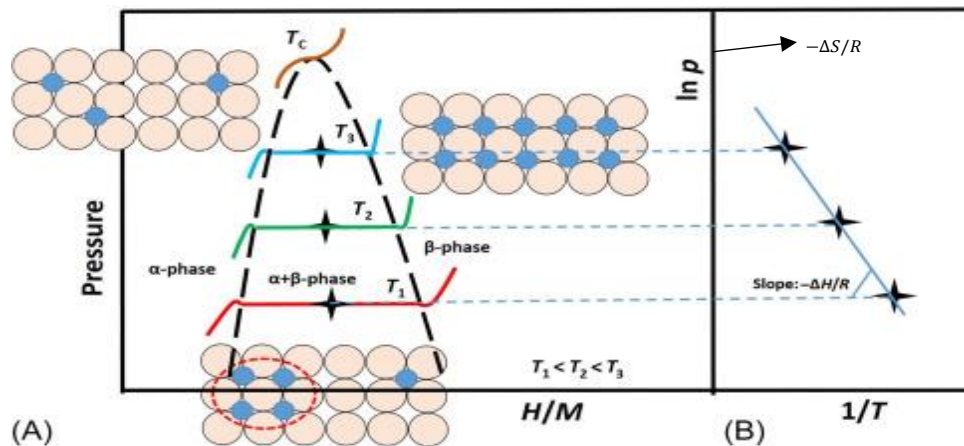


Figure 27 From the PCT diagram to the Van't Hoff plot for an ideal case

This diagram is very important because it can compare different hydrides from a thermal stability point of view; the straight line indicates the pressure and temperature values at which the hydride must work in order to have good kinetic: the lower bound represents lower temperatures (higher  $1/T$ ), below which the hydrogenation-dehydrogenation processes result too slow, while the upper bound is given by a temperature too high to have a good stability in the process/hydride. The line slope depends by the enthalpy variation and is negative during the absorption.

Several empirical models allow the estimation of the stability and concentration of hydrogen in an intermetallic hydride. The maximum amount of hydrogen in the hydride phase is given by the number of interstitial sites in the intermetallic compound. More in general the Miedema's rule on reversed stability states that the more stable an intermetallic compound, the less stable the corresponding hydride and the other way round. This model is based on the fact that hydrogen can only participate in a bond with a neighbouring metal atom if the bonds between metal atoms are at least partially broken. The stability of metal hydrides is presented in the form of Van't Hoff plots: the most stable ones have high, negative formation enthalpies, so a higher slope.

Practical hydrating metals do not show perfectly flat plateaux or zero hysteresis. The reversible capacity,  $\Delta(H/M)_r$ , is conservatively defined as the plateau width, which can be considerably less than the maximum capacity,  $\Delta(H/M)_{max}$ . In practice, depending on

available pressure and temperature ranges, engineering capacity is usually somewhere between the two values. The principal hydride properties are:

- **Activation:** it is the hydrating procedure of a metal for the first time that brings it up to maximum H-capacity and hydrating/dehydrating kinetics. When hydrogen is first applied to a hydrating material, the reaction is usually not immediate: the ease of initial hydrogen penetration depends on surface structures and barriers, such as catalytic species and oxide films on the metal surface. These are formed after a prior exposure to air and have to be dissociated in the first cycles. In most of the cases, the activation process consists in two parts: the first one is the penetration of a small amount of H<sub>2</sub> through the natural oxide layer with the begin of nucleation of the  $\beta$ -phase, with the incubation time that ranges from seconds to days. The second step consists in the fragmentation of large grains into highly cracked smaller particles due to the expanding hydride phase, which increases the surface area for hydrogen absorption and in some way cleans the area, resulting in improved inlet and outlet of hydrogen in interstices.
- **Decrepitation:** it means the self-pulverization of large particles into powder, resulting from the volumetric expansion (15 – 30 %) that follows to H<sub>2</sub> absorption and the brittle nature of hydrating alloys. This phenomenon occurs primarily during the activation process, as mentioned above. The morphology of decrepitated powder (~10 [ $\mu$ m]) affects the heat transfer and also the tendency of powder migration into undesirable places like valve seats. This effect can be easily limited with proper gas filters with pore sizes of ~ 1 [ $\mu$ m]. The fine powder can also pack in the container, resulting in local high mechanical stresses which can even bring to the tank rupture. This aspect is discussed in detail in the section 3.6;
- **Hysteresis:** It is a phenomenon in which there are 2 different pressures for absorption and desorption, respectively upper and lower than the ideal one which must be considered instead of the equilibrium pressure calculated from the Van't Hoff equation. There are different models that try to explain physically the related causes and the most correct equation to use is the following:

$$\text{Hysteresis} = \frac{1}{2} R_g T \ln \left( \frac{P_{D_{eq}}}{P_{A_{eq}}} \right) - RT \ln \left( \frac{P_D}{P_A} \right) \quad (11)$$

With  $P_{D_{eq}}$  &  $P_{A_{eq}}$  represent the mid plateau desorption and absorption pressures.

Hysteresis is a measure of energy loss during an absorption/desorption cycle that has its origin in the strains associated with the metal from internal defects like dislocations and stacking faults. This inefficiency decreases with increasing temperature, thanks to a relaxation process and has a value which depends by the considered alloy. Generally speaking, it goes from 0 to more than 2 and it is fundamental to evaluate, since the operating pressures during absorption and desorption depend by the new values of pressures found considering this phenomenon:

$$P_{\text{supply}} > P_{\text{ABS}} , P_{\text{delivery}} < P_{\text{DES}}$$

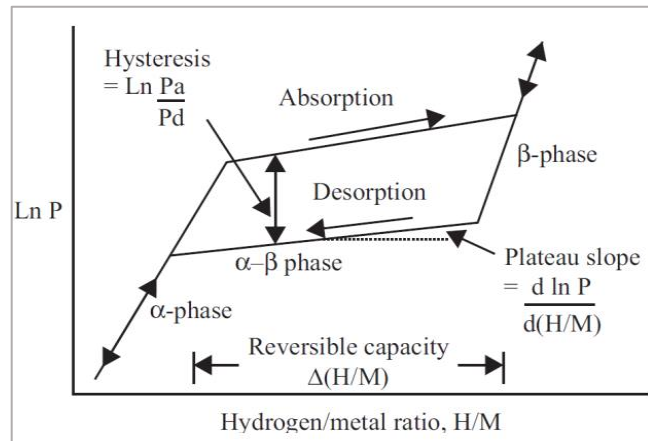


Figure 28 Simplified representation of a hysteresis loop in a PCT diagram. A simplified equation of h. evaluation is also written on the top left and will be used for the case study. [38]

- **Plateau slope:** Real materials rarely have a flat plateau, so pressure during absorption and desorption doesn't keep constant but increases with the concentration. So, Van't Hoff plots are not 100% precise, but they preserve a good and reliable approximation.

$$S_f = \frac{d(\ln p_{eq})}{d(H/M)} \quad (12)$$

This can be a function of the metallurgy, since hydrides of pure elements below the critical temperature tend to exhibit relatively flat plateaus, due to the energetic

equivalence of interstitial sites. Alloys of two metals have randomly variable environments around each interstitial site, resulting in a variable local affinities for, hydrogen atoms. The slope tends to increase as result, even far from the critical temperature. Metallurgical segregation often occurs during preparation, especially with multicomponent intermetallics, so that annealing treatments are mandatory after the synthesis of intermetallic compounds, that must be produced with elements as pure as possible. This leads to an increase of material cost even higher than the 100% of the raw material today. This aspect will be discussed more in detail.

- **Gaseous impurity resistance:** Sandrock judges this as the second most important hydride property next to PCT ones. Trace of contaminants, such as  $\text{H}_2\text{O}$ ,  $\text{CO}$ ,  $\text{CO}_2$  can react with the hydrating alloy particle leading to decreased capacity and/or kinetics. Therefore the system insulation from external environment must be guaranteed in a very effective way, with a consequent increase of investment costs. There are four classic types of alloy-impurity interactions: poisoning, retardation, reaction.
  - Poisoning: results in severe and rapid H-capacity loss with cycling, due to the formation of a monolayer surface coverage that deactivates the dissociative chemisorption of hydrogen molecules. Typical poisons include  $\text{CO}$  and sulphur-containing gases. Kinetic remains untouched in the remaining unpoisoned material. Poisoned alloy can be regenerated with difficulty by heating and flushing with pure  $\text{H}_2$ .
  - Retardation: results in losses of absorption/desorption reaction rates without loss in H-capacity. Typical retardant compounds are  $\text{NH}_3$ ,  $\text{CO}_2$ ,  $\text{O}_2$  or  $\text{CO}$  (above  $100\text{ }^\circ\text{C}$ ). This effect can be solved by simply switching back to high purity  $\text{H}_2$ .
  - Reaction: results in a bulk corrosion of the alloy with irreversible capacity loss. The main reactant that brings to this damage is oxygen in long-term exposures.
- **Cyclic stability:** One important parameter to consider for hydrogen storage applications is the ability of the material to conserve its properties after extensive

usage, due to loss of crystallinity and disproportionation of the intermetallic. These effects are an intrinsic and lead to isotherm distortion and to the loss of H-capacity even with absolutely pure H<sub>2</sub> feeding. Disproportionation is a behavioural discrepancy between absorption and desorption in which part of the absorbed hydrogen is not successively released and stays inside metal interstices, due to anomalous strong metal bonding between H-M. It is accelerated with increasing temperature, so it can definitively be neglected in the case study in chapter 4, that will be characterized by only 5 deep cycles in an entire year of operation.

- **Safety:** Let's consider a severe tank rupture during the desorption process: only hydrogen in gaseous phase will be instantly released in the environment, since the desorption is immediately stopped. In fact, during normal operation, the pressure inside the reaction bed is slightly depressurized to ~0.5 [bar] and now the powder is exposed to the ambient pressure, decreasing the most important driving force ( $\Delta p$ ); moreover, the heat supply ceases suddenly, so, as conclusion, hydrogen explosion is very unlikely. Safety problem usually centres around pyrophoricity (the tendency for a hydride powder to burn when suddenly exposed to air) and toxicity, resulting from an accidental ingestion or inhalation of powders in case of accident.
- **Alloy cost:** It is one of the most important issues for large scale applications and, currently, is one of the causes that doesn't enable a commercialization of this technology. It is influenced by several factors including raw material cost, melting and annealing costs, metallurgical complexities and profit. Metallurgy is very important in this field (crystal structure and microstructure factors) to achieve the optimum hydrating properties discussed above. The overall cost can easily raise by more than 100% of raw material cost.
- **Kinetics:** It is successively elaborated, but generally, many room temperature hydrides have excellent intrinsic kinetics. Moreover, for stationary applications, it is somewhat less important because of relatively slow cycling of storage tanks.

For storage applications, a hydrogen storage alloy is needed to be characterized by low cost, easy activation, good resistance to gas impurities, low temperature and pressure operations, thanks to low  $|\Delta H_F|$ , that is, weak H-M bonds.

The theoretical maximum volumetric hydrogen density in a metal hydride, assuming a closed packing, is 254 [kg/m<sup>3</sup>], which is 3.6 times the density of liquid hydrogen. The maximum hydrogen capacity ever recorded is 150 [kg/m<sup>3</sup>] in Mg<sub>2</sub>FeH<sub>6</sub> and Al(BH<sub>4</sub>)<sub>3</sub>. It is strongly related to the temperature and the specific surface areas of the chosen materials.

### 3.2. Kinetics

Thermodynamics can give only information related on the driving force which control on the general transformation, but kinetic is fundamental in the same way since it studies the transformation velocity; fast absorption and desorption processes are important requirements (more relevant in automotive applications). It indicates the reactant concentration variation in the unit time, which is a complex process that puts together a gas motion (whose properties change in time) in a porous media, heat and mass transfer.

When an atom in metastable equilibrium, with a free energy  $G_I$ , goes in a new state with a lower value  $G_F$ , the driving force is  $\Delta G = G_F - G_I$ . Often, the pursue of the minimum free energy requires an intermediate state passage, characterized by a higher free energy value, called activation state. In the last decades several mathematical models have been done to describe the hydride absorption-desorption kinetics. The most used and recognised are the models used by A. Jemni and S.B. Nasrallah:

$$\dot{V}_{ABS} = C_a \cdot \exp\left(-\frac{E_a}{RT}\right) \cdot \ln\left(\frac{p}{p_{eq}}\right) \cdot (\rho_{ss} - \rho_s) \quad (13)$$

$$\dot{V}_{DES} = C_d \cdot \exp\left(-\frac{E_d}{RT}\right) \cdot \frac{p_{eq} - p}{p_{eq}} \cdot \rho_s \quad (14)$$

Where  $\dot{V}$  are the absorption and desorption volumetric flow rate,  $C_a$  &  $C_d$  [ $s^{-1}$ ] are fitting parameters that can be obtained experimentally,  $E_a$  &  $E_d$  are the absorption and desorption activation energies  $\rho_s$  &  $\rho_{ss}$  are the hydride density in the current and saturated conditions. One problem relies on the determination of the hydride density, that increases during the absorption and depends by temperature, but there is no model today able to describe its behaviour.

- Absorption: the equation can be approximately considered as temperature dependent, only, if hydrogen pressure is kept constant. It is characterized by three main parts: the first one is an Arrhenius-type equation, so temperature dependent (the reaction is encouraged by a temperature increase); the second is a ratio between inlet and equilibrium pressure, so the higher the supply pressure the higher the  $H_2$  absorption rate, which increase exponentially; finally, the third part takes into account the metal / alloy fraction that has been hydrogenated: hydrides near to the saturation condition tend to absorb hydrogen slower and slower until nullify the process in the end (saturated hydride). If the temperature increases, the first member only goes; since the second member varies more quickly than the first one with temperature the time necessary to fill a metal hydride tank decreases with a temperature decrease
- Desorption: The equation is similar to the previous one in the first part. The pressure part is not logarithmic anymore and its contribution is always negative with respect to the volumetric flow rate, except when operating in vacuum conditions. Finally, the flow rate is directly proportional to the hydride density and so decreases during the process.

### 3.3. Ternary hydrides classification [38]

Ternary Interstitial Hydrides Ternary interstitial hydrides can be classified as  $AB_5$ ,  $AB_2$ ,  $AB$ ,  $AB_3$ ,  $A_2B$  type compounds with a metal A, which forms a stable metal hydride, which are strongly exothermic hydrogen absorbers (e.g. Mg, Ti, Zr, La) and another transition metal B that are either endothermic or very weakly exothermic hydrogen absorbers (e.g. Ni, Fe, Co, Mn).



two different plateaus and a significant hysteresis ( $\sim 0.6$ ). The most suitable compounds for low temperature fuel cells are TiFe itself with Mn- and Ni- substituted versions on the B-side, that facilitate the activation process and partially solve the problems related to low gaseous impurity resistance. They show good volumetric and gravimetric reversible H-capacities, competitive with the best AB<sub>5</sub> and AB<sub>2</sub>.

Their favourable PCT properties and low costs are counterbalanced by other problems that affects TiFe-type alloys, which have greatly reduced their commercialization. TiFe cannot be activated at room temperature and must be heated to 300 – 400 [°C] at 30 – 40 [bar] before hydrogen begins to penetrate the passive surface layer in the first stage of activation. This process can take 200 [h] to fully activate since TiFe has a significant fracture strength. A small starting particle size helps to speed up the activation process (e.g. ball milling). The activation process is different from AB<sub>2</sub> and AB<sub>5</sub>, since they don't pulverize as much, but the internally highly cracked particles tend to develop a higher surface area (0.5 m<sup>2</sup>/g vs 0.2 m<sup>2</sup>/g of LaNi<sub>5</sub>). Kinetics is instead slower compared to others and resistance to gaseous impurities is lower, making these compounds more fragile to treat in reality, with a consequent improvement of investment costs. Finally for all TiFe-type alloys the cyclic stability is excellent if only the lower plateau is used (no capacity

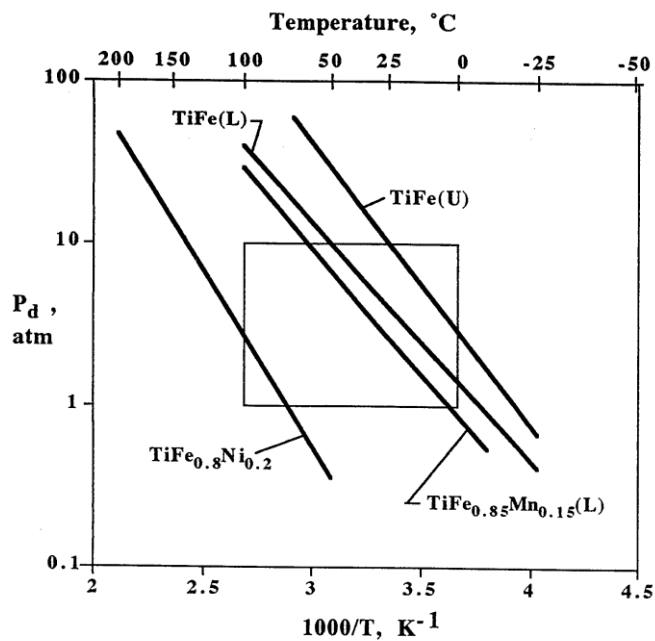


Figure 31 Different AB compounds in the Van't Hoff plot, with emphasis on pressure and temperature ranges we are interested into for PEMFC coupling. "U" means upper plateau, "L" lower plateau

losses resulted in 30000 cycles) and these alloys are the one characterize by the maximum safety since they are not pyrophoric and do not contain toxic elements.

### 3.3.2. AB<sub>2</sub>

The first studies for hydrogen storage in Laves phases were performed in 1967 and the AB<sub>2</sub> compounds have been extensively studied for their hydrogenation properties as their capacity to absorb large amounts of hydrogen up to 2 [H/M] (A= Sc, Ti, Y, Zr, Nb, Hf, Rare Earth and B=V, Cr, Mn, Fe, Co, Ni). These compounds have good hydrogen storage capacity, very high versatility, fast kinetic, long cycling life (good disproportionation resistance), and low cost (compared to AB<sub>5</sub>). Almost all the practical compounds come from the Laves phases with 2 main structures: C14, C15, both with tetrahedral interstices.

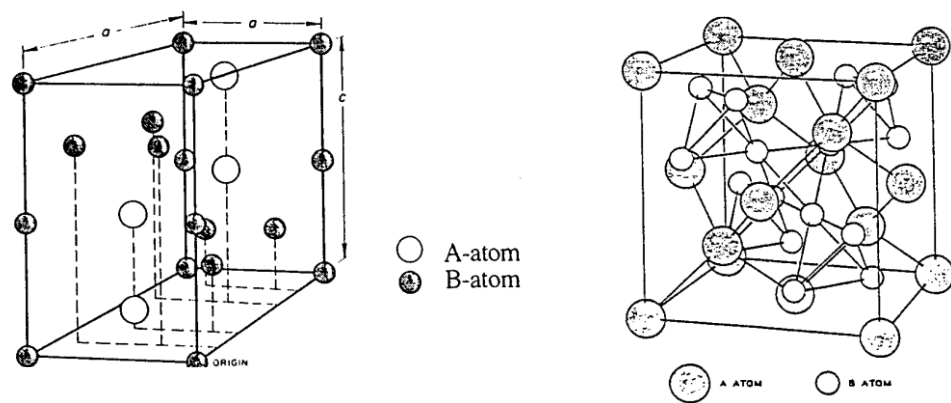


Figure 32 Structures of the C14 (hexagonal) and C15 (cubic) Laves phase

A big number of different compounds have been created and tested with a large number of possible choices, as it can be found in [38]

Unfortunately AB<sub>2</sub> are characterized by narrower plateaus compared to AB<sub>5</sub>, but they offer a cost significantly lower. Most of Laves phase intermetallic compounds (which were not exposed to air for a long time) activate at room temperature with sufficient H<sub>2</sub> pressure and incubation times higher than AB<sub>5</sub>, especially if they are characterized by high Ti, Cr, V content. To facilitate the process, the material may be heated up to a few hundred °C under H<sub>2</sub> atmosphere.

The decrepitation is a common effect in the activation process for these compound, especially for high Mn contents, which guarantees an extremely fine powder, with particle size of less than  $1\mu\text{m}$ , which would cause additional problems with local mechanical stresses in the storage tank and possible entrainments of fine MH particles out of the reactor. There are no problems regarding the kinetic properties but they are quite more sensitive to gaseous impurities than  $\text{AB}_5$ . The effect of  $\text{CO}$  is comparable with  $\text{AB}_5$ , but effects of  $\text{O}_2$  and  $\text{H}_2\text{O}$  are worse. There are less experimental data than  $\text{AB}_5$  on cyclic stability, but it seems to be good for compounds based on  $(\text{Ti,Zr})(\text{Mn,Cr})_2$  with an average loss of H-capacity due to disproportionation of  $\sim 5\%$  during 2000 A/D cycles with high purity  $\text{H}_2$  feeding. They are more problematic from the safety point of view, exhibiting pyrophoric behaviours, especially for alloys rich in Zr and Mn; they are not considered toxic, but the right precautions should be taken in any case.

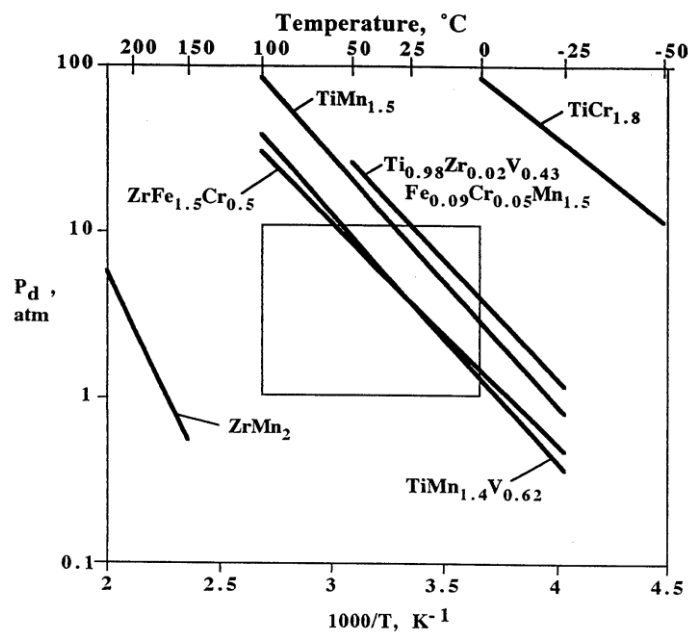


Figure 33 Different  $\text{AB}_2$  compounds in the Van't Hoff plot, with emphasis on pressure and temperature ranges we are interested into for PEMFC coupling

### 3.3.3. $\text{AB}_5$

$\text{LaNi}_5$  and its substituted derivatives represent the most studied and best-known hydrogen storage compound family. This is not only because of the simplicity of the metallurgy (they can be prepared in tonnage quantities by conventional metallurgical techniques such as vacuum induction melting); they are surely the most versatile (owing their ability to

accept wide substitution ranges which allow to tune the thermodynamic properties) and commercially important family of reversible MH. Almost all the AB<sub>5</sub> intermetallic compounds crystallize with the hexagonal D<sub>2</sub> structure (derivative to the C14 laves phase with a variety of tetrahedral and octahedral interstices).

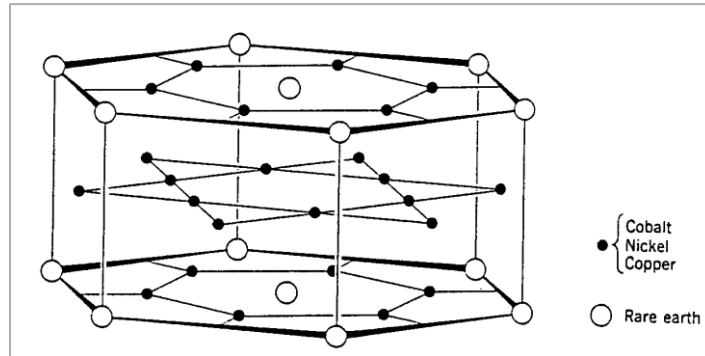


Figure 34 The D<sub>12</sub> AB<sub>5</sub> structure

They were accidentally discovered at the Philips Eindhoven Labs in 1969 and have found to have unequalled activation properties at room temperature, kinetics, and reactivity. The main drawbacks of these materials are the limited weight (reversible) capacity that never exceed 1.3 wt.%, with the high material cost compared to AB and AB<sub>2</sub>, due to the presence of rare earth materials. Activation of the AB<sub>5</sub> compounds is generally easy: freshly crushed alloy will usually activate at room temperature without prior heating, in a time depending by the H<sub>2</sub> applied pressure that must be higher than the absorption plateau, which can go from seconds to several hours. This time decreases if the powder has not been exposed to air for a long time before the activation. These compounds quickly decrepitate into powder with particle sizes on the order of a few tens of μm, with surface areas on the order of 0.2 m<sup>2</sup>/g (not including internal cracks). Their kinetic is very high if the powder heat transfer is optimum and continuous during operations. Gaseous impurity effects are quite good compared to other two families described. CO gives an immediate and severe damage proportional to his content, constituting only a monolayer able to deactivate hydrogen absorption, forming Ni-carbonyl bonds; its effects become weaker with increasing in temperature, since the bond Ni-CO becomes unstable and carbon is desorbed in form of CH<sub>4</sub>. O<sub>2</sub> and H<sub>2</sub>O results in a first retardation effect and then a long-term reaction effect, as anticipated in 3.3. The partial substitution of Al on B side results in increased resistance to these effects. AB<sub>5</sub> alloys are also subjected to

disproportionation with a dramatically improved resistance resulting with a partial B-side substitution with Al or Sn. They unfortunately usually bring to a decreased H-capacity, especially in mixed mismatch metals on the A-side. Finally, these materials are pyrophoric when exposed suddenly to air and composed by toxic elements. Particular safety measurements need to be taken as consequence, but, under normal operations, they are safe to use.

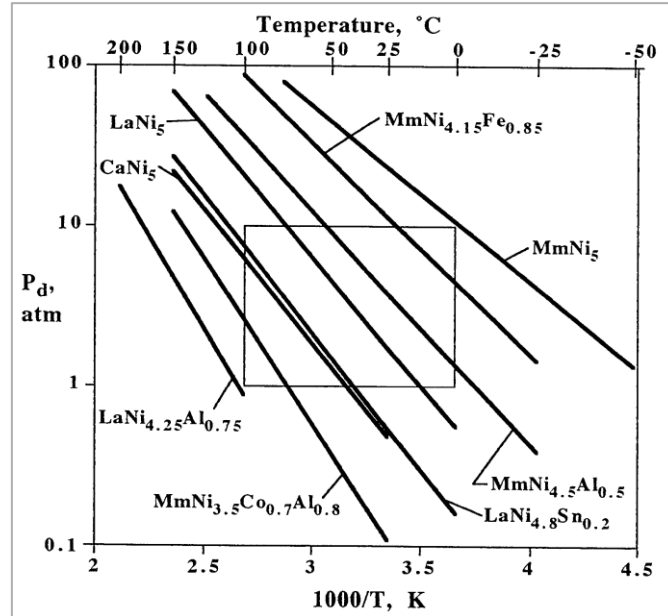


Figure 35 Different AB<sub>5</sub> compounds in the Van't Hoff plot, with emphasis on pressure and temperature ranges we are interested into for PEMFC coupling

### 3.3.4. Others

In addition to the intermetallic families discussed above, several others have been shown capable of reversible hydrating/dehydrating reactions. Examples include AB<sub>3</sub>, A<sub>2</sub>B<sub>7</sub>, A<sub>6</sub>B<sub>23</sub>, A<sub>2</sub>B<sub>17</sub>, A<sub>3</sub>B and others. Most structures involve long-period AB<sub>5</sub> and AB<sub>2</sub> stacking sequences and are thus crystallographically related to these two classic families. Although none of these have attained commercial levels of interest, AB<sub>3</sub> and A<sub>2</sub>B<sub>7</sub> phases do have PCT properties, which are in the desired ranges.

### 3.4. Today's best options

Thousands of alloys have been tested and studied over the last 40 years and the best ones in terms of thermodynamic, properties, cost, cycling and experience have been selected among the MH families previously focused.

#### 3.4.1. $\text{TiFe}_{0.85}\text{Mn}_{0.15}$ – AB [49]

Among hydrogen storage materials, TiFe has the advantages of a large absorption capacity, good kinetics for hydrogen absorption and desorption after activation, suitable equilibrium pressures (5–10 [bar]) and low cost. It has the great disadvantage of not being easily activated at room temperature due to the formation of titanium oxide layer on the metal surface, so both high-pressure and high temperature are required to achieve a reproducible absorption/desorption of the maximum amount of hydrogen in the compound. PCT curves on absorption and desorption show a large hysteresis effect that has been suggested related to the apparent existence of two  $\beta$  phases with different hydrogen content ( $\text{TiFeH}$ ,  $\text{TiFeH}_{1.4}$ ). It has been demonstrated that these effects depend on the sample history and that an annealing treatment ( $\sim 800$  [°C] for 80 [h]) subsequent to the activation (400 [°C], 50 [bar]) releases lattice strain induced by hydrogen absorption. Many activation methods have been investigated such as ball-milling, ion implantation, high-pressure torsion, cold rolling, Pd doping, to ease the activation but they decrease the hydrogen storage capacity.

A common method to modify the hydrogen sorption properties of a hydride is the insertion of substituting elements. For this compound, V, Mn or/and other transition metals are widely used to partially substitute Fe. For example, when a small amount of Mn is substituted for Fe, activation is promoted and the resistance to contamination by impure gases is increased. It has been shown that these metal substitutions modify the surface properties of TiFe and favour the formation of secondary phases.  $\text{TiFe}_{0.85}\text{Mn}_{0.15}$  in particular, has proven to be more attractive owing to the lower cost of Mn, the easier activation (simply by crushing the material into a powder), the reduced

desorption equilibrium plateau pressure at ambient temperature (from 4.1 to 2.6 [bar] at 25 [°C]) and the slightly hysteresis reduction. An increased stability is given by the higher value of the reaction enthalpy compared to TiFe, 29.5 vs 28.1 [kJ/mol].

Many uncertainties are still present regarding the behaviour of different  $\text{TiFe}_{1-x}\text{Mn}_x$  compounds and recently, especially after the big earthquake in Japan in 2011, stationary energy storage using hydrogen has attracted much attention again. TiFe is one of the ideal materials for energy storage because of low cost and ambient working temperature. Research on activation of TiFe has been re-started.

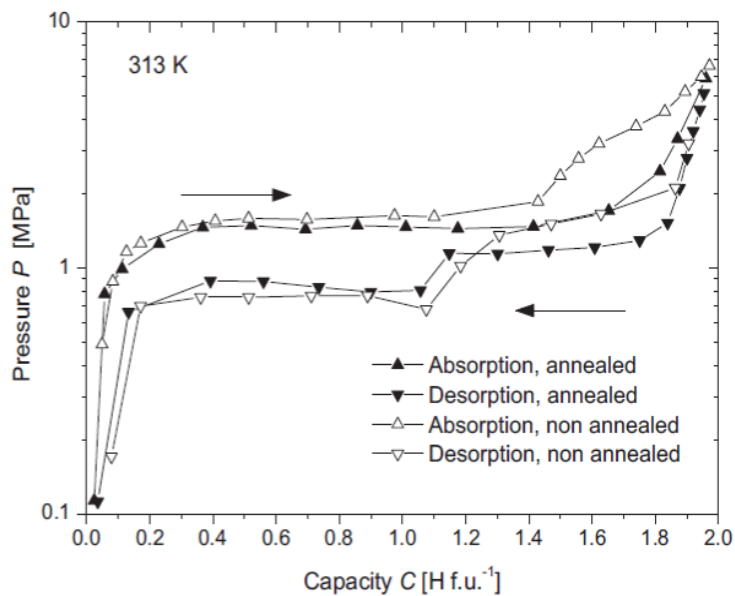


Figure 36 Pressure-composition curves at 313 K of TiFe nonannealed (empty symbols) and TiFe annealed at 1073 K (full symbols)

### 3.4.2. $\text{TiMn}_{1.5} - \text{AB}_2$

$\text{TiMn}_{2-x}$  compounds have interesting hydriding properties for applications, like good kinetic, long-term hydrogen storage capacity, and good resistance to impurities. The  $\text{TiMn}_{1.5}$  is the only intermetallic compound with suitable thermodynamic properties for a fuel cell coupling, but specific data on the literature are not easy to find. Basing on Sandrock comments [33] and on data present on its report, a hypothetical adoption has been considered in chapter 4, but it will be the one with largest uncertainties among the other selected materials.

### 3.4.3. $\text{LaNi}_{4.8}\text{Sn}_{0.2} - \text{AB}_5$ [50]

It is the most studied compound for its hydrogenation properties. It absorbs about 1.0 H/M ( $\text{LaNi}_5\text{H}_6$ ) and has the largest hydrogenation capacity compared to other  $\text{AB}_5$  near atmospheric pressure which makes it the base compound for hydrogen storage applications. The splendid quality of the  $\text{LaNi}_5$  that has been responsible for the early interest in this compound, is to have its plateau pressure very close to room pressure at room temperature offering, prior to any modification, the possibility of a simple reversible storage of hydrogen. No other intermetallic compound offers at the same time high hydrogen capacity, formation and decomposition close to room temperature and pressure and high kinetics, reactivity, and reversibility.  $\text{LaNi}_5$  melts congruently and thus is easily produced from laboratory scale up to industry scale by melting. The easy activation (three complete cycles at 20 [bar] for 30 minutes) of  $\text{AB}_5$  compounds was successfully explained by spontaneous surface segregation with selective oxidation of the rare earth La and formation of metallic Ni precipitates, which catalyse the hydrogen dissociation–recombination reaction. Figure 20 shows the hydrogen storage capacity of this compound as a function of absorption-desorption cycles.  $\text{LaNi}_5$  is indeed very bad in conserving the storage capacity along cycling. Fortunately, substitution by certain elements (like Ge and Sn) allows to considerably improve the cycling behaviour. Any substitution provokes a reduction of the capacity in an amount approximately proportional to the quantity of the substituting element, whose rate depends on the element itself.

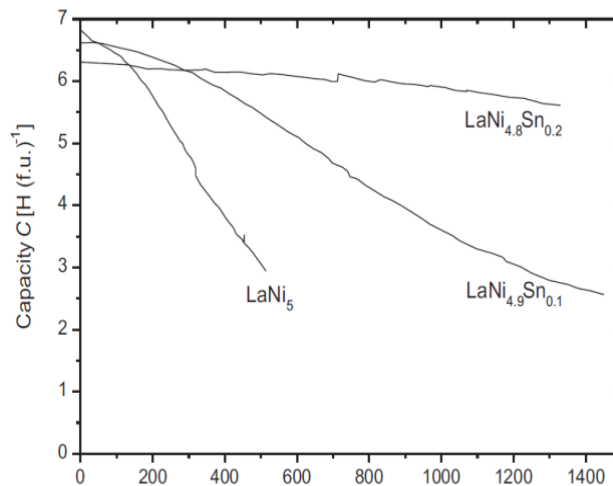


Figure 37 Hydrogen capacity as a function of cycle number for  $\text{LaNi}_5$  and two Sn substituted compounds

LaNi<sub>4.8</sub>Sn<sub>0.2</sub> is recognized as one of the more resistant hydrides. According to Laurencelle et al. it loses only the 2.2 % of H-capacity after 1000 A/D cycles with pure hydrogen, with a perfect preservation of the crystalline structure (consistent hydrogen properties) and kinetics, and a slight reduction of hysteresis due to a lowering of the absorption plateau pressure

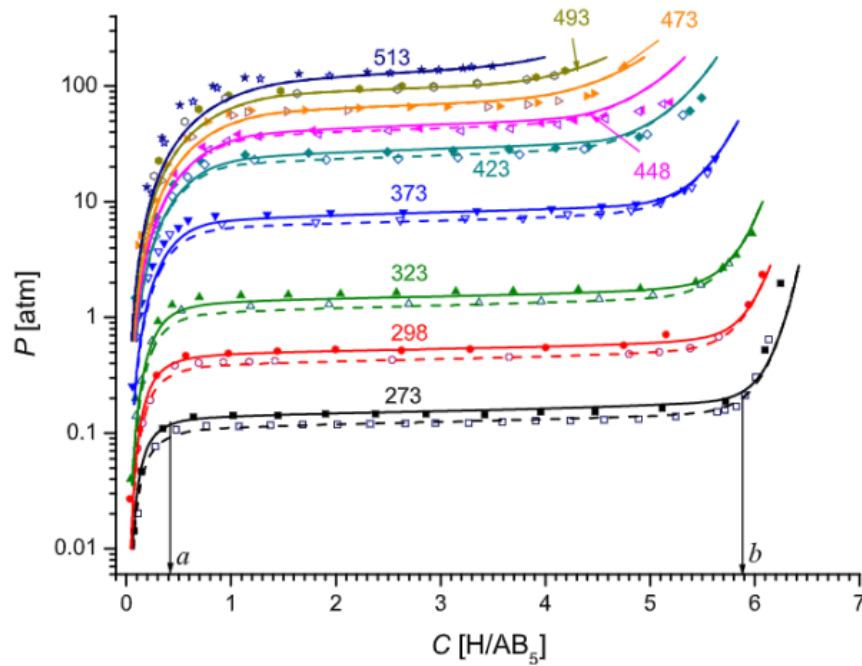


Figure 386 LaNi<sub>4.8</sub>Sn<sub>0.2</sub> PCT isotherms with experimental points highlighted [46]

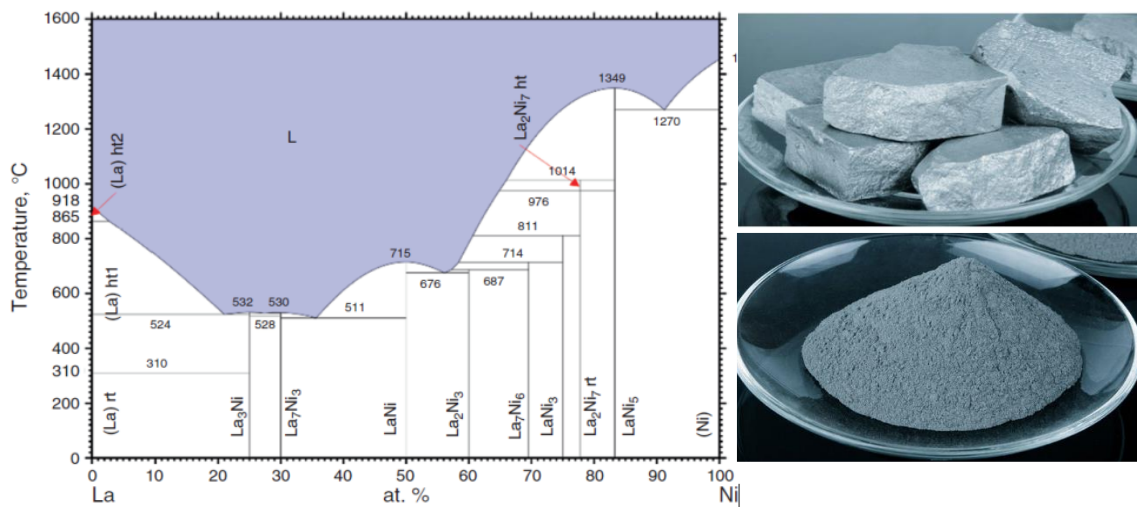
In practice, this would be the best material to use but, in chapter 4, LaNi<sub>5</sub> will be considered anyway for three main reasons: all sellers contacted for this work, especially for the economical part in chapter 4, affirm to use the intermetallic without tin-doping, and they all<sup>5</sup> guarantee that the MH reactors are able to withstand 1000 – 3000 A/D deep cycles without lose more than the 15 % of hydrogen capacity. Moreover, LaNi<sub>4.8</sub>Sn<sub>0.2</sub> is characterized by a desorption pressure at 25 °C of 0.5 [bar], so the desorption must be carried out at almost vacuum conditions, that would be complex in the case-study later described. Finally, the minimum operational temperature given by equation 19 in section 3.7, is 57 [°C], while the operations will be characterized by a medium temperature of 25 [°C].

<sup>5</sup> Sadly, I don't have any legal permission to make known the sellers that I have contacted with reserved e-mails.

### 3.5. Synthesis of intermetallic compounds [42]

The preparation of intermetallic compounds requires the knowledge of the corresponding phase diagrams. These are available for many systems of interest and give basic information on the existence and homogeneity ranges of solid solutions and intermetallic phases, on the solidification reactions, and possible solid-state transformations. These data are important to determine the method of preparation, the heat treatments, the composition shift, etc. Even for compounds which melt congruently and can be obtained directly from the liquid, an annealing treatment is required to improve the homogeneity and eliminate micro segregations.

As an example, the La-Ni phase diagram has been the subject of many investigations and the most recent is presented in Figure 21, that shows the existence of eight different intermetallic compounds.



Figures 39, 40, 41 Binary phase diagram of the La-Ni system and LaNi<sub>5</sub> chunks and powder

LaNi<sub>5</sub> melts congruently at 1349 [°C] and if the process of solidification is not carried out correctly, the alloy may develop distinct liquidus and solidus temperatures (being no more congruent) and second phases, resulting in a reduction of H-capacity. So, post-solidification homogenization heat treatments are used to reduce this undesirable effects and flatten the plateau. A congruent melting is also observed for La<sub>3</sub>Ni and La<sub>7</sub>Ni<sub>3</sub> at 532 and 530 [°C], respectively, while four other La-Ni intermetallic (La<sub>2</sub>Ni<sub>3</sub>, La<sub>7</sub>Ni<sub>16</sub>, LaNi<sub>3</sub>,

and  $\text{La}_2\text{Ni}_7$ ) can crystallize through a peritectic reaction.  $\text{AB}_5$  is usually made commercially by vacuum induction melting of the elements.

The Fe-Ti binary phase diagram, in Figure 22, shows only two intermetallic compounds,  $\text{TiFe}_2$  and  $\text{TiFe}$ , that present both a broad homogeneity range.  $\text{TiFe}_2$  displays a congruent melting at 1427 [°C], whereas  $\text{TiFe}$  is peritectic at 1317 [°C]. Solid solutions of Ti in Fe and Fe in Ti exists also with maximum concentrations of 10 and 25 at%, respectively.

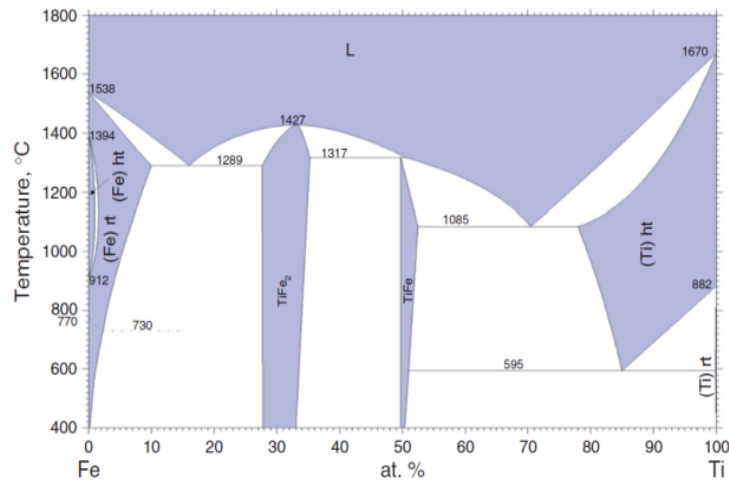


Figure 43 Binary phase diagram of the Ti-Fe system

To prepare an alloy or an intermetallic compound, it is important to determine the conditions of preparation at each step. As the chemical purity of the final material depends on a large extent on the impurity level of the constituents, it is worth to carefully check the purity of the elements used. Some elements, like rare earth metals, are very sensitive to oxidation and should be cleaned and handled under inert atmosphere before melting. To synthesize an intermetallic compound one can use melting techniques, single crystal growth but also rapid solidification, powder metallurgy, and mechanical milling. To synthesize an intermetallic compound melting techniques can be used, such as single crystal growth, but also rapid solidification, powder metallurgy, and mechanical milling.

Finally, the commercial production of  $\text{AB}_2$  compounds is more difficult than  $\text{AB}_5$  compounds since it requires a great metallurgical care. In fact, they are characterized by high melting points of the principal elements and standard techniques (VIM in conventional oxide crucible) are almost impossible to perform. Typical  $(\text{Ti,Zr})(\text{Mn,Cr})_2$

commercial alloys should be melted by vacuum-arc or argon-arc skull techniques using a cold copper crucible to minimize contamination.

### 3.6. Tank Design [44], [45]

Many MH reactors have been developed and the based configurations roughly fall in three categories depending on the geometry of the reaction bed:

- Tubular reactor: this typology is characterized by a central hydrogen artery in which the gas flows while the alloy powder is packed in the annular space around it. The heat exchange is usually by an external air flow. This configuration is used for heat pump systems or for little storage applications, with units characterized by maximum outer diameters of 30 [mm] and cylinder height up to 0.3 – 0.5 [m] (aspect ratio >10). The main advantages regards the simple manufacture and management of single units and the flexibility of hydrogen capacity; the reactor is relatively easy to scale up by increasing the number of units, which are modular and can work independently.

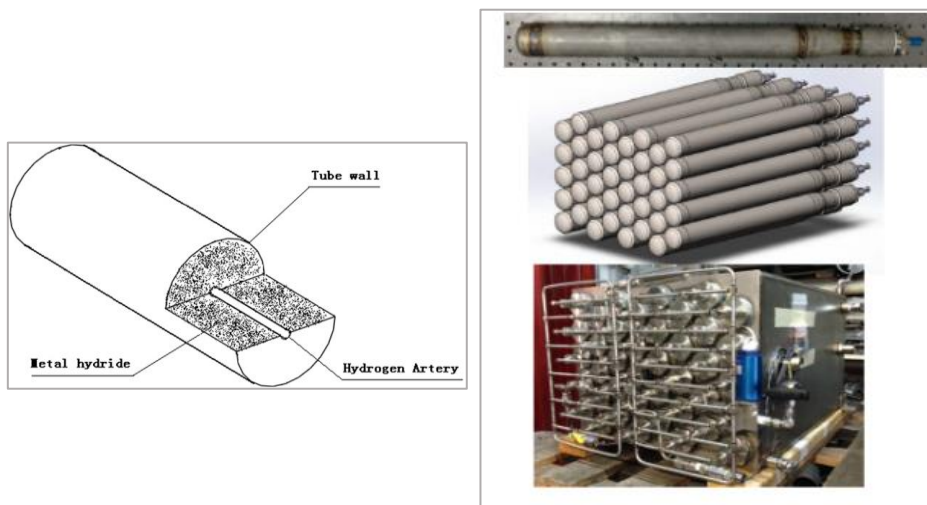


*Figure 44 Schematic of a tubular reaction bed and practical disposition of units to minimize the encumbrance (hexagonal compact honeycomb structure) in a compression system.*

- Disc reactor: the reaction bed now has a flat shape with an aspect ratio smaller than 1. It is characterized by a large heat transfer area that increases the reaction kinetics for a thin MH bed. It can hold only a small amount of powder and it is technically difficult to increase.

- Tank or chamber reactor: this is the typology taken into consideration from now on, since it is the only one characterized by the possibility of large hydrogen storage capacities. A cylinder chamber of a considerable size is used as reaction bed. It is filled with MH powder characterized by a low thermal conductivity. This may bring to local hot spots and mechanical stress which would decrease the reactor lifetime critically, so the heat exchange must be improved by some embedded elements, such as tube bundles, heat pipes and spiral coil, so to uniform temperature distribution and the reaction rate.

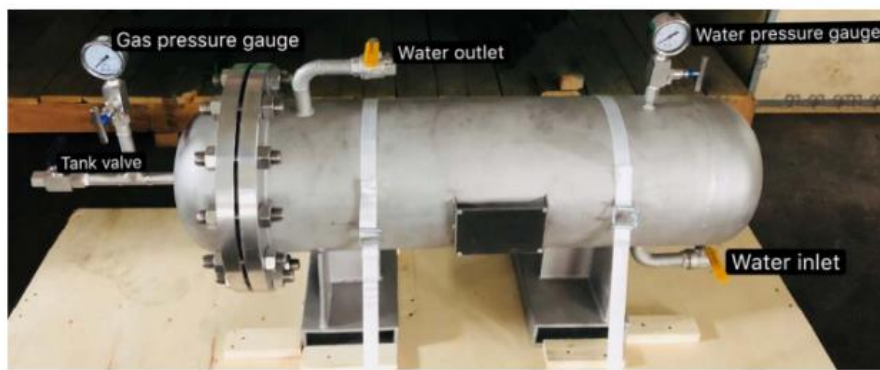


Figure 45 Commercial MH reactor with internal water-based heat exchange

Generally, MH reactors are characterized by:

- A gas-proof containment, in which the material in powder is placed, that isolates the MH powder and hydrogen from the environment and must withstand to temperatures and pressures related to the uptake and release of hydrogen within the bed;
- A system for  $H_2$  input/output and its distribution inside a MH bed. It also ensures the filtering of gas in the release phase, in order to avoid that fine particles of MH material go outside, causing additional problems. The filter pores size must take into consideration the decrepitation process that involves the powder in the first cycles, causing the pulverization into fine particles in the order of 10 [ $\mu m$ ]. Filters or screens with  $\sim 1$  [ $\mu m$ ] pores are simple measure to avoid this problem;
- A heat management system that considers heating/cooling of the reaction bed for absorption /desorption. These operations must be as much homogeneous as possible in the MH bed for a correct operation and can be characterized by an internal or external system. While the absorption reaction is accompanied by the release of heat

which needs to be removed from the system, for desorption heat needs to be supplied.

This reaction heat has a great bearing upon the system performance as it controls the MH bed temperature, which in turn controls the equilibrium pressure.

The metal hydride storage tank requires significant amounts of heat to be removed/supplied from/to the material. In order to improve the bed heat transfer without introducing a large temperature difference, two means can be considered according to Fourier's law: reducing the heat transfer distance or increasing the thermal conductivity that, considering the low thermal conductivity of MH powders ( $\sim 1$  [W/m/K]), is a challenging problem. The most common solutions include:

- Internal heat-conductive matrices such as heat conductive metal foams in aluminium or copper, internal cooling tubes, especially in large-size applications, transverse or longitudinal fins or complex wire configurations within the MH bed. The most popular option is the Al foam with porosity >90 % and thermal conductivity >100 [W/m/K], principally thanks to its very low cost.
- MH compacts, mixing them with some binder materials, e.g. Al powder and graphite. They can be encapsulated with a thin layer of copper and it has been proved experimentally that it has good structure stability and enables excellent heat transfer in the bed. The main application of this is into tubular tanks.
- External heat transfer. The  $H_2$  discharge dynamics depends on the intensity of the heat exchange between the heating-cooling fluid and the wall of the container.

In both internal and external heating and cooling systems, MH tanks are preferred to be long with small diameters, due to shorter heat transfer distance and better heat dissipation.

There is no scarcity of studies on design of metal hydride hydrogen storage systems but studies on large-scale systems are far less than those on small-scale. Further investigation of large-scale practical systems is important keeping in view the issues that are unique to these systems, such as creation of hot spots, parasitic system weight, volumetric efficiency, etc. Moreover, while every heat transfer enhancement results in improved system performance, it also leads to reduced gravimetric and volumetric capacities, due

to the adoption of different systems to increase thermal conductivity and the effectiveness of the heat management, such as porous metal foam and stainless-steel shell-in-tube systems, which increase the overall system weight. So, as the bed dimension increases, the number and layout of heat and mass transfer elements must be determined carefully to meet the requirement for a good performance. In this sense the computational fluid dynamics techniques play a fundamental role.

Another problem to take into consideration is the lattice expansion during hydrogenation that can cause the occurrence of large mechanical stresses on the containment wall if free space is not provided to allow this phenomenon. The pulverization of the MH particles during cyclic absorption/desorption results in their concentration in the bottom part of the vessel, which creates particularly strong local stresses, even during the first absorption cycle. This phenomenon can cause significant deformations or even rupture of the containment, reducing the stability lifetime of the tanks. Current measures to avoid damages are the following: put the reactor in horizontal, enable the powder dilatation in case of hydrogen absorption leaving a free space in the discharged state, decrease the packing fraction of the powder and pre-processing the powder. Nasako et al. [46] carried out an extensive study of this problem and concluded that the stress of the vessel will occur only if:

$$\phi = \phi_0 \cdot \left[ 1 - (\beta - 1) \cdot \frac{c}{c_s} \right] > 0.61 \quad (15)$$

Where  $\phi$  and  $\phi_0$  are the actual and initial packing fractions,  $\beta$  is the expansion ratio,  $c$  and  $c_s$  are the actual and saturated hydrogen concentration. The most effective demonstrated measure to face up the problem today is the pre-processing of powder that consists in confining the pulverization and movement of MH particles by encapsulation or mix with organic additives or silicon oil. In the next chapter these measures will be taken into consideration by leaving the 25% of void volume to make the powder free to dilate, upon absorption of hydrogen and considering the pre-processing of powders by increasing their cost of the 50 % to stay conservative in the economic evaluation

The integration into FC power system requires important considerations to ensure the overall system effective operation. This involves several different factors:

- The required amount of stored hydrogen must be achieved within the space and weight constrains of a particular application;
- The hydrogen storage system has to provide sufficient  $H_2$  supply to the FC when operating at a maximum rated power for a specified time;
- The refuelling of the storage system has to take reasonably short time and the hydrogen mass transfer must be uniform;
- The material-related properties, the specified performances are also affected by the features of the containers in which the MH material is placed. Furthermore, the rates of  $H_2$  supply both from MH tank and, especially, to the MH tank will be greatly dependent on the size, geometry and layout of the MH container.

These dependencies are quite complicated and often require numerical modelling (CFD) followed by quite expensive experimental verification.

### 3.7. Plant layout [47]

This work is focused on the possibility of coupling hydrogen storage systems based on MH usage with fuel cell and electrolyzers. This particular layout is possible between low

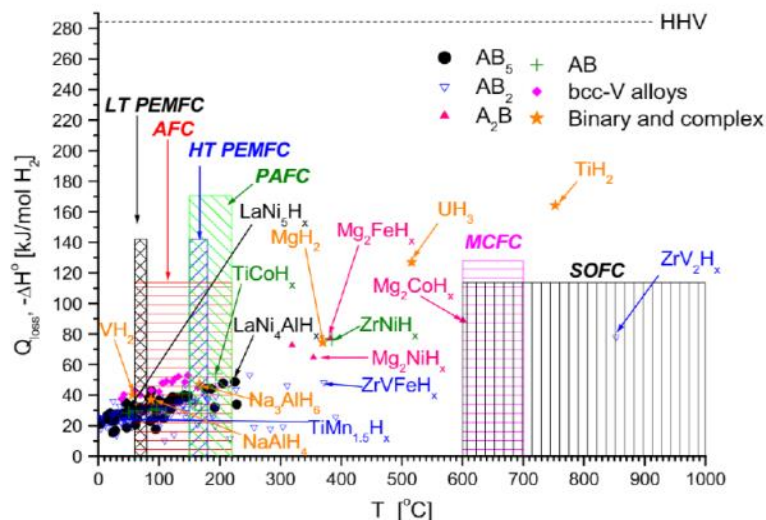


Figure 46 Potential various metal hydrides with the associated heat losses in different types of fuel cells. The operation temperatures of the MH's correspond to  $H_2$  plateau pressures of 10 [bar] [37]

temperature fuel cell systems and intermetallic compounds, as found by Lototsky et al. [37]. There are three operative situations to take under consideration: power production, MH tank refuelling and long-term storage.

- **Power production**

In such a system, hydrogen is supplied from the MH tank at a pressure,  $p_{FC}$ , which depends on the MH operating temperature and can be estimated using the Van't Hoff equation. In the fuel cell hydrogen is converted to electricity net to its efficiency, that determines the fraction of chemical energy released during the electrochemical oxidation of the fuel cell into electric energy.

$$\eta_{FC} = \frac{E_{el}}{E_{TOT}} \quad (16)$$

The remaining energy can be expressed as heat losses, dissipated in the environment or stored in sensible or latent forms.

$$Q_{loss} = E_{TOT} - E_{el} = E_{TOT}(1 - \eta_{FC}) \quad (17)$$

This energy can be used to provide the correct hydrogen supply by enabling the decomposition of intermetallic hydride. As seen previously, this process is endothermic and requires a heat supply equal to the absolute value of the hydrogenation enthalpy (approximation). Assuming  $E_{TOT}$  equal to the lower hydrogen heating value ( $LHV_{H_2} = 120 [MJ/kg_{H_2}]$ ), a further estimation of the conditions at which  $H_2$  supply from the MH to the FC can be provided without additional energy input, i.e. by only using heat losses during FC operation can be made:

$$|\Delta H_0| \leq Q_{loss} = LHV(1 - \eta_{FC}) \quad (18)$$

The plateau pressure at the operating temperature must be higher than the pressure required by the fuel cell of hydrogen supply (0,5 [bar]). So, the operation temperature must satisfy the following requirement:

$$T_{OP} \geq \frac{\Delta H^0}{\Delta S^0 + R \ln p_{FC}} \quad (19)$$

Therefore, the feasibility of thermal integration of a MH with a FC requires the thermodynamic properties of its reversible interaction with  $H_2$  ( $\Delta H^0$  &  $\Delta S^0$ ) to satisfy the two equations above. Most of the intermetallic compounds are suitable for low temperature FC applications, as it can be noticed in the previous figure. Hydrogen supply from “low-temperature” MH requires quite modest energy input (10 – 30% of the LHV) of the released heat  $Q_{loss}$ . This means that thermal integration of these materials with the BoP of the FC stack does not require high heat transfer efficiency and can be simply achieved capturing the warm air from the exhaust of the cooling system of the FC module.

Considering the starting process, a buffer tank is needed to provide  $H_2$  for the duration of the start-up that the FC takes to reach the nominal temperature ( $\sim 70 - 80$  [°C]). The required buffer capacity may be estimated supposing a linear increase of fuel cell stack current and voltage in one hour or more, with the same increment value until the right operational configuration is reached.

- **Refuelling**

The MH should be coupled with a hydrogen supply (electrolyser or compressed gas) and heat management system that cools the tank down during the exothermic hydrogen absorption by means of the same heat transfer mechanism of the previous case. The heat collected is then rejected or collected in a thermal energy storage, such as a PCM layer, and can be used to start the desorption process when the fuel cell is asked to intervene. This heat will be considered as a waste later, since it is characterized by a temperature too low to be involved in a further usage. Considering instead high temperature applications, involving complex hydrides instead of intermetallic, the heat generated has a higher

exergy content, so the metal hydride reactor can function as both chemical and thermal energy storage. Tens of academic researches and experimentations have been already conducted in this field.

○ **Long-term storage**

This is the simplest operating condition, due to the fact that the metal hydrides which have been formed after hydrogen absorption by selected HSA are stable enough to make the long-term storage energy loss negligible. The MH bed pressure must be higher than the equilibrium pressure at ambient temperature, which doesn't exceed the 10 – 15 [bar].

A coupled with a MH hydrogen storage and supply system in shown in Figure 27. The integration of storage systems, balance of plant and fuel cell components together are optimized utilizing system models which track hydrogen flow, humidification

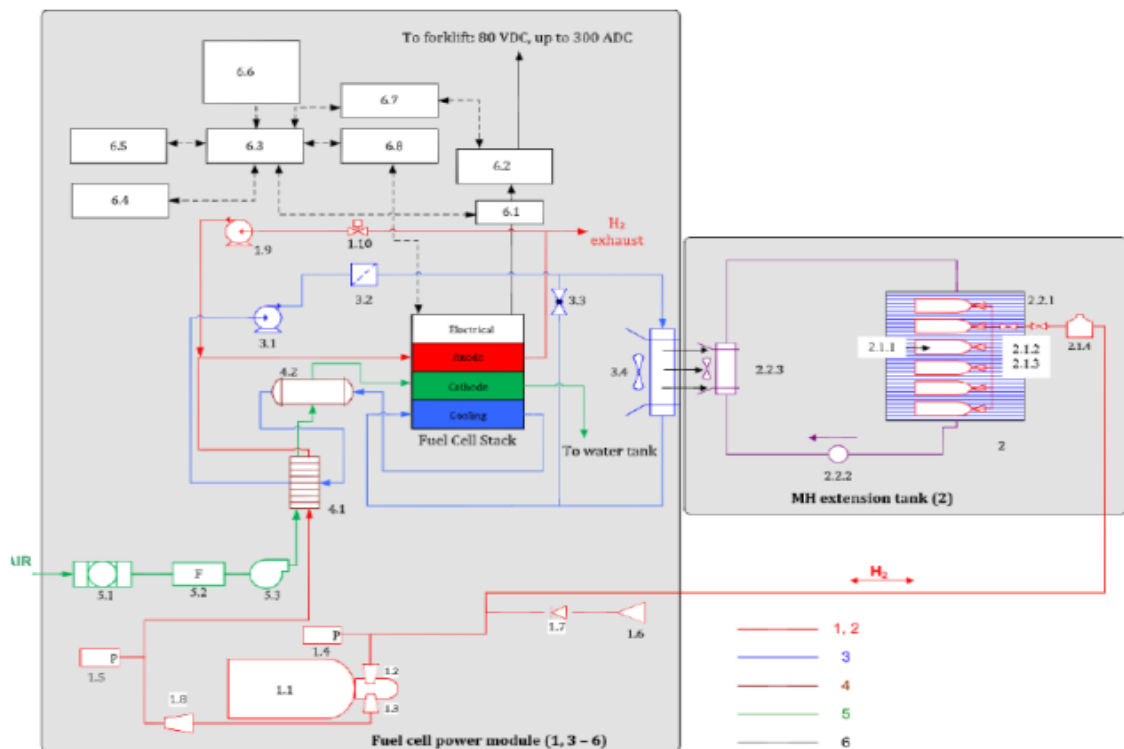


Figure 47 Integration of a MH hydrogen storage extension tank in FC system [47]:

- 1 – Hydrogen storage and supply subsystem, 1.1 – gas cylinder, 1.2,1.3 – adapters, 1.4, 1.5 pressure sensors, 1.6 – refuelling receptacle, 1.7 – check valve, 1.8 – reducer, 1.9 – recirculation pump, 1.10 – purge valve.
- 2 – MH extension tank: 2.1 – hydrogen subsystem, 2.1.1 MH containers, 2.1.2, 2.1.3 – shut-off valves, 2.1.4 – gas filter, 2.2 – thermal management subsystem, 2.2.1 – water tank, 2.2.2 – circulation pump, 2.2.3 – radiator.
- 3 – FC stack cooling subsystem: 3.1 – coolant pump, 3.2 – DI filter, 3.3 – bypass valve, 3.4 – radiator.
- 4 – fuel/oxidant conditioning, 4.1 – reactants conditioner, 4.2 – humidifier assembly.
- 5 – air supply subsystem, 5.1 – filter, 5.2 – flow meter, 5.3 – compressor.
- 6 – electrical components, 6.1 – contactor, 6.2 – Li-ion battery, 6.3 – system master controller, 6.4 – compressor motor controller, 6.5 – cell voltage monitor, 6.6 – BoP sensors, 6.7 – battery sensors, 6.8 – stack sensors

requirements by the PEMFC, water and thermal management issues as well as the numerous other system components required to allow for a fully functioning hydrogen storage system. But here the MH system is not linked with the fuel cell directly but passes through the gas cylinder.

*Table 4 Principal thermodynamic characteristics of the selected intermetallic compounds*

Alloys	Hydrides	$\rho$	Slope	Hysteresis	$p_{abs}$ (25°C)	$p_{des}$ (25°C)	$\Delta H$	$\Delta S$	$T_{op\_min}$
		kg/m <sup>3</sup>	/	/	bar	bar	kJ/mol	kJ/mol/K	°C
TiFe.85Mn.15	TiFe.85Mn.15H	6500	0,62	0,92	6,44	2,57	29,5	0,107	18,24
TiMn1,5	TiMn1,5H2	6400	0,93	0,57	14,66	8,29	28,7	0,114	-7,99
LaNi5	LaNi5H6	8300	0,13	0,13	2,02	1,78	30,8	0,108	28,11
Lani4,8Sn0,2	Lani4,8Sn0,2H6	8400	0,19	0,22	0,61	0,49	32,8	0,105	57,37

## 4. Application to the off-grid plant in Ginostra (Sicily)

### 4.1. Introduction [52]

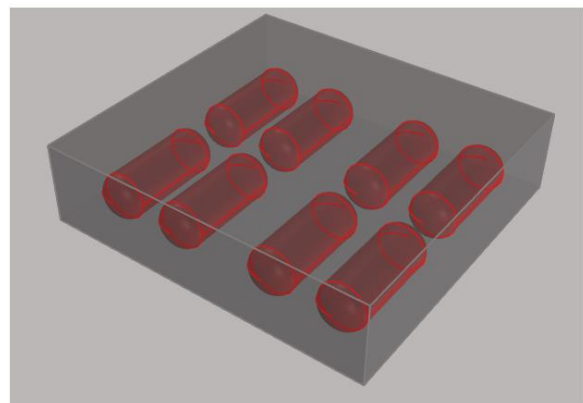
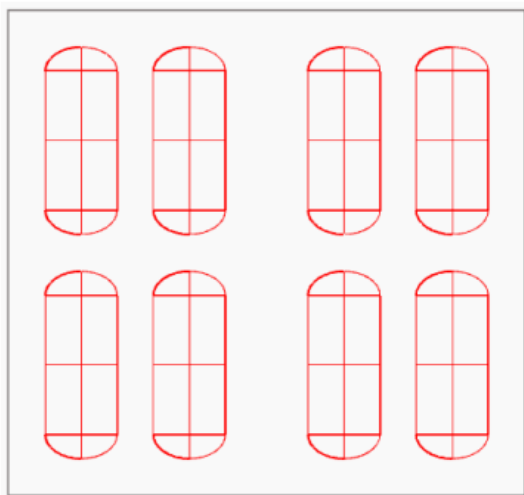
REMOTE is a 4-year project (2016-2020), under the EU's Horizon 2020 programme. REMOTE has the objective to demonstrate the technical and economic feasibility of fuel cell-based  $H_2$  energy storage solution in 4 isolated off-grid remote areas that will be fed mostly or totally by renewable electricity. In these locations the link with the national grid and the transport of fuel cost too much; moreover, some of them are in protected national areas with fragile wildlife and plants, so the main target is to become fully zero-emitting by renewable generation (PV and wind). To stabilize the local grid an energy storage is needed and two solutions will be applied: a Li-ion battery, with very efficient charge and discharge, and hydrogen storage that will function as seasonal storage into an integrated P2P system, characterized by alkaline electrolyzers and a PEM fuel cells. Lastly, diesel generators are needed as final back-up system.

The DEMO taken into consideration in this last chapter will be built in Ginostra, Sicily, an island village not connected to the Italian distribution and transmission grid and to the local Stromboli Island grid. It's characterized by residential loads only: the village counts about 40 people living there during the year, who increase to 200 during summertime thanks to tourism. Currently, the site load is covered diesel generators (304 [kW]), with the fuel that must be transported by helicopter, leading to a very high cost of electricity. The proposed solution consists in the adoption of a 170 [kW] pre-existing PV power plant that can directly cover the load or can charge a special 600 [kWh] Li-Ion battery or a 50 [kW] alkaline electrolyzers (two 25 [kW] modules) to produce hydrogen in case of overproduction, especially in summer. Hydrogen is then stored and re-electrified by a 50 [kW] PEMFC system (two 25 [kW] stacks) when the energy required is higher than the PV coverage, minimizing the conventional diesel generator utilization. The battery has the priority on both charge and discharge phases to maximize the overall system efficiency, while the hydrogen storage will be constituted by 8 tanks of 2.7 [ $m^3$ ] each, operating at maximum tolerable

pressure of 30 [bar]; so, the maximum capacity is 52.7 [ $kg_{H_2}$ ] but the maximum operative value allowable is assumed to be 50 [ $kg_{H_2}$ ] because of the maximum operative pressure of 28 [bar] (corresponding to 49.2 [ $kg_{H_2}$ ])

Table 5 Principal Ginostra power plant components with specifications

	Size	Efficiency	Operative Range
<b>PV</b>	170 [kW]	14 %	–
<b>Battery</b>	600 [kWh]	95 %	0.2 – 0.8
<b>P2G</b>	2x25 [kW]	63 %	0.2 – 1
<b>G2P</b>	2x25 [kW]	50 %	0.15 – 1
<b>H<sub>2</sub> Storage</b>	21.6 [ $m^3$ ] 50 [kg] 1.64 [MWh]	–	0 – 28 [bar]



Figures 48, 49, 50 Front, top and perspective views of the compressed gas based system

The 8 Hydrogen pressure vessels are located in a proper room (8.4 x 7.9 x 2.1 [m]) with a suitable ventilation system for safety reasons (DM 21/08/2006). The final preliminary results obtained in MATLAB, with proper input data (yearly solar irradiance and yearly load with 1 [h] time-step).

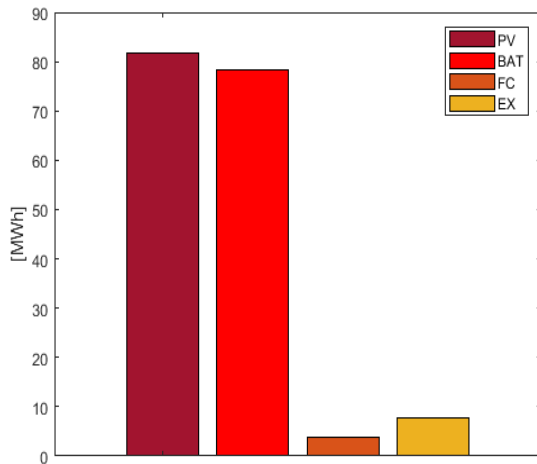


Figure 51 Load coverage in MWh: Direct Photovoltaic 81.7, Battery 78.3, G2P 3.8, External Source 7.7

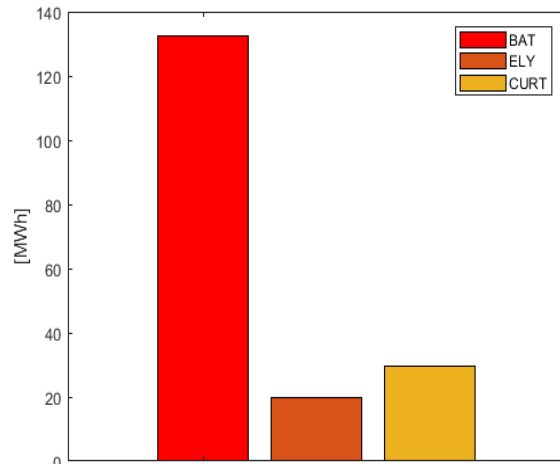


Figure 52 Net RES surplus utilization in MWh: Battery 132.4, P2G 19.9, Curtailment 29.7

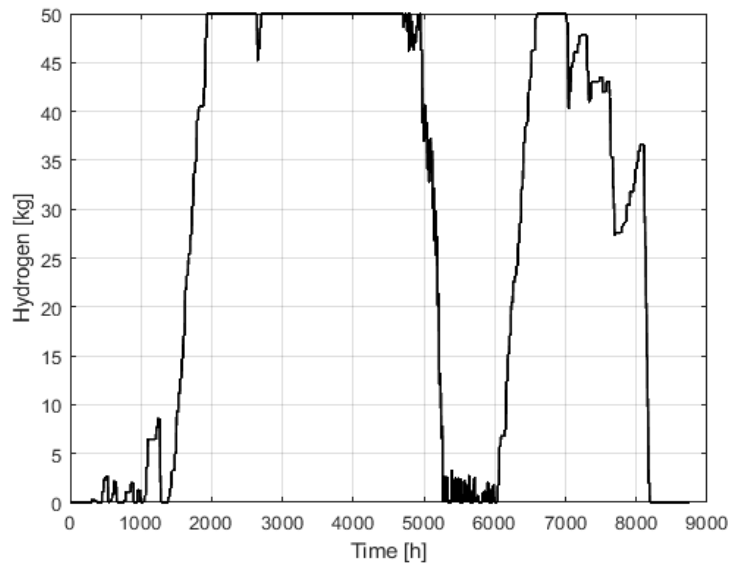


Figure 53 Hydrogen storage progress during the reference year; full equivalent cycles calculated = 4.5, assumed 5 [cycles/year]

In figure 31 it is appreciable that hydrogen is collected especially during spring and autumn, since the tourism season has not started yet and the solar irradiance starts to become higher, overwhelming largely the daily energy demand. Hydrogen is used during summer when the inhabitants of the island quadruple, and in winter as the solar irradiance becomes too weak and daytimes too short to cover the daily loads.

## 4.2. MH-based storage system adoption

The aim of this section is to demonstrate the technological feasibility of the metal hydride adoption to store the same amount of hydrogen of the previous case highlighting advantages and disadvantages from a technical and economical point of view. The materials chosen are the ones studied in detail in the previous chapter:  $LaNi_5$ ,  $TiFe_{0.85}Mn_{0.15}$ ,  $TiMn_{1.5}$ , primarily because they are the alloys with the highest collected experience, in the relative family, during the last decades. Their principal characteristics are shown in tables<sup>6</sup> 5, 6:

As already said, the reversible quantities are referred to the plateau region of the PCT diagram, but the real hydrogen capacity during operation is between the two values. The reversible capacities only are taken into account to remain conservative later on.

Table 6 Maximum and reversible hydrogen capacities for selected HSA

Alloys	Maximum Capacity			Reversible Capacity		
	H/M	%wt	[kg_H2/m <sup>3</sup> ]	dH/M	/wt	[kg_H2/m <sup>3</sup> ]
TiFe.85Mn.15	1	1,90%	123,5	0,8	1,50%	83,69
TiMn1,5	0,99	1,86%	119,04	0,65	1,15%	63,61
LaNi5	1,08	1,49%	123,67	0,93	1,20%	87,04

A particular attention is given to the  $LaNi_5$  which is the only material that has collected enough experience to be commercialized. In fact, systems based on its usage are the only ones which can be easily found on the web with accurate thermodynamic properties, operational configurations, system lifetime data and costs.

### MH based hydrogen storage reactor

The layout taken into consideration is a multi-tubular shell-and-tube reactor (described in [44]). Since 1.64 [MWh]  $H_2$  must be stored reversibly, several large-size reactors will be required and they will be disposed in canisters to optimize the system encumbrance. Heat transfer to/from the MH bed is an important factor to ensure efficient hydrogen storage, so, a cylindrical design is chosen to guarantee sufficient heat transfer area, ease in handling and

<sup>6</sup> All materials data have been taken from [38]

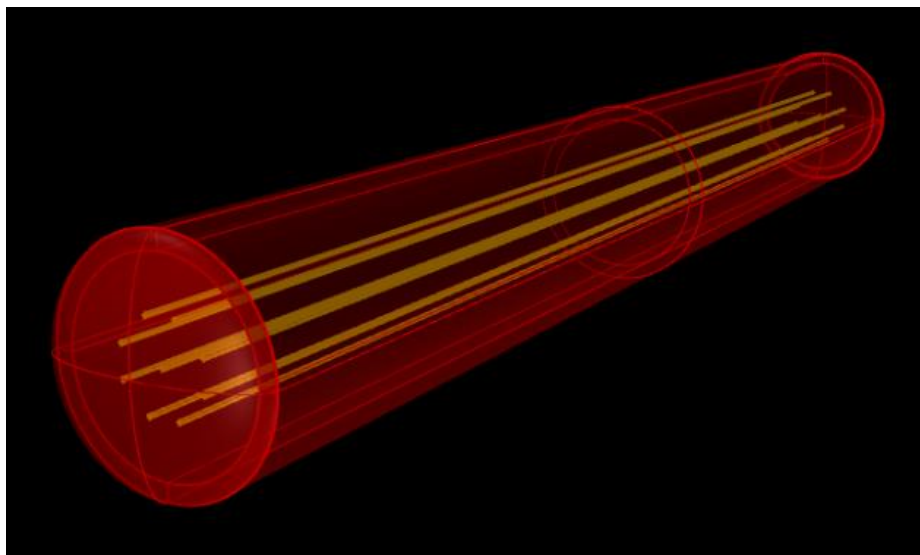
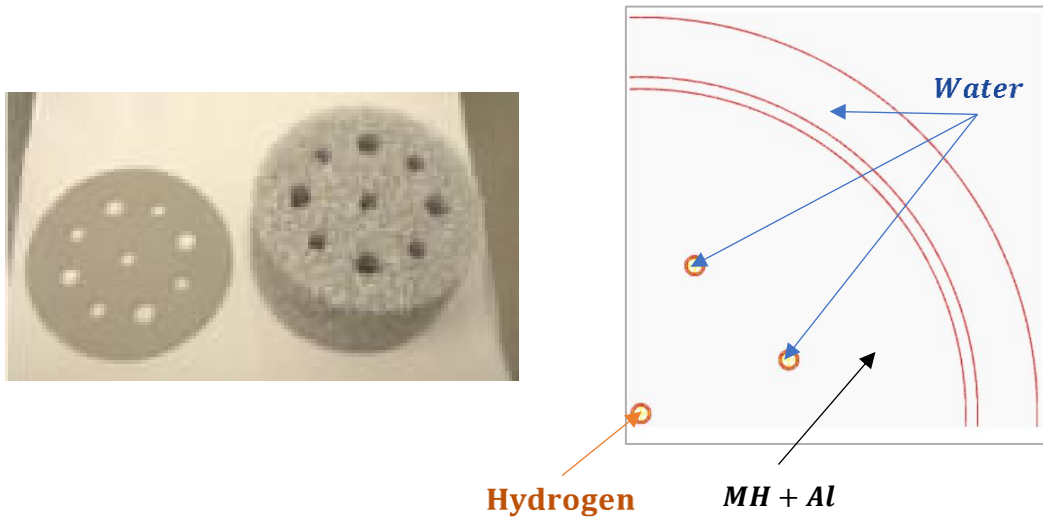
portability. Improvements in heat transfer uniformity and efficiency are required, with the addition of a 3 [cm] thick water jacket and 8 cooling tubes in which pure water will flow through, in order to have a more uniform and safe heat transfer in the reaction bed. A central pipe will function as hydrogen filter and artery to assure the right charge and discharge processes. Afzal & Sharma [44] found that thermal conductivity and supply/delivery pressures have the most significant impact on the system performance, overshadowing the effects of other parameters. The thermal conductivity value of a generic MH powder of porosity 50% is usually very poor, around 1 – 2 [ $W/m/K$ ], so an aluminium foam of porosity 91% is adopted, to have a final a value of 10 – 12 [ $W/m/K$ ]. The final heat transfer coefficient value assumed with these hypothesis is 500 [ $W/m^2/K$ ]<sup>7</sup>.

Table 7 Main technical specifications of the MH tank adopted

External Diameter ; thickness	cm	16.90 ; 0.60
Reactor Length	m	1.650
Cooling Tubes D ; thickness	cm	0.50 ; 0.10
Empty reactor weight	kg	64.00
Water Jacket	cm	3.00
Total Volume	lt	37.01
MH Volume <sup>8</sup>	lt	24.39

---

<sup>8</sup> Net of MH powder porosity, cooling tubes volume, aluminium foam volume and the fraction left empty in discharged reactor (25%).



Figures 54, 55, 56 Typical aluminium matrix for thermal conductivity enhancement, schematic 2D plot of the MH reactor front view, 3D plot of the single reactor (drawn in Rhinoceros 5)

The typical reactor and tubes material is stainless steel 316, particularly indicated to withstand to hydrogen embrittlement, even if it is not a so problematic issue in this application.

The reaction bed must be maintained at constant temperature of 25 [°C], neglecting the transient patterns during the processes. In fact the bed temperature always increases in the first part of the absorption, reaching peak values that depend on the material and the supply

hydrogen pressure. The considered hydrides can withstand to 1000-3000 deep cycles before having a 10-15 % capacity loss (supply reference on  $LaNi_5$  and  $TiFe_{0.85}Mn_{0.15}$  only, no data on  $TiMn_{1.5}$ ). The number of equivalent deep cycles have been found by programming in MATLAB for the general case (figure 39), and it has been found a value of 5 per year. So, the theoretical system lifetime is above 100 years in this operating conditions (with pure hydrogen).

Table 8 Total amount of HSAs required, H-content, MH-content for single t. and total number of t. per HSA required

Alloys	Volumetric den kg_H/m <sup>3</sup>	TOTAL_MH		H2_Tank				MH_tank	Number_units
		kg	m <sup>3</sup>	kg	Nm <sup>3</sup>	mol	kWh	kg	#
TiFe.85Mn.15	83,69	3803,6	0,585	1,020	11,436	506,190	34,016	79,255	48
LaNi5	87,04	4670,1	0,563	1,061	11,893	526,438	35,376	101,203	47
TiMn1,5	63,61	4927,8	0,770	0,776	8,691	384,705	25,852	78,036	64

### o Charge phase

Hydrogen exiting from the electrolyser at 30 [bar] goes directly to the MH reactors since the high pressure is positive from the hydrogen absorption viewpoint. Afzal & Sharma found that this supply pressure increases the hydrogen absorption rate of about 10% compared to 25 [bar], highlighting how important this parameter is; moreover, this value is usually the upper limit at which hydrogen can be supplied in MH reactors in available commercial devices.

Absorption is highly exothermic, characterized by an irregular pattern of the released heat, which makes necessary a continuous water flow at ambient temperature or lower. The lower the temperature the more effective the heat removal and the reaction rate consequently. It has been assumed 25[°C] but it could depend by external conditions. The average reaction bed temperature depends by the alloy considered and it increases with the supply pressure, but generally speaking, peak temperatures would not exceed 50 – 60 [°C] ([47]) in the first 30 – 50 [s] of the process at 30 [bar]. The outlet water temperature assumed is 50 [°C]. Clearly, these value are not precise and should be founded with accurate numerical simulation (CFD).

In Ginostra the filling process can be performed one reactor at a time to follow the low full operation hydrogen production rate by the 2 alkaline electrolyzers of  $0.72 [kg_{H_2}/h]$ . The absorption process has been assumed to be completed after 1.5 [h] per tank (from published data on seller websites and from [47]). The thermal energy necessary to absorb (and desorb) a hydrogen mole in a  $\left(\frac{M}{x}\right)$  mole equal to the reaction enthalpy difference ( $\alpha \rightarrow \beta$ ), the thermal power and the consequent water flow rate (per reactor) can be calculated.

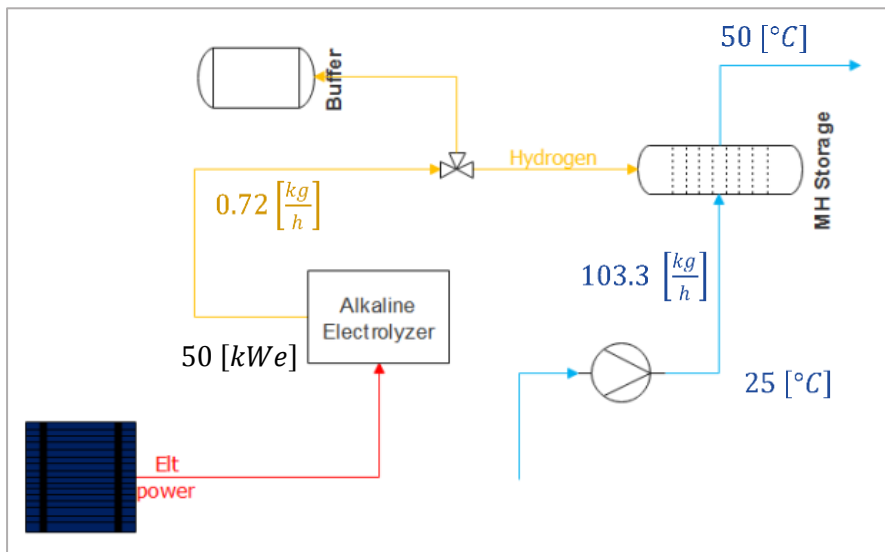


Figure 57 Schematic representation of the charging process at nominal operating conditions

Table 9 Calculation steps for the absorption process, with reference to the single tank only

Alloys	Q	$\Phi$	G_H2O	v	Time_total
	MJ	kW	kg/h	m/s	h
TiFe.85Mn.15	14,93	2,77	95,13	1,382E-03	72,0
LaNi5	16,21	3,00	103,29	1,500E-03	70,5
TiMn1,5	11,04	2,04	70,34	1,022E-03	96,0

In this application charging time is not an important issue compared to the automotive case. The system appears to be technically complex and the software to manage the entire process expensive because both water and hydrogen streams have to flow into reactors selectively one at a time until the process is complete. Moreover, when the hydrogen content fluctuates a lot (figure 40), especially during winter and summer the reactors involved in that continuous ON/OFF behaviour have to be different year by year so to avoid the degradation of the single units.

### ○ Discharge phase

The main requirement in this phase is the nominal hydrogen flow that must be assured to the fuel cell stack, equal to  $3 \left[ \frac{kg_{H_2}}{h} \right]$  ( $\sim 16$  [h] *autonomy with the full charge*). Assuming the entire storage full of hydrogen, now all reactors are involved together in the discharge process. Water at 50 [°C] is needed to flow in the tubes and in the water jacket to give the amount of heat required, theoretically equal to the quantity of the previous case. To heat up the water, fuel cell exhausts are used to perform a low-temperature heat recovery in a stainless steel, double-pipe air/water heat exchanger to be dimensioned later using the logarithmic mean temperature difference method for the three different materials. The nominal hydrogen flow rate exiting from the single reactor can be estimated: it is lower than commercial reactors of the same size. This effect can be realistic since water in nominal conditions may be sent at 80 – 90 [°C], but in case of heat recovery from the fuel cell exhausts, water temperature is limited by the exhausts temperature and low specific heat. An advanced layout may be thought with a  $H_2$  burner out of the cell which can increase both temperatures of FC exhausts and process water, so to have better performances.

Regarding the hydrogen buffer required for the system start-up, it must contain the amount of hydrogen, able to bring the fuel cell at nominal operations. It can be estimated equal to  $\approx 1,0$  [kg] assuming a linear increase of FC current, voltage and temperature in a 1[h] start-up, stored as compressed gas at 28 [bar] (420 [lt]), so that no further compression is needed. So the hydrogen that needs to be stored in MH reactors is now equal to 49 [kg]  $\equiv 549$  [ $Nm^3$ ]  $\equiv 1633$  [kWh].

The steps of calculation are explained in detail in the following points:

- First of all, the FC exhausts must be analysed taking into account the input data: FC stacks overall power in nominal conditions (50 [kWe] with air 32720 [ $Nm^3/h$ ]  $\equiv 0.8$  [kg/s]), the amount of heat extracted by the cathode air (54.7 [kWth]), the overall efficiency (50%). The operating FC conditions can be calculated:

Table 10 Single 25 [KW] Fuel Cell operation parameters

$I_{stack}$	715 [A]
$V_{cell}$	0.7 [V]
$n_{cell}$	50
$G_{H_2}$	1.5 [kg/h]
Fuel Utilization	0.9
Excess Air	1.6
$T_{OP}$	80 [°C]
Efficiency	50 %

- The physical properties and chemical composition of the exhausts coming out from the fuel cell cathode must be found, paying attention that this gas cannot be considered air anymore. A part of the oxygen contained in the inlet air has reacted with hydrogen while nitrogen is an inert gas that does not participate in the reaction in the fuel cell.

$$G_{O_2} = G_{air} \cdot 0.233 - \frac{I}{4F} \cdot \bar{M}_{O_2} = 0.130 \left[ \frac{kg}{s} \right]$$

Where  $F=96485$  [ $A \cdot s/mol$ ], Faraday constant.

$$G_{N_2} = G_{air} \cdot 0.767 = 0.622 \left[ \frac{kg}{s} \right]$$

$$G_{MIXGAS} = G_{O_2} + G_{N_2} = 0.752 \left[ \frac{kg}{s} \right]$$

$$y_{O_2} = \frac{\frac{G_{O_2}}{\bar{M}_{O_2}}}{\frac{G_{O_2}}{\bar{M}_{O_2}} + \frac{G_{N_2}}{\bar{M}_{N_2}}} = 0.154$$

$$y_{N_2} = 1 - y_{O_2} = 0.846$$

Now the “MIXGAS” specific gas constant can be calculated:

$$R_{MIXGAS} = R_{N_2} \cdot x_{N_2} + R_{O_2} \cdot x_{O_2} = 290.5 \left[ \frac{J}{kgK} \right]$$

Finally, supposing the new mixture saturated, with saturated steam pressure at 70 [°C] equal to 0.3119 [bar], and the outlet cathode air pressure 2 [bar], the water fraction can be found as:

$$x_{H_2O_{cat,out}} = x_1 = \frac{R_{MIXGAS}}{R_{H_2O}} \cdot \frac{p_{sat}(70^\circ C)}{p_{cat,out} - p_{sat}(70^\circ C)} = 0.116$$

$$G_{H_2O} = x_{H_2O} \cdot G_{MIXGAS} = 0.087 \left[ \frac{kg}{s} \right]$$

A fraction of this humid MIXGAS will flow in the tube-in-tube heat exchanger to heat up the water which will cause the hydrogen desorption in the cylindrical MH tanks. The enthalpy of this humid gas needs to be calculated

$$cp_{MIXGAS} = x_{N_2} \cdot cp_{N_2} + x_{O_2} \cdot cp_{O_2} = 1,020 \left[ \frac{kJ}{kgK} \right]$$

$$h_{MIXGAS} = cp_{MIXGAS} \cdot (T - T_0) = 71,40 \left[ \frac{kJ}{kg} \right]$$

$$h_1 = h_{wat,v} \cdot x_1 + h_{MIXGAS} \cdot (1 - x_1) = 369,0 \left[ \frac{kJ}{kg} \right]$$

With

$$h_{wat,v}(70^\circ C) = 2626.9 \left[ \frac{kJ}{kg} \right], cp_{N_2} = 1,042 [kJ/kg/K], cp_{O_2} = 0,910 [kJ/kg/K].$$

After that this flow crosses the tube-in-tube heat exchanger, it will be cooled down to 55 [°C]. The calculated pressure losses inside the HEX are largely negligible and the new water fraction is calculated assuming again a saturated gas flow,  $x_2 = 0.055$  with  $p_{sat}(55^\circ C) = 0.1615 [bar]$ . The new enthalpy at this temperature can be calculated considering that a certain amount of water condenses. The heat released per unit mass of MIXGAS is finally determined:

$$h_{MIXGAS} = cp_{MIXGAS} \cdot (T - T_0) = 45,90 \left[ \frac{kJ}{kg} \right]$$

$$h_2 = h_{wat,v} \cdot x_1 + h_{MIXGAS} \cdot (1 - x_1) = 186,1 \left[ \frac{kJ}{kg} \right]$$

$$q = (h_1 - h_2 - (x_1 - x_2) \cdot h_{wat_{liq}}) = 166,9 \text{ [kJ/kg]}$$

With  $h_{wat,v}(55^\circ\text{C}) = 2601,0 \left[ \frac{kJ}{kg} \right]$ ,  $h_{wat_{liq}}(70 - 55^\circ\text{C}) = 261,6 \text{ [kJ/kg]}$ .

Water and vapour enthalpies can be found on thermodynamic tables or in books [54]. They need to be found in this way since both inlet and outlet exhausts fluxes have been considered in saturated conditions.

- The water inlet temperature is 25 [°C] and it's needed at 50 [°C] to supply the heat for the desorption process. Different flow rates are needed for the different materials involved, since they are characterized by different reaction enthalpies. The calculations have been made fixing the value of hydrogen flow rate at FC nominal power, so that the total heat must be given in  $49.0/3 = 16.32 \text{ [h]}$ .

Table 11 Operating conditions of the discharging process

Alloys	Q	Time	Φ	G_H2O	
	MJ	h	kW	kg/h	kg/s
TiFe.85Mn.15	716,77	16,32	12,20	699,3	0,19
LaNi5	762,07	16,32	12,97	743,5	0,21
TiMn1,5	706,63	16,32	12,02	689,4	0,19

Dividing these values per the number of reactors, the water flow rate per unit can be evaluated and then the water velocity inside the cooling tubes and the water jacket. Coming to the reactor, its bed temperature is considered at constant temperature (25 [°C] again), and water for hydrogen desorption releases the heat required, cooling down from 50 to 35 [°C]. The pressure in the bed must stay below the equilibrium value, otherwise the desorption will stop. A pressure value of 0.5 [bar] in hydrogen artery is enough low and easy to pursue, connecting the MH beds with a slightly depressurized ambient. A further decrease of pressure or water temperature increase would enhance the speed of the entire process.

- Only a part of the MIXGAS is needed to heat up the water to 50 [°C] for the desorption. The flow rate values are equal to 0,122 [kg/s] for  $\text{TiFe}_{0.85}\text{Mn}_{0.15}$  (16,2 % of the total), 0,129 [kg/s] for  $\text{LaNi}_5$  (17,23 %), 0,120 [kg/s] for  $\text{TiMn}_{1.5}$  (15,9 %). The temperature of exhaust out of the HEX has been assumed equal to 55 [°C]
- Finally, the tube in tube heat exchanger can be dimensioned using the logarithmic mean temperature difference method. The HEX typology adopted is the counter-current one.

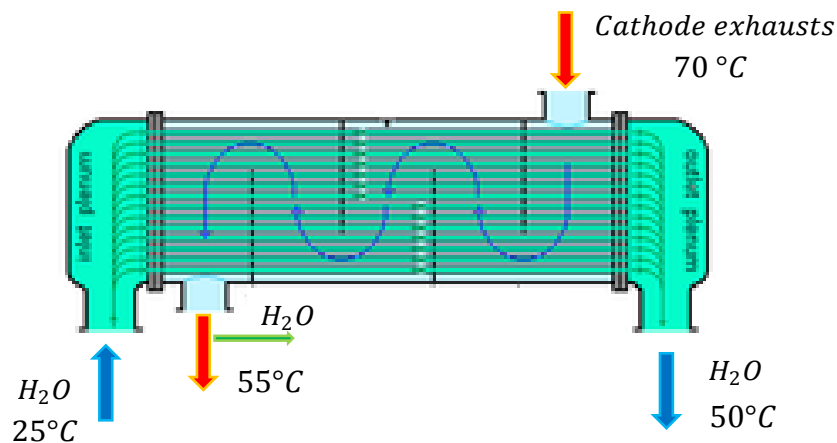


Figure 58 Schematic representation of the air/water heat exchanger

$$\Delta T_1 = 30,0 \text{ °C}$$

$$\Delta T_2 = 20,0 \text{ °C}$$

$$\Delta T_{ml} = \frac{\Delta T_1 - \Delta T_2}{\ln\left(\frac{\Delta T_1}{\Delta T_2}\right)} = 24,66 \text{ °C}$$

A corrective factor for this typology has been found equal to 0.9 and the air/water global heat transfer coefficient 100 [W/m<sup>2</sup>/K].

$$A = \frac{\Phi}{F \cdot U \cdot \Delta T_{ml}}$$

Since the value in the three cases has been found between 9 – 9.7, a 10 [m<sup>2</sup>] commercial heat exchanger has been chosen with 400 [mm] diameter and 2.2 [m] length [43].

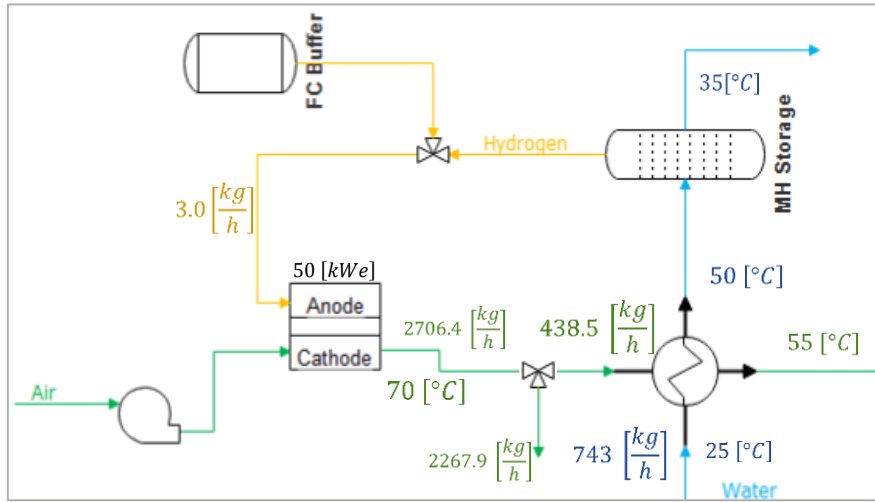


Figure 59 Schematic plant layout in the desorption process in LaNi5 case

### 4.3. Economic assessment

The economic evaluations have been carried out basing on the estimation given by 2 different sellers, whose MH tanks are all based on the usage of LaNi<sub>5</sub> and others belonging to the same family of intermetallics. So, this part is only focused on this alloy since it is the only one commercially available. The methods of thermal conductivity enhancements were not shared, so the configuration seen in the previous section is considered (shell-in-tube with 91 % porous aluminium foam and 25 % of vacuum space). The average costs on the market today are very high compared to compressed gas systems, mainly due to the current maturity level of the technology, which is not totally out of the prototyping stage or even the R&D in the design process.

$$1920 - 2400 \left[ \frac{\text{USD}}{\text{Nm}^3_{\text{H}_2}} \right] \equiv 645 - 810 \left[ \frac{\text{USD}}{\text{kWh}} \right]$$

These costs are referred to simple systems which consider only the costs of tank, hydrogen storage alloy, labour cost gas filters and tank sensors (flowmeters, pressure gauges, thermocouples, etc.). So an additional investments of 400.000 USD has been added to consider the complex piping system, the software implemented to regulate the operations

and the power electronics which connect all components (Balance of Plant). Finally, the safety system can be assumed as the same of the compressed gas system and part of the BoP.

Alloys costs have been evaluated through values in [38] in [USD/kg<sub>Raw mat</sub>]. The report was written in 1997, so they can be adjusted through the Chemical Engineering Plant Cost Index (CEPCI). These values must be further enhanced considering the price of all treatments required, such as pulverization, activation, encapsulation, etc. LaNi<sub>5</sub> and TiMn<sub>1.5</sub> prices have been enhanced by 2 times and TiFe<sub>0.85</sub>Mn<sub>1.5</sub> by 2.3 times. The cost of aluminium foam is also included here, but it is less important economically than other components. The labour cost has been considered the 18 % of the total cost, since it has to be carried out by high specialized workers (currently), while a remaining part of the total cost is left empty with a 8.96 %.

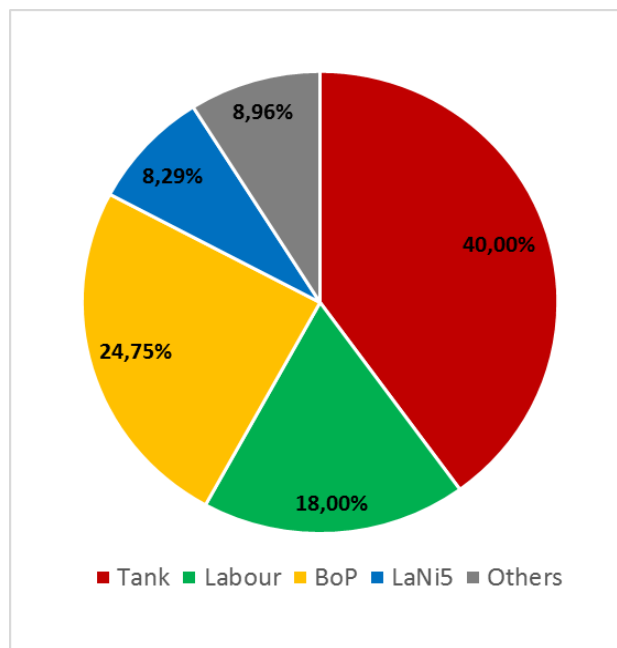
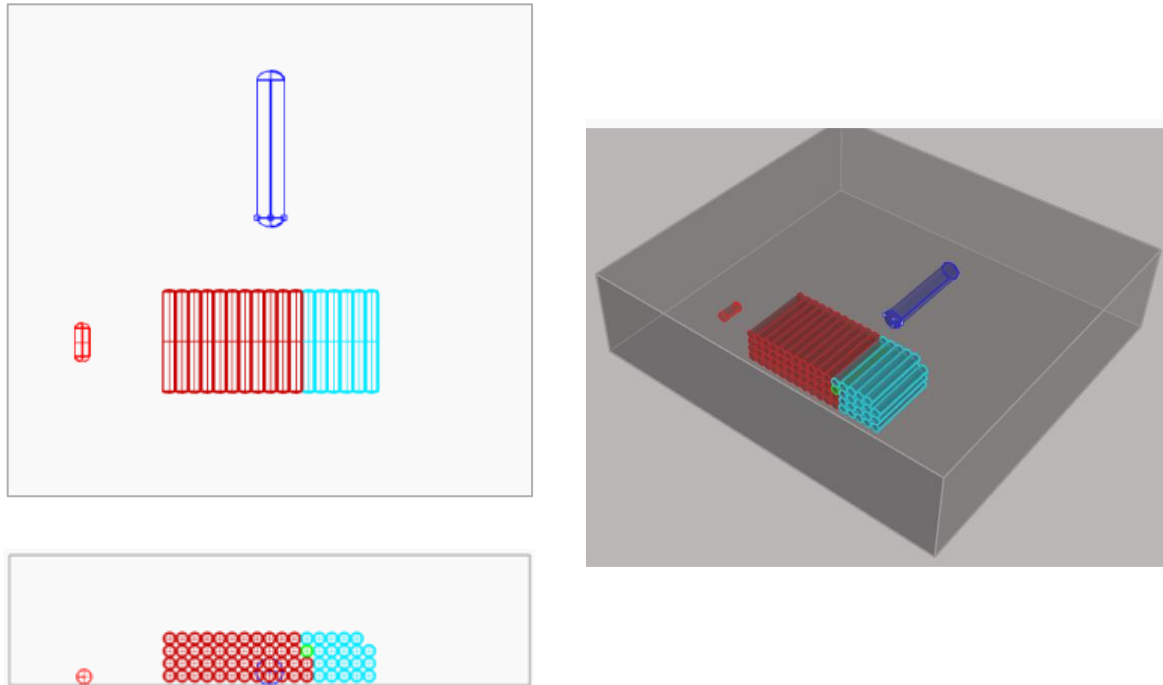


Figure 60 Division of fixed costs in a large-scale MH hydrogen storage system

Table 12 Final plant costs

<b>Total plant cost in USD</b>	1.619.000,00
<b>\$/kg<sub>H<sub>2</sub></sub></b>	33.056,00
<b>\$/kWh</b>	991,70

The specific costs are still too high to be competitive in commercial applications.



*Figures 61, 62, 63 Final plant layout with MH-based tanks adopted for hydrogen storage ( red-LaNi<sub>5</sub>, green-TiFe<sub>0.85</sub>Mn<sub>1.5</sub>, cyan-TiMn<sub>1.5</sub>), the blue device is the air/water HEX and the container on the left is the hydrogen buffer. The improvements in encumbrance are evident*

#### **4.4. Possible future trends [56], [57], [58]**

The final values calculated in the last section are clearly a prove of the unfeasibility of this kind of storage system from the economic point of view. In this last section a possible future trend is showed, based on the learning curve tool. There are several causes behind the phenomenon of learning curves, but the principal rule is the following: the greater the cumulative production of a good, the greater this experience and the lower the product cost will be over time, since the manufacturing process can be optimized, resources can be saved and competitors in the market increase. The learning curve came into prominence during World War II when Army Air Force scientists noticed that the cost for a given aircraft model declined with increased production in accordance with a fairly predictable formula. Each time the cumulative production doubled, cost declined by a fixed percentage. In the aircraft

industry, at that time, this reduction was about 20%. This assumes that repetitive production costs will decrease due to learning by the manufacturing staff - by increasing yields, increasing operation throughput, improved tooling, substituting equipment for labour, eliminating unnecessary steps, and process improvement and substitution. Technological learning is a major aspect in the assessment of potential cost reduction for emerging energy technologies with low numbers of cumulative productions. Since common approaches for the estimation of learning effects require an observation of the production cost development over several magnitudes of cumulative production volumes, they are obviously unsuitable for emerging technology which have not yet reached high market penetration.

The learning curves represent the relationship between the cost of a product and the experience expressed in cumulative production of that product:

$$C_x = C_0 \cdot \left(\frac{X}{X_0}\right)^{-r} \quad (20)$$

Where  $C$  denotes the costs at a given time,  $X$  is the cumulative production at that time,  $C_0$  are the initial costs at a cumulative production of  $X_0$  and  $r$  is the learning rate. The other parameters that are interesting to evaluate are the so-called progression ratio,  $PR = 2^{-r}$ , that denote the cost reduction when the cumulative production is doubled and the learning rate that is its complement to the unit,  $LR = 1 - PR$ .

To be acceptable, this kind of study needs an enough amount of data on productions and production costs that are not present in this application. So, following the research conducted by Bohm and al. [50], the learning factors will be 5% for independent standard parts, peripheral parts that are specific to the technology are defined with 8% and technology decisive parts are set to 15%. The BoP module is analysed by dividing the system into its subcomponents, since the theory of technological learning can be applied to every single component and then summed up to an overall curve.

$$C(X_t) = \sum_{i=1}^n C_{0i} \cdot \left(\frac{X_t}{X_{0i}}\right)^{-r_i} \quad (21)$$

Where  $X_{0i}$  and  $C_{0i}$  are the cumulative number of component  $i$  produced at time 0 and their costs,  $X_t$  is the cumulative production of the overall system only (simplification) and  $r_i$  are the learning parameters.

The main part of the BoP is has been assumed as the piping system, due to its complexity (nine tubes per reactors), followed by the software for the operations control and the power electronics with the circulation pumps. The reliability and safety of the operations are strictly linked to the effectiveness of the thermal management, so redundant pumps may be required for groups of 4 to 8 reactors with a further increase of investments in this part to assure a proper operation without any human intervention (REMOTE goal). The software should be able to manage automatically all signals coming from flowmeters, pressure and temperature sensors of each reactor and P2P systems all together making it very expansive, especially for a plant first of its kind like this one. A gas filter for each reactor is needed in order to avoid entrainments of MH particles that can easily congest valves and pipes; for shell-in-tube reactors the filter is usually mounted on the gas inlet/outlet but it is considered

Table 13 Learning rates assumed for BoP components

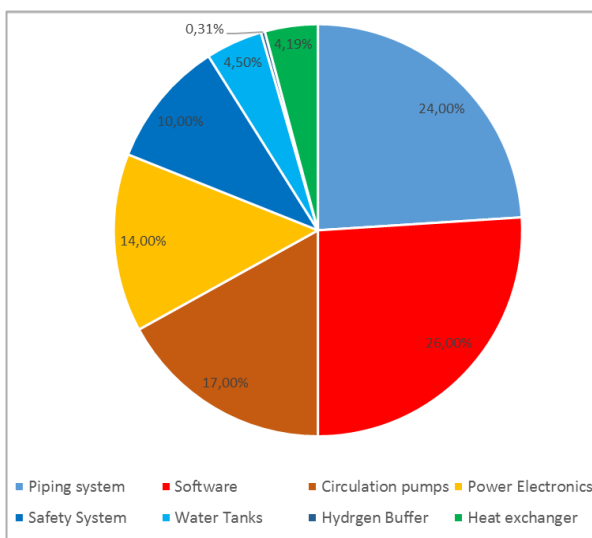


Figure 64 Balance of Plant subsystems cost division

System	Learning Rate
Power Electronics	15 %
Piping System	10 %
Circulation Pumps	5 %
Software	15 %
Safety system	5 %
Heat Exchanger	5 %
Hydrogen Buffer	5 %

separately from the reactor itself in this study. A final BoP learning rate can be easily calculated, equal to 10,3 %.

Considering the reactor, another method is applied (based on the reference [49]) that consists in the division of a so-called “system module” in two essential parts: material cost and residual cost. The material cost (SS 316) can be easily found [51] and its learning rate is fixed to 5 %, while the residual costs are all the remaining with a learning rate assumed equal to 15 %. The calculated learning rate value is 14.7 %. Finally the construction/labour value is assumed 15 % and the LaNi<sub>5</sub> equal to 10%. Other costs regarding additional systems not considered in this work, due to its qualitative nature, takes the 10 % of the initial cost and the respective learning rate has been fixed conservatively to 5 %.

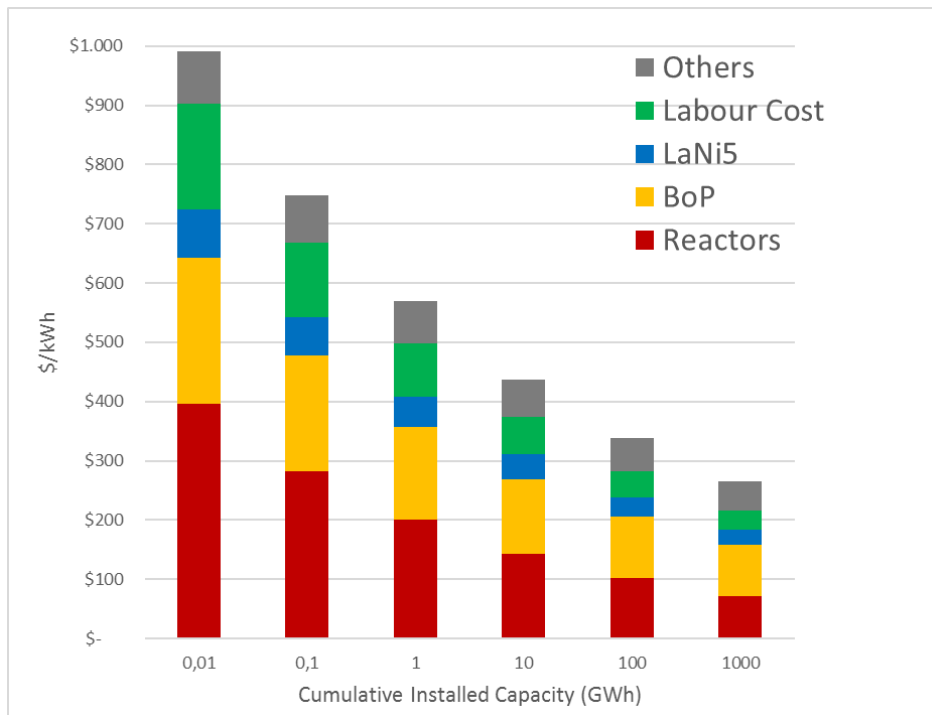


Figure 657 System learning curve

The final learning rate of the overall system is equal to 12,3 %, that is a medium value for emerging technology. From one side this result is optimistic, because saying that 100 GWh of hydrogen one day will be stored in intermetallics metal hydride is a pure hypothesis, but, from the other side, several assumptions made from the beginning of this work are conservative, together with the single low learning rates values assumed. So the result can be evaluated as realistic in this sense, but with high uncertainties, clearly.

The final cost obtained with 100 GWh capacity installed worldwide is around 265,4 [\$/kWh] that is too high yet compared to today's compressed hydrogen system cost that is around 30 [\$/kWh], but it seems to be a competitive cost comparing it with other energy systems in table 1.

## Conclusions

This master's thesis explores the principal environmental problem that represent the biggest threat ever faced up by mankind in its history, according to scientists all around the world: climate change. The energy sector is in the middle of a large and difficult energy transition that has its primary goal on the complete supersede of conventional, carbon/oil-based energy systems by sustainable, clean energy resources. The increased penetration of renewable energy carries the problem of intermittency in the electric grid, that needs new flexibility to manage it. Energy storage is expected to become fundamental in the next decades and hydrogen as its principal energy carrier. The focus is then moved to the main hydrogen technologies available today, and, clearly, on its storage technologies. The design for high internal pressures storage tanks (200 – 800 [bar]) results in a considerable wall thickness, very high encumbrance and moderate system safety. The container of a liquid hydrogen systems is not as stable and is more sensitive to external loads while in the metal hydride storage devices, hydrogen is chemically bonded and a gaseous release can take place if the container is destroyed but comes to a stop for lack of heat input, making this storage option intrinsically safe.

The main topic is the study of innovative materials for hydrogen storage that can host it reversibly in form of solid solutions. These materials are studied from late 70s and are the metal hydrides, in particular the intermetallic group. These ones are characterized by high efficient packing of H-atoms within the interstices among the metal atoms, the high volumetric densities of hydrogen (higher than  $\text{GH}_2$  and usually even  $\text{LH}_2$ ), low operational temperature and pressure, ultra-pure hydrogen (99.999 %) release, important safety improvements. The fact that the gravimetric capacity reaches values below the 2% makes them unsuitable for automotive applications but potentially advantageous for stationary applications and for hydrogen transportation (if the total weight is still in the application constraints, clearly). All these advantages can be appropriate especially in Power-to-Power backup systems, in off-grid locations to make these totally powered with renewable energy with no carbon dioxide emissions and low land occupation. The main

disadvantage relies on the fact that these new storage systems are still largely in the research & development stage, or just beyond the prototyping stage (depending on the alloy and the reactor typology), that make MH systems too expensive for commercial applications. Moreover, large-scale plants, like the one described in this work, seem to be very complicated to construct and manage.

So, this technology can be extremely useful for a large set of applications, that go from hydrogen storage, to heat pump, gas separation and thermal compression without moving parts and others. Focusing especially on the storage application, it would be interesting and advantageous compared to compressed gas systems only after the proper investments in next years and low land requirements by the considered plant. If encumbrance is not a problem, compressed gas systems have to be preferred in any case, with a consequent acceptance of a decreased safety; not a big problem, considered the number of years of experience with hydrogen in gaseous form. By the way, regarding the technical experience with early stage technologies, this is the principal problem regarding all hydrogen green applications and one of the principal goal of the REMOTE project exactly this: gain experience of maturing technologies that, maybe one day, will be in the foreground in the world energy sector. The main tool that companies all around the world could use to decide to invest in a technology that has not matured yet is the learning curve. The transformation of the energy system to facilitate the intensive use of renewable energies is based on the assumption that the technology costs concerning the generation applications and storage of renewable energy will decrease in future, so technological learning is a major aspect in the assessment of potential cost reductions for emerging energy technologies.

To conclude, an important ongoing European project has been commissioned by EU with an investment of 2 Million euros to provide a hydrogen storage tank based on a solid-state carrier, that will be part of a renewable energy plant exploiting the use of H<sub>2</sub> as energy vector for stationary energy storage: the HyCARE project. In this project carried on by a team of the department of chemistry of the university of Turin, the energy produced by renewable sources is used to produce H<sub>2</sub> from water through an electrolyser.

The gas is then stored in the HyCARE tank using a solid-state carrier. A heat storage system based on phase change materials collects the heat produced by the renewable plant, the electrolyser and from the metal hydrides, during H<sub>2</sub> absorption. The collected heat is used for the desorption from the metal hydride to release hydrogen and finally, the released H<sub>2</sub> supplies a fuel cell (FC), producing electricity.

The tank used for storage will be based on an innovative concept, linking hydrogen and heat storage to improve energy efficiency and to reduce the footprint of the whole system. It will be connected to a 20 kW Proton Exchange Membrane (PEM) electrolyser as hydrogen provider and a 10 kW PEM fuel cell as hydrogen user. The tank will be installed in the site of ENGIE Lab CRIGEN, a research and operational expertise centre dedicated to new energy sources and emerging technologies. It aims to store more than 50 kg of hydrogen in a metallic powder that can contain reversibly more than 100 [kg<sub>H<sub>2</sub></sub>/m<sup>3</sup>] with a final round-trip efficiency higher than 70%.

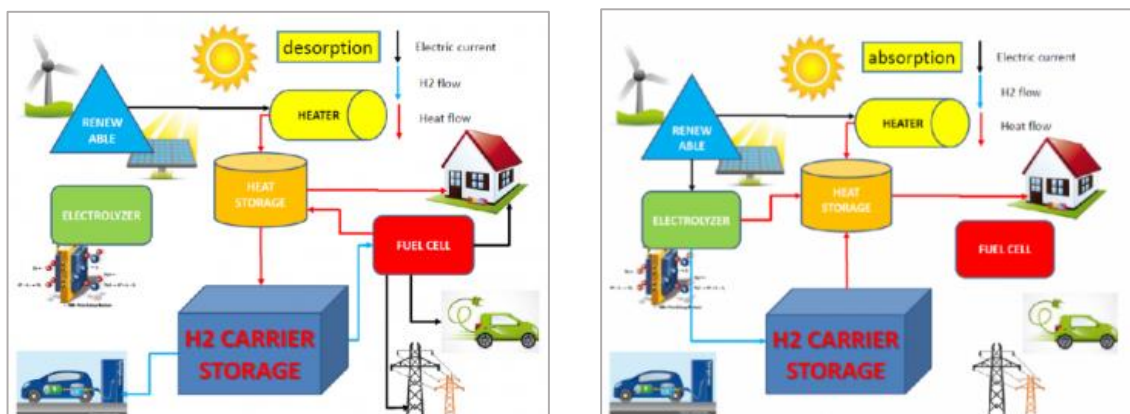


Figure 668 Qualitative representation of flows of hydrogen, heat and electricity during hydrogen production and usage in HyCARE project

This large and recent project (April 2019) has been cited because it is the first of this kind and it is almost identical to the final layout that has been described qualitatively in the case study in the last chapter, and the results that it will have deserve surely attention and further deepening.

# APPENDIX

	HSA	Density	Maximum Capacity			Reversible Capacity		
		g/cm <sup>3</sup>	H/M	%wt	rho_V	dH/M	/wt	rho_V
	/							
AB2	TiCr1,8	6	1,25	2,43%	145,8	0,45	0,85%	45,19
	Ti0,98Zr0,02V0,43Fe0,09Cr0,05Mn1,5	5,8	0,99	1,90%	110,2	0,7	1,30%	63,61
	TiMn1,5	6,4	0,99	1,86%	119,04	0,65	1,15%	63,61
	ZrFe1,5Cr0,5	7,6	1,03	1,50%	114	0,62	0,90%	55,24
	TiMn1,4V0,62	5,8	1,14	2,15%	124,7	0,56	1,10%	51,89
	ZrMn2	7,4	1,2	1,77%	130,98	0,6	0,90%	48,54
AB5	LaNi5	8,3	1,08	1,49%	123,67	0,93	1,20%	87,04
	LaNi4,25Al0,75	7,6	0,77	1,13%	85,88	0,53	0,78%	51,89
	Lani4,8Sn0,2	8,4	1,06	1,40%	117,6	0,92	1,24%	85,37
	CaNi5	6,6	1,05	1,87%	123,42	0,55	0,99%	56,91
	MmNi3,5Co0,7Al0,8	7,6	0,85	1,24%	94,24	0,36	0,53%	36,82
	MmNi5	8,6	1,06	1,46%	125,56	1,24	1,40%	87,04
	MmNi4,15Fe0,85	8,1	0,82	1,14%	92,34	0,9	0,90%	63,61
	MmNi4,5Al0,5	8,1	0,85	1,20%	97,2	0,83	0,83%	58,59
AB	TiFe	6,5	0,976	1,86%	120,9	0,79	1,50%	83,69
	TiFe,85Mn0,15	6,5	1	1,90%	123,5	0,8	1,50%	83,69
	TiFe0,8Ni0,2	6,5	0,7	1,30%	84,5	0,42	0,80%	48,54

	HSA	dH	dS	P abs(25°C)		P des(25°C)		T des(1atm)	Plateau	
		kJ/mol	kJ/mol/K	bar	atm	bar	atm	°C	Slope	Hysteresis
	/									
AB2	TiCr1,8	20,2	0,111	202,5	182	179,6	159	-91	0,11	0,12
	Ti0,98Zr0,02V0,43Fe0,09Cr0,05Mn1,5	27,4	0,112	32,6	11	10,9	10,9	-28	-	1,1
	TiMn1,5	28,7	0,114	14,7	8,4	8,3	8,3	-21	0,93	0,57
	ZrFe1,5Cr0,5	25,6	0,097	13,9	4	3,9	3,9	-10	0,34	1,26
	TiMn1,4V0,62	28,6	0,107	14,4	3,6	3,6	3,6	-5	-	1,4
	ZrMn2	53,2	0,121	0,0	0,001	0,0	0,0	167	0,99	0,74
AB5	LaNi5	30,8	0,108	2,0	1,8	1,8	1,8	12	0,13	0,13
	LaNi4,25Al0,75	44,1	0,117	0,4	0,024	0,0	0,0	104	0,23	2,7
	Lani4,8Sn0,2	32,8	0,105	0,6	0,5	0,5	0,5	39	0,19	0,22
	CaNi5	31,9	0,101	0,6	0,5	0,5	0,5	43	0,16	0,19
	MmNi3,5Co0,7Al0,8	39,8	0,115	0,4	0,11	0,1	0,1	73	0,2	1,2
	MmNi5	21,1	0,097	39,0	23	22,7	22,7	-56	1,65	0,54
	MmNi4,15Fe0,85	25,3	0,105	15,8	11,2	11,1	11,1	-32	0,17	0,36
	MmNi4,5Al0,5	28	0,105	5,4	3,8	3,8	3,8	-6	0,11	0,36
AB	TiFe	28,1	0,106	4,0	4,1	4,0	4,0	-8	0,64	0
	TiFe,85Mn0,15	29,5	0,107	6,4	2,6	2,6	2,6	3	0,62	0,92
	TiFe0,8Ni0,2	41,2	0,119	0,1	0,1	0,1	0,1	73	0,05	0,36

	HSA	Cost	
		\$/kg	\$/g H
	/		
AB2	TiCr1,8	\$8,64	\$1,02
	Ti0,98Zr0,02V0,43Fe0,09Cr0,05Mn1,5	\$4,82	\$0,37
	TiMn1,5	\$4,99	\$0,44
	ZrFe1,5Cr0,5	\$10,90	\$1,21
	TiMn1,4V0,62	\$29,40	\$2,67
	ZrMn2	\$11,29	\$1,25
AB5	LaNi5	\$9,87	\$0,77
	LaNi4,25Al0,75	\$9,68	\$1,24
	Lani4,8Sn0,2	\$9,69	\$0,78
	CaNi5	\$7,56	\$0,76
	MmNi3,5Co0,7Al0,8	\$13,25	\$2,50
	MmNi5	\$7,94	\$0,64
	MmNi4,15Fe0,85	\$7,12	\$0,79
	MmNi4,5Al0,5	\$7,17	\$0,86
AB	TiFe	\$4,68	\$0,37
	TiFe,85Mn0,15	\$4,83	\$0,32
	TiFe0,8Ni0,2	\$5,50	\$0,68

Tables with all hydrogen storage alloys found, with respective properties and costs. Values in red are the ones for which the respective compounds have been discarded in the final selection.



Final learning curve calculation procedure

	Reactors	Labour Cost	BoP	LaNi5	Others	
<b>%</b>	<b>40,00%</b>	<b>18,00%</b>	<b>24,75%</b>	<b>8,29%</b>	<b>8,96%</b>	<b>Final</b>
	\$ 647.569,27	\$ 291.406,17	\$ 400.683,49	\$ 134.244,72	\$ 145.019,53	\$ 1.618.923,17
0,01	\$ 396,67	\$ 178,50	\$ 245,44	\$ 82,23	\$ 88,83	\$ 991,69
0,1	\$ 281,94	\$ 126,37	\$ 193,58	\$ 65,32	\$ 79,17	\$ 746,39
1	\$ 200,40	\$ 89,46	\$ 154,04	\$ 51,89	\$ 70,56	\$ 566,35
10	\$ 142,44	\$ 63,34	\$ 123,66	\$ 41,21	\$ 62,89	\$ 433,53
100	\$ 101,24	\$ 44,84	\$ 100,12	\$ 32,74	\$ 56,05	\$ 334,99
1000	\$ 71,96	\$ 31,74	\$ 81,74	\$ 26,00	\$ 49,95	\$ 261,40
<b>LP</b>	<b>14,8%</b>	15,0%	<b>10,3%</b>	10,0%	5,0%	<b>12,3%</b>

# BIBLIOGRAPHY & SITOGRAPHY

## Chapter 1

- [1] François-Marie Bréon (France), William Collins (UK), Jan Fuglestedt (Norway), Jianping Huang (China), Dorothy Koch (USA), Jean-François Lamarque (USA), David Lee (UK), Blanca Mendoza (Mexico), Teruyuki Nakajima (Japan), Alan Robock (USA), Graeme Stephens (USA), Toshihiko Takemura (Japan), Hua Zhang (China), *Climate Change 2013: The Physical Science Basis, chapter 8: “Anthropogenic and Natural Radiative Forcing”*, pg. 569-7400, Working Group I contribution to the Fifth Assessment Report of the Intergovernmental Panel on Climate Change (IPCC)
- [2] [<https://www.co2.earth/daily-co2>]
- [3] Robinson, M.; Dowsett, H. J.; Chandler, M. A. *Pliocene role in assessing future climate impacts*. *Eos*. 89 (49) (2008): 501–502. doi:10.1029/2008EO490001
- [4] [<https://www.noaa.gov/news/july-2019-was-hottest-month-on-record-for-planet/>]
- [5] [<https://www.power-technology.com/projects/peterhead-carbon-capture-and-storage-ccs-project-scotland/>]
- [6] [<https://ourworldindata.org/>]
- [7] [<https://nsidc.org/arcticseaicenews/>]
- [8] Collins M., Knutti R., *Long-term Climate Change: Projections, Commitments and Irreversibility*, report IPCC, chapter 12
- [9] [<https://www.who.int/news-room/detail/02-05-2018-9-out-of-10-people-worldwide-breathe-polluted-air-but-more-countries-are-taking-action>]
- [10] UNEP, *Global Trends in Renewable Energy Investment 2019*, Copyright © Frankfurt School of Finance & Management gGmbH (2019).
- [11] Renewables now, Renewables 2019, Global status report, [<https://www.ren21.net/gsr-2019/>]
- [12] International Energy Agency, *Global Energy Outlook 2018*
- [13] IEA, *Energy Technology Perspectives 2018*; KPMG International

- [14] World Economic Forum, *Forecasting effective energy transition*, 2019, © 2019 World Economic Forum, © 2019 World Economic Forum
- [15] [<https://www.worldsteel.org/publications/position-papers/steel-s-contribution-to-a-low-carbon-future.html>]
- [16] International Renewable Energy Agency, *Electricity storage and renewables: costs and markets to 2030*, ISBN 978-92-9260-038-9, 2017
- [17] DG ENER Working Paper, *The future role and challenges of Energy storage*, Report by European commission (2012)
- [18] O. Schmidt, A. Hawkes, A. Gambhir & I. Staffell, *The future cost of electrical energy storage based on experience rates*, Nature Energy volume 2, Article number: 17110 (2017)

## Chapter 2

- [19] [<https://www.iea.org/tcep/energyintegration/hydrogen/>]
- [20] *The Future of Hydrogen, seizing today's opportunities*, Report prepared by the IEA for the G20, Japan, June 2019;
- [21] [<https://hydrogeneurope.eu/index.php/hydrogen-applications>]
- [22] Italian article on the website "Rinnovabili.it"  
[<http://www.rinnovabili.it/energia/idrogeno/idrogeno-prodotto-rinnovabile-economico-gas/>]
- [23] *How hydrogen empowers the energy transition*, report prepared by the Hydrogen Council, January 2017
- [24] [<https://www.iea.org/reports/tracking-energy-integration/hydrogen>]
- [25] Kasper T. Møller, Torben R. Jensen, Etsuo Akiba, Hai-Wen Li, *Hydrogen - A sustainable energy carrier*, Progress in Natural Science: Materials International, January 2017;
- [26] Rahul Krishna, Elby Titus, Maryam Salimian, Olena Okhay, Sivakumar Rajendran, Ananth Rajkumar, J. M. G. Sousa, A. L. C. Ferreira, João Campos Gil and Jose

Gracio, *Hydrogen Storage for Energy Application*, © 2012 Titus et al., licensee InTech;

- [27] Website of US Department of Energy, page focused on hydrogen storage  
[<https://www.energy.gov/eere/fuelcells/hydrogen-storage>]
- [28] [<https://www.iea.org/reports/tracking-energy-integration/hydrogen>]
- [29] L. Schlapbach, A. Züttel: *Hydrogen-storage materials for mobile applications*, Nature, 414 (15 Nov. 2001), 353-357
- [30] Niedzwiecki (Quantum Technologies): “Storage”, Proc. Hydrogen Vision Meeting, US DOE, Washington, 15-16 Nov. 2001;
- [31] T. Autry, A. Gutowska, L. Li, M. Gutowski, J. Linehan: “Chemical Hydrogen Storage: Control of H<sub>2</sub> Release from Ammonia Borane”, DOE 2004 Hydrogram Program Review, 24-27 May 2004, Philadelphia, USA
- [32] Prof. Dr. Detlef Stolten, Dr. Debrnd Emonts, *Hydrogen Science and Engineering, Materials, Processes, Systems and Technology*, © 2016 Wiley-VCH Verlag GmbH & Co. KGaA, chapters 27, 28, 31
- [33] [[https://en.wikipedia.org/wiki/Hydrogen\\_embrittlement](https://en.wikipedia.org/wiki/Hydrogen_embrittlement)]
- [34] [<https://www.brighthubengineering.com/machine-design/118961-fusion-of-inox-steel-and-embrittlement-issues/>]

### Chapter 3

- [35] Prof. Dr. Detlef Stolten, Dr. Debrnd Emonts, *Hydrogen Science and Engineering, Materials, Processes, Systems and Technology*, © 2016 Wiley-VCH Verlag GmbH & Co. KGaA, chapter 32
- [36] Martin Dornheim, *Thermodynamics of Metal Hydrides: Tailoring Reaction Enthalpies of Hydrogen Storage Materials*, (2011), DOI 10.5772/21662  
[<https://www.intechopen.com/books/thermodynamics-interaction-studies-solids-liquids-and-gases/thermodynamics-of-metal-hydrides-tailoring-reaction-enthalpies-of-hydrogen-storage-materials>]

- [37] Reilly J., Sandrock G. 1980 Hydrogen storage in metal hydrides. Scientific American, 242 2 5118 5129, 0036-8733
- [38] Gary Sandrock, *State of the art review of hydrogen storage in reversible metal hydrides for military fuel cell applications*, SunaTech, Inc. for the Department of the Navy Office of Naval Research (1997)
- [39] Gary Sandrock, *A panoramic overview of hydrogen storage alloys from a gas reaction point of view*, Journal of Alloys and Compounds 293-295 (1999) 877-888
- [40] Database of pyrophoric materials  
[\[https://www.chem.purdue.edu/chemsafety/PyrophoricChemicals.php\]](https://www.chem.purdue.edu/chemsafety/PyrophoricChemicals.php)
- [41] Database with thousands of tested hydrogen storage alloys  
[\[https://hydrogenmaterialssearch.govtools.us/\]](https://hydrogenmaterialssearch.govtools.us/)
- [42] Emil Burzo, *Landolt-Börnstein: Numerical data and functional relationships in science and technology; Group VIII: Advanced Materials and Technologies, Volume 8, Hydrogen Storage Materials*, pp.7-9, 13-18, 60-63, 512-515, 213-264 © Springer-Verlag GmbH Germany 2017, ISBN 978-3-662-54259-0
- [43] Billur Sakintuna, Farida Lamari-Darkrim, Michael Hirscher, *Metal hydride materials for solid hydrogen storage: A review*, International Journal of Hydrogen Energy 32 (2007) 1121 – 1140
- [44] Mahvash Afzal, Pratibha Sharma, *Design of a large-scale metal hydride-based hydrogen storage reactor: Simulation and heat transfer optimization*, international journal of hydrogen energy 43 (2018) 13356-13372
- [45] F.S. Yang, G.X. Wang, Z.X. Zhang, X.Y. Meng, V. Rudolph, *Design of the metal hydride reactors – A review on the key technical issues* International Journal of Hydrogen Energy 35 (2010) 3832 – 3840.
- [46] Nasako K, Ito Y, Hiro N, Osumi M, *Stress in a reaction vessel by the swelling of a hydrogen absorbing alloy*, Journal of Alloys and Compounds (1998) 264:271-6
- [47] Mykhaylo V. Lototsky, Ivan Tolj, Lydia Pickering, Cordellia Sita, Frano Barbir, Volodymyr Yartys, *The use of metal hydrides in fuel cell applications*, Progress in Natural Science: Materials International 27 (2017) 3-20

- [48] Mykhaylo V. Lototskyy, Moegamat Wafeeq Davids, Ivan Tolj, Yevgeniy V. Klochko, Bhogilla Satya Sekhar, Stanford Chidziva, Fahmida Smith, Dana Swanepoel, Bruno G. Pollet, *Metal hydride systems for hydrogen storage and supply for stationary and automotive low temperature PEM fuel cell power modules*, International Journal of Hydrogen Energy 40 (2015) 11491 – 1497.
- [49] Poojan M., Aguey-Zinsou K.F., *Titanium-iron-manganese (TiFe<sub>0.85</sub>Mn<sub>0.15</sub>) alloy for hydrogen storage: reactivation upon oxidation*, International Journal of Hydrogen Energy 44 (2019) 16757 – 16764;
- [50] Laurencelle F., Dehouche Z., Goyette J., *Hydrogen sorption cycling performance of LaNi<sub>4.8</sub>Sn<sub>0.2</sub>*, Journal of Alloys and Compounds 424 (2006) 266-271
- [51] R.B. Schwarz, A.G. Khachaturyan, *Thermodynamics of open two-phase systems with coherent interfaces: Application to metal-hydrogen systems*, Acta Materialia 54, 313-323, (2006).

## Chapter 4

- [52] [<https://www.remote-euproject.eu/>]
- [53] [[https://www.alibaba.com/product-detail/Stainless-steel-double-pipe-heat-exchangers\\_60226814038.html](https://www.alibaba.com/product-detail/Stainless-steel-double-pipe-heat-exchangers_60226814038.html)]
- [54] [[https://www.alibaba.com/product-detail/Metal-Hydride-H2-storage-tank\\_1055956548.html?spm=a2700.7724838.2017115.1.52f077c1Kg2oyn](https://www.alibaba.com/product-detail/Metal-Hydride-H2-storage-tank_1055956548.html?spm=a2700.7724838.2017115.1.52f077c1Kg2oyn)]
- [55] Cengel Y. A., Boles M.A., *Thermodynamics, an engineering approach, fifth edition*, McGraw-Hill, June 3, 2004, ASIN: B003I01E40, Table A-4
- [56] Miguel A. Reguero, *An Economic Study of the Military Airframe Industry, Wright-Patterson Air Force Base*, Ohio, Department of the Air Force, October 1957, p. 213.
- [57] Schoots K., Ferioli F., Kaer G.J., van der Zwaan B.C.C., *Learning curves for hydrogen production technology: An assessment of observed cost reductions*, International Journal of Hydrogen Energy 44 (2019) 30789 – 30805

- [58] Bohm H., Goers S., Zauner A., *Estimating future costs of power-to-gas – a component-based approach for technological learning*, International Journal of Hydrogen Energy 33 (2008) 2630 – 2645
- [59] [<http://www.meps.co.uk/Stainless%20Price-eu.htm>]

## Ringraziamenti

Al termine di questo viaggio, sembrato interminabile, ma che adesso sembra essere volato via in un lampo, posso affermare che mai e poi mai sarei riuscito a superare qualsiasi prova, esame, sfida da solo. Il tanto lavoro che ha preso ore, giorni, mesi del mio tempo questi anni ha però dato i suoi frutti e questo lo devo a tutti coloro che mi sono stati vicini, sia nei bei momenti che in quelli più bui.

Al Professor Massimo Santarelli va la mia più sentita riconoscenza per il suo tempo dal valore inestimabile che mi ha concesso, nonostante i mille impegni. Confrontarsi con un esperto tanto rinomato ai più alti livelli è stato un privilegio di cui farò tesoro per tutta la mia carriera. Grazie professore.

Ai miei genitori, più unici che rari, grazie di avermi permesso di vivere un'esperienza indimenticabile in questa città stupenda e di aver sempre mantenuto il loro sorriso intatto, nonostante la nostalgia in questi due lunghi anni. Spero tanto di avervi reso fieri di me.

A Giuseppe, Marica, Chiara, Ciccio, Antonio e Luca ringrazio di cuore per avermi fatto tornare il sorriso in OGNI momento. Qualsiasi giorno diventa una festa quando ci siete.

A Zia Finella, Pino, Angela, Biagio, Domenico, Luciana, Andrea, Gimmy, Vincenza, Giuseppe, Zio Luigi e Zia Gianna, grazie di rendere tutti insieme questa famiglia la più meravigliosa, unita e forte che ci sia al mondo. Farne parte è una fortuna inestimabile.

A Letizia, grazie per esserci sempre.

A Michele, Anna, Alex e ai nonni Angela, Nicola, Uccia e Pasquale, grazie di avermi accolto nella vostra bellissima famiglia. Quando sono con voi mi sento sempre a casa.

A quei matti di Gianluca, Cosimo, Luigi e Fabio, grazie per le risate infinite. Anche se questi 5 anni ognuno ha preso la sua strada, quando torniamo insieme il tempo vola e questo non è da tutti. Spero sempre in una Reunion stile 2010...

A Dorian, grazie per le risate, l'assoluta, indiscussa sincerità nei consigli e nelle strigliate (a volte un po' cattive). Non sarei quello che sono senza te, ma naturalmente lo sai già!

A Rosanna, grazie per questa stupenda amicizia che ormai va avanti da quasi 15 anni e che, sicuramente, non finirà mai.

Ad Antonio, grazie per quest'amicizia di 25/25 anni. Abbiamo ancora centinaia di derby Roma-Inter da guardarci insieme!

A Mariachiara, Alessandra, Bea, Silvia, Savino, Felician, Giampiero, Arianna, Angela e Silvio, grazie per avermi fatto capire fino in fondo il detto: "Chi trova un amico trova un tesoro" Vi voglio bene!

A Serena, grazie davvero di tutto: del tempo trascorso insieme a ridere, piangere, festeggiare, discutere o a pianificare il prossimo weekend per riabbracciarci finalmente

dopo settimane, se non mesi. Essere arrivati fino a qui è stato possibile soprattutto grazie a te, ricordalo sempre. Affrontare questi due anni tanto distanti ci ha portato via qualcosa, ma ci ha dato molto di più: adesso sento che non esistono più orizzonti troppo distanti per noi due, insieme.

A me stesso vorrei solo ricordare un domani, semmai rileggerò per nostalgia queste righe: Mari calmi non fanno buoni marinai.

Grazie A Tutti.